Structure-activity investigation on laccases by computational and site directed mutagenesis studies

by

Azar Delavari

Universitat Politecnica de Catalunya

Structure-activity investigation on laccases by computational and site directed mutagenesis studies

A thesis submitted for the degree of

Doctor of Phylosophy

by

Azar Delavari

This work has been carried out at the Laboratory of Molecular Engineering, of the Molecular and Industrial Biotechnology Group, Department of chemical engineering, under the direction of Prof. Juan Jesús Perez.

Prof. Juan Jesús Perez

Barcelona, July 2016

ABSTRACT

Laccase belongs to multi copper oxidase enzyme family (EC 1.10.3.2). It has three different copper sites, type 1 (T1), type 2 (T2) and type 3 (T3). The function of the T1 site is shuttling electrons from the substrate to the trinuclear copper cluster. During the catalytic cycle of laccase, four electrons are removed from four substrate molecules, which are finally transferred to reduce oxygen to two water molecules. Comparison of the kinetic parameters using several laccases and several substrates has shown that the reaction rate of laccase correlates with the redox potential difference between the T1 copper and the substrate. Their capacity to oxidize a wide range of substrates makes them very attractive for the industry and are growing in importance for environmentally-friendly synthesis. Thus, they are used on a large scale for industrial purposes.

Due to the industrial importance of laccases an enormous interest has been put forward to improve their physicochemical properties using protein engineering. Today, the use of novel computational methods, and cutting-edge directed evolution techniques, supported by the know-how generated during the last two decades on laccase structure–function relationships, can aid implementation of laccases at industrial scale. Moreover, computational simulations can reveal targets for protein engineering to be explored by site-directed mutagenesis (or semi-rational approaches). In this work we tried to use computational methods for studying interaction of different substrates with laccases and structural activity of the enzyme.

One of the goals of this thesis is to characterize the binding pocket of diverse laccases and describe the mechanism of oxidation of substrate in laccase active site. For this purpose we have used three laccase structures with diverse redox potential values, including a high redox potential (HRPL), a low redox potential (LRPL) and one bacterial laccase, to study the differences in active site of this enzyme. First we did geometry optimization of substrates. We found that ABTS, one of the main substrates of laccase in industry, with the two benzothiazoline groups in the same planar in the case of $ABTS^{2-}$ and $ABTS^{1-}$, whereas the two fused rings show a 30º twist when the two nitrogens of azine group are protonated. The experimentally pKa measurement of ABTS also supported this finding.

Then, we performed molecular docking studies and analysed the data to find which residues are involved in the interaction with substrates. Our results indicate that bacterial laccase (1UVW) has less hydrophobic and aromatic residues in the activity site in comparison to other fugal structures of this study, as a result, find a pose that interacts with residues needs more energy. We carried out the docking process with protonated Asp/Glu, conserved residue in fungal laccases. The scores were worse except in case of ABTS, that we obtained better score. All in all, the results of molecular docking illustrates that ligands bound near His. In fact, the hydrogen of N_e of His is oriented to the oxygen atom of the phenolic substrate which is the path for electron transfer from substrate to the enzyme. Subsequently, we evaluated the effect of protonation state of a conserved residue in fungal laccase, Asp/Glu, through molecular dynamics simulation. The results illustrate that water molecules have role in the interaction of DMP with MaL structure.

For industrial use of laccase, the current challenge is to obtain improved laccases with desirable physicochemical characteristics such as a higher redox potential. The present study is also aimed at applying a computational method that permits the calculation of the redox potential by taking into account the different residues in binding pocket environment in order to suggest possible mutations. We used QMMM-2QM-MD approach for one of the fungal laccase structure (3FU8) in order to calculate redox potential value. The result indicates that the difference in redox potentials changes from 7-17 to 74-92 kJ/mol if the redox state of T1Cu and DMP in the other subunit change and we correctly predict that CuT1ox/DMPred state is more stable than the CuT1red/DMPox state.

Afterwards, we have started experimentally performing mutations on binding pocket of laccase in order to find if those residues effect on redox potential value. We performed mutagenesis on MtL T2 structure that has 76% of identity to MaL which our computational studies was performed on its structure. We made a combinatorial library for position 192 and 296 in MtL T2. In our screening assays the clone contained A192P and L296W (3H12) mutation and clone contained A192P and L296L (19G8) showed activity with violuric acid 1.23 and 1.33 fold higher than parental type, respectively. Moreover, the clone

contained A192R and L296W (15H11) and clone with mutation A192R and L296L (5B4) showed higher activity with molybdenum hexacyanide in comparison to parental type.

Thermostability of the different mutants along directed evolution did not vary significantly, so the final mutant showed thermostability profiles equivalent to the parental type MtLT2. Besides, the activity of parental type and all mutants were optimal at pH 4.0 for ABTS. The kinetic measurements indicated that the mutant that had substitution of A192R, 5B4, did not indicate better affinity to ABTS since Arg residue is more bulky than Ala. k_m value of 19G8 that has Pro192 in binding pocket is lower than 5B4 mutant which indicates that it has more affinity to phenolic substrates since the binding pocket is more hydrophobic and allows a better fit for phenolic structures binding site T1.

After characterization of mutants experimentally, we analyzed the mutants by computational study. First, we compared the wild type structure with P192P and A296L which is similar to 19G8 mutant and P192R and A296L which makes it similar to 5B4 mutant. There was a difference in case of P192R and A296L, the binding pocket is tighter than the wild type. In molecular docking simulation it did not show differences and ligands could bind there. We calculated the redox potential value of the structure similar to 19G8 mutant. The redox potential value is 167 kJ/mol that illustrates increasing in the value.

Overall, by making different mutagenesis library on MtL T2 laccase, we found that combination of position 192 and 296 has effect on redox potential of this structure. The combination of Pro and Leu, which are hydrophobic residues, or Pro and Trp, which add aromatic residue to the active site lead improvement in activity of enzyme with molybdenum compound (E°= 780 mV vs. NHE) and violuric acid (E°= 912 mV vs. NHE). Since there was no improvement in kinetic constants of the interaction between ABTS and DMP as a ligand and enzyme, consequently, the improvement in activity refers to redox potential property. Aside from that, the computational prediction of redox potential of MaL in the same position with the same residue showed increasing in the value.

PREFACE

"Four years ago I started this project as a molecular engineering project, but it turned out to be long battle against a small molecule. This thesis is the report of this long process. It cannot express the long days spent in the lab, battling shoulder to shoulder with my fellow scientists and friends, the joy for screening of mutagenesis library, the hope for good results, the sadness and tiredness with each failed attempt."

During my previous years of study, before starting PhD, I looked for industrial issues and tried to find a project that could bridge the gap between Research and Industry by developing innovative solutions, which I could found by present PhD thesis.

Among the industrial enzymes, over the years, several industrial applications demand laccases, as a result of their broad oxidative capabilities and it becomes very attractive candidates for protein engineering. Laccase belong to multi copper oxidase enzyme family. One of the remaining challenges in laccase engineering is the increasing of the redox potential at the T1 Cu site beyond the nature limits (above +800 mV) without sacrificing neither the stability nor the catalysis. Moreover, despite that the mechanism for substrate oxidation has been studied for several years, it has not been fully elucidated and it is still controversial.

This dissertation is aimed at developing a procedure for exploitation of laccases in different industrial fields. It demonstrates a rational approach in order to understand structure-activity of laccase by applying computational methods. The project originally consisted of three parts. First, it provides information on laccase mechanism and approaches that have been used computationally and experimentally (literature overview). Then the second part it contains the computational methods to obtain goals such as, characterization of the binding pocket of diverse laccases, description of the substrate oxidation mechanism in active site, calculation of the redox potential value. Finally, in the last part, it deals with experimental

strategies to improve one of the important properties of laccase, redox potential value, in order to combat one of the restriction of using this enzyme in industry.

I hope this work and the achieved results be of interest to students and researchers in industrial biotechnology as well as to everyone interested in basic research in protein structure, molecular engineering, computational chemistry and enzyme biochemistry. Metalloproteins such as laccase present many challenges when they come to computational modeling. However, in the forthcoming years, it is expected that the combination of laboratory evolution with both rational and semi-rational strategies, including molecular dynamics and quantum mechanics/molecular mechanics simulations, will lead to the development of laccases with exciting biotechnological properties and produced at high titers while enhancing our understanding, at the molecular level, of the mechanisms that govern the behavior of this thrilling group of oxidoreductases.

Azar Delavari

Barcelona,

July 2016

ACKNOWLEDGMENTS

This research project would not have been possible without the support of many people. I am especially grateful to my supervisor, Professor Juan Jesus Perez for accepting me as a Ph.D student. I would like to thank him for professional help regarding some parts of this thesis and for providing a continuous funding stream to my post-graduate education. I feel grateful to the Universitat Politecnica de Catalunya for awarding me predoctoral scholarship FPI-UPC in four academic years (2012 - 2016).

My greatest appreciation to Professor Ulf Ryde in Theoretical Chemistry department of Lund University. He is full of brilliant ideas and deep insights about multicopper proteins. Thanks to him for dedicating his time to me, answering my questions and guiding me even after I left there, although he was busy to supervise his post graduate students. I learned a lot of issues during my stay in his group. Also, great thanks to Geng, who helped me to carry out some QMMM calculations of my thesis.

Unique thanks must be given to Dr. Miguel Alcalde who gave me the opportunity in order to work in his lab, Institute of Catalysis and Petrochemistry, CSIC (Madrid), Directed Enzyme Evolution lab, to carry out mutagenesis experiments of my project. Thanks to him for enabling me to work with such an interesting enzyme!

Further, my special thanks to Dr. Alcalde's lab members,

Xavi, none have put so much time with me on my project as you have. Ivan, you have been helping me a lot during my stay in Madrid. Patri and David, you have always been ready to answer my questions. Berni, Javi and Pati, you have helped me by showing me how instruments and robots function in the lab. I wish you all, the best.

I would like to express my acknowledgement to my officemates Lourdes, Patri such a nice person who played the role of my older sister; I tried to listen to your recommendations on scientific or nonscientific issues, and Cecy, who learned some Persian words and tried to use them in her talks with me.

Thank to you for many, many nice times together and a lot of fun. Thanks for being there to make difficult moments, easier for me.

Thanks must also be given to my Iranian friends Bahar, Mahdieh, Behrooz and Hamed that helped me not to feel homesick by creating nice moments together what I really needed to continue my PhD.

I take the opportunity to show my appreciation for some other people that mean a lot to me which is somewhat besides the PhD…

I am lucky to have you Mam, thank you for your love and support even from that distance. Thanks to Dad who always wishes the best for people around and finally, I want to express my gratitude to my husband, Mostafa, for his intimate love and sacrificial accompanying that have brought and will continuously bring happiness into my life.

TABLE OF CONTENTS

II. Experimental material and methods

ABBREVIATIONS, ACRONYMS AND SYMBOLS

ABTS   2,2´-azino-bis(3-ethylbenzothiazoline-6-sulphonic acid)

Amp   ampicillin

bp   base pair

BSA   bovine serum albumin

DMSO   dimethyl sulfoxide

dNTPs   desoxynucleotides

dH_2O distilled water

DMP   2,6-Dimethoxyphenol

DNA   deoxyribonucleic acid

$E°$ standard redox potential

E. coli   *Escherichia coli*

EDTA   ethylenediaminetetraacetic acid

EPR   electron paramagnetic resonance

ESP   electrostatic potential

HRPL   high redox potential laccase

IvAM   in vivo assembly of mutant libraries

IVOE   in vivo overlapping extension

K   kelvin degree

kb   kilo base

LB	lysogeny broth
LRPL	low redox potential laccase
M	molar
MCO	multicopper oxidase
MD	molecular dynamics
MM	molecular mechanics
MOE	molecular operating environment
ng	nanograms
OD	optical density
PCET	proton coupled electron transfer
PCR	polymerase chain reaction
pH	*potentia Hydrogenii*
QM	quantum mechanics
QMMM	quantum mechanics/molecular mechanics
RESP	restrained electrostatic potential
rpm	revolutions per minute
RT	room temperature
SC	synthetic complete
S. cerevisiae	*Saccharomyces cerevisiae*
SOC	super optimal broth plus glucose

T	temperature
TAE	tris-acetat-EDTA
TNC	thri-nuclear copper center
U	units of enzyme
XYD	2,5-xylidine
YNB	yeast nitrogen base
YPD	yeast extract peptone D-Glucose

Amino acids

A   alanine (Ala)

C   cysteine (Cys)

D   aspartate (Asp)

E   glutamate (Glu)

F   phenylalanine (Phe)

G   glycine (Gly)

H   histidine (His)

I   isoleucine (Ile)

K   lysine (Lys)

L   leucine (Leu)

M   methionine (Met)

N   asparagine (Asn)

P   proline (Pro)

Q   glutamine (Gln)

R   arginine (Arg)

S   serine (ser)

T   threonine (Thr)

V   valine (Val)

W   trptophan (Trp)

Y   tyrosine (Tyr)

LIST OF FIGURES

LIST OF TABLES

1. INTRODUCTION

1.1. Physico-chemical properties and structure of laccases

Laccases are enzymes that belong to the group of the oxidoreductases, facilitating a redox reaction while regenerating themselves. Laccases often occur as isoenzymes or monomers that oligomerize to form multimeric complexes (Claus et al., 2002). Each isoenzyme has four copper atoms that enable to individually carry out the catalytic process of laccases. The molecular mass of the laccase monomers ranges from 40 to 130 kDa with a covalently linked carbohydrate. The carbohydrate moiety typically consists of mannose, N-acetylglucosamine and galactose, which may contribute to the high stability of the enzymes (Claus et al., 2002; Gianfreda et al., 1999).

The systematic name of laccase, benzenediol: oxygen oxidoreductases (EC 1.10.3.2), is somewhat misleading, as the substrate range of laccases is much wider. Laccases are able to oxidize diverse phenols: mono-, di-, and polyphenols, aminophenols, polyamines, as well as methoxy-substituted phenols (Thurston, 1994) and several other compounds and aryl diamines (Rodríguez Couto and Toca Herrera, 2006; Wells et al., 2006). Thus, the phenolic subunits of lignin are also natural substrates for laccases. Aminophenols and phenylenediamines are also good substrates for laccases, but arylamines are usually weak substrates (Bertrand et al., 2002). Laccase oxidizes the molecule with a simultaneous radical formation, which can spontaneously rearrange to cleave the aromatic rings or promote their polymerization (Fiţigău et al., 2013; Sun et al., 2013).

Their capacity to oxidize a wide range of substrates makes them very attractive for the industry and are growing in importance for environmentally-friendly synthesis. Thus, they are used on a large scale for industrial purposes such as the textile industry; removal/degradation of a number of environmental pollutants (Auriol et al., 2008); dye decolorization (Yang et al., 2015), synthesis of antioxidants highly valuable in food applications, removal of phenols in wastewaters (Sukan and Sargin, 2013); pulp and paper industry (Kunamneni et al., 2008; Valls et al., 2010); and in the modification of polymers such as chitosan

(Aljawish et al., 2012). Recently, they have applications in other field such as biofuel cells (Zheng et al., 2015).

Three-dimensional structural analysis of several fungal, bacterial and plant laccases reveals a structure with three sequentially arranged cupredoxin-like domains; each of them exhibiting a greek key β-barrel topology, being highly related to small copper proteins such as azurin and plastocyanin (Dwivedi et al., 2011; Giardina et al., 2010). The cupredoxin domain is distinctive for all blue copper-containing proteins, for example, azurin (one domain), nitrite reductase (two domains), laccase (three domains), and ceruloplasmin (six domains) (Murphy et al., 1997; Nakamura and Go, 2005). All these blue copper-containing proteins have apparently evolved from the same ancestor protein. Although the exact evolutionary pathway of laccases is not yet completely understood, laccases most certainly have evolved through gene duplication and divergence of cupredoxin domains (Zhukhlistova et al., 2008).

Laccase contains four copper atoms (Figure 1.1), which have been classified into three types based on the absorption and Electronic Paramagnetic Resonance spectra. Specifically, they are called type 1 (T1), type 2 (T2) and type 3 (T3) copper. Type 1 (T1) or paramagnetic "blue" copper has an intense absorption at 600-610 nm, which is caused by the covalent copper-cysteine bond and confers the typical blue color to the multicopper proteins. The T1 copper has a trigonal coordination with two histidines and one cysteine (Giardina et al., 2010; Palmer et al., 1999). In bacterial laccase the axial ligand is formed by methionine (Gunne et al., 2014). The lack of a coordinated axial ligand to the T1 copper of fungal laccases is arguable, because other multicopper oxidases, such as plastocyanin, ascorbate oxidase, human ceruloplasmine, and tree laccases, have a methionine at this position coordinated to the T1 copper (Giardina et al., 2010). However, based on sequential analysis, in fungal laccases the amino acid at the axial position is leucine or phenylalanine and this is unable to coordinate to copper.
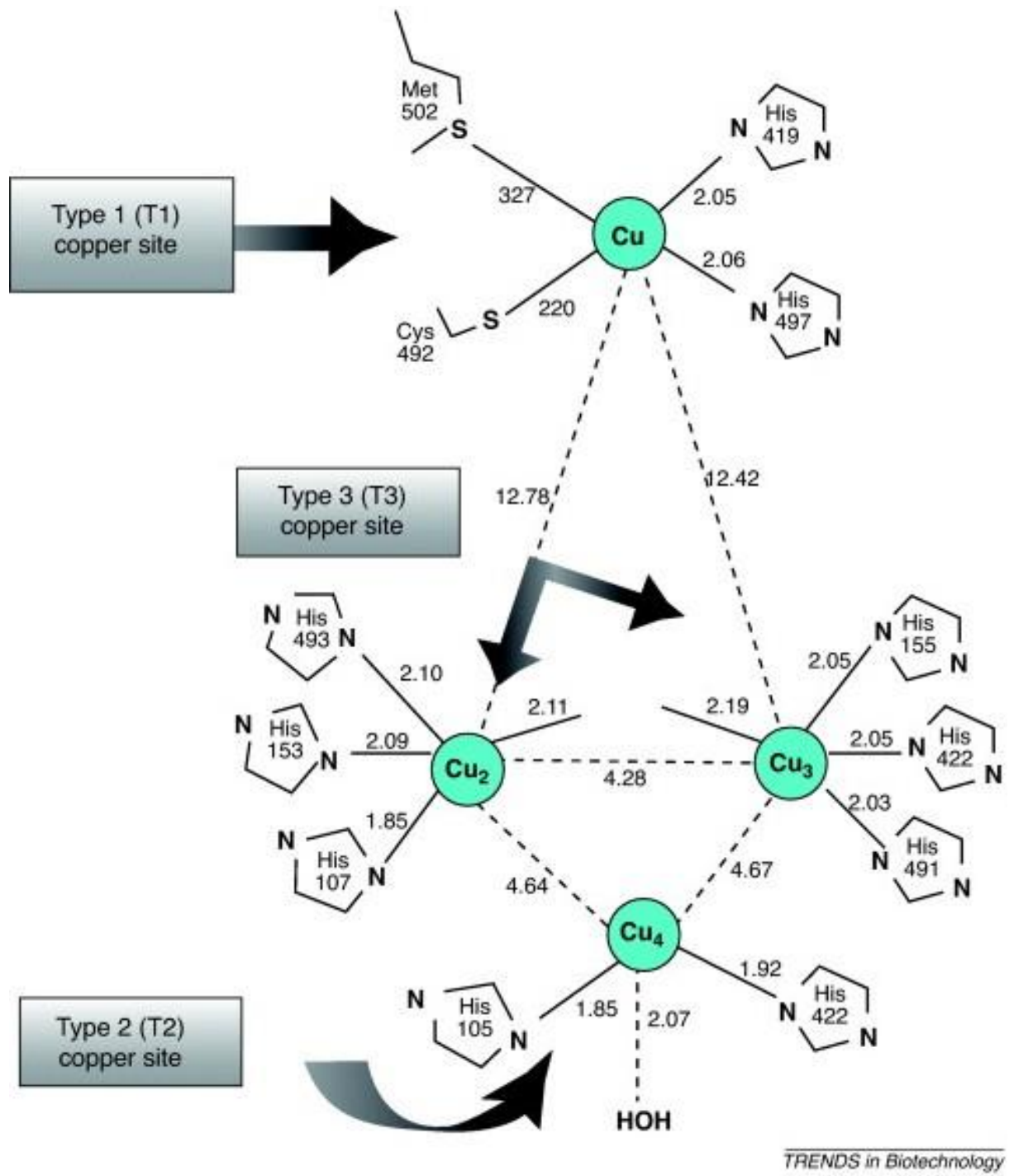
Figure 1.1. Three types of copper found in laccase (Santhanam et al., 2011).

Type2 (T2) or paramagnetic "non-blue" copper has no visible absorption spectrum and is coordinated by two histidines and a water molecule. Finally, the two T3 coppers are antiferromagnetically coupled through a bridging hydroxide; thus, the resulting diamagnetic T3 site is EPR silent. Type3 (T3) is a diamagnetic coupled binuclear copper center, with an absorption band at 330 nm. Each of the T3 coppers is coordinated to three histidines in addition to the bridging hydroxide (Giardina et al., 2010). The eight histidines coordinating the trinuclear cluster (TNC) occur in a highly conserved pattern of four HXH motifs.

Based on a comparison of over 100 sequences of fungal and plant laccases, a laccase signature sequence has been found (Dwivedi et al., 2011; Kumar et al., 2003). This signature sequence, differentiates laccases from other multicopper oxidases, and comprises four amino acid sequences L1–L4, in which all the copper-coordinating amino acid residues are found. The stretch of 11-12 residues binding the 4 coppers is conserved among the laccases family. Comparison of the 3D structure of laccases of diverse species, suggests that all the laccases are folded in a similar manner and the distances of the 12 ligating amino acids are very similar in all of them (Dwivedi et al., 2011). All laccases are organized in three sequentially arranged cupredoxin-like domains. The cupredoxin domains are mainly formed by β-barrels (Greek-key motif) comprising β-sheets and β-strands arranged in sandwich conformation. The substrate is bound in the active site, in a cleft at the surface of the enzyme, and oxidized by the T1 site. The size and the shape of substrate-binding cavity varies among different laccases (Kallio et al., 2009).

7.1. Catalytic mechanism of laccase

The redox process involves the oxidation of a substrates by hydrogen abstraction with the concomitant reduction of oxygen to water. Figure 1.2 illustrates the catalytic mechanism. Oxidation of the substrate produces an intermediate, the substrate reduces the T1 site, which transfers the electron to the trinuclear cluster T2/T3. Here, two possible mechanisms for reduction of the TNC are conceivable: either T1 and T2 sites together reduce T3, or each copper on the cluster is sequentially reduced by electron transfer starting from T1. Once the enzyme is completely reduced, one oxygen atom is bound with the T2

and T3 copper ions, and the other oxygen atom is bound with the other copper ion of T3, forming the peroxide intermediate. Subsequently, the peroxide bond (O-O) is broken to produce a native intermediate (fully oxidized form), which will end the catalytic cycle with the reduction of oxygen to water. Sometimes the native intermediate is converted to a completely oxidized cluster called the "resting" form, where the T2 copper is isolated from the coupled T3 coppers. In this form, the T1 can still be reduced by the substrate, but the electron transfer is too slow to be significant (Jones and Solomon, 2015; Solomon and Lowery, 1993; Wherland et al., 2014). The use of molecular oxygen as the oxidant and the fact that water is the only by-product are very attractive catalytic features, rendering laccases as excellent 'green' catalysts (Riva, 2006; Thorum et al., 2010). The function of the T1 site is long-range intramolecular electron transfer, shuttling electrons from the substrate to the TNC, 13 Å away (Gasparetti, 2012).
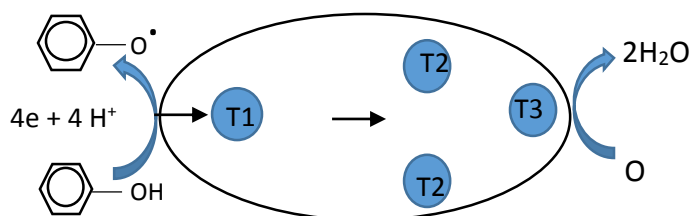
Figure 1.2. Catalytic mechanism of laccase.

During the catalytic cycle of laccase, four electrons are removed from four substrate molecules, which are finally transferred to reduce oxygen to two water molecules. The oxidized substrates can be also involved in further non-enzymatic reactions. Electrons needed for this process are obtained through the oxidation of a variety of substrates, but not much is known about the mechanism of proton transfer during this process. Recently, site directed mutagenesis studies suggest that Asp112 of CueO (Asp 116 in CotA) (Kataoka et al., 2009), a conserved residue that is located in the exit channel in close proximity to the T2 copper ion, plays an important role in the protonation process.

Comparison of kinetic parameters using several laccases and several substrates has shown that the reaction rate of laccase correlates well with the redox potential difference between the T1 copper and the

substrate (Xu, 1996). Based on this result, it was suggested that the electron transfer occurs through an outer-sphere mechanism, that is, the electron is transferred through space rather than through a chemical bond. Another similar study, involving velocity measurements in D_2O using a phenolic substrate, confirms that the proton exchange is fast and the rate-determining step is indeed the electron transfer (Tadesse et al., 2008). The electron transfer from the substrate results in a radical cation, which is then deprotonated at a fast rate. However, the redox potential also must be adequately low, appropriate for reducing the substrate, so that the T1 copper is able to abstract the electron from the substrate (Giardina et al., 2010).

1.3. Protein engineering of laccases

Due to the industrial importance of laccases an enormous interest has been put forward to improve their physicochemical properties including redox potential and kinetic parameters using protein engineering. Protein engineering is the discipline dealing with the design of new enzymes or proteins with new or desirable functions. The prospects for protein engineering, such as X-ray crystallography, chemical DNA synthesis, computer modelling of protein structure and folding were discussed and the combination of crystal structure and protein chemistry information with artificial gene synthesis was emphasized as a powerful approach to obtain proteins with desirable properties (Ulmer, 1983). The major goal of protein engineering is the generation of novel molecules, intended as both proteins endowed with new functions by mutagenesis and completely novel molecules.

Diverse techniques of mutagenesis/ screening have been introduced, expanding the possibility of modifying a protein properties. The most classical method in protein engineering is the so-called "rational design" approach which involves "site-directed mutagenesis" of proteins (Arnold, 1993). Site-directed mutagenesis allows introduction of specific amino acids into a target gene. Rational design is an effective approach when the structure and mechanism of the protein of interest are well-known.

In many cases of protein engineering, however, there is limited amount of information on the structure and mechanisms of the protein of interest. Thus, the use of "Directed evolution" that involve

"random mutagenesis and selection" for the desired protein properties was introduced as an alternative approach. Application of random mutagenesis could be an effective method, particularly when there is limited information on protein structure and mechanism. The only requirement here is the availability of a suitable selection scheme that favours the desired protein properties (Arnold, 1993). Directed evolution requires significant screening effort for the analysis of thousands of clones. The availability of reliable screening methods to differentiate the best mutants from the rest is one of the main bottlenecks for evolutionary design.

In recent years, the demonstrated potential of laccases in a range of applications has motivated the progress of laccase engineering efforts. Today, the use of novel computational methods, and cutting-edge directed evolution techniques, supported by the know-how generated during the last two decades on laccase structure–function relationships, can aid implementation of laccases at industrial scale. Moreover, computational simulations can reveal targets for protein engineering to be explored by site-directed mutagenesis (or semi-rational approaches). Some research groups applied computational studies such as molecular docking, molecular dynamics and quantum mechanics/molecular mechanics on multicopper oxidases (MCO) such as laccase.

1.3.1. Rational approach

What makes the MCOs so interesting for a computational bioinorganic chemist? We can conceive at least three reasons. The first is the inherent (in vacuo) instability of many plausible intermediates in the catalytic cycle of MCOs (i.e. the geometrical arrangements of the TNC as a consequence of the four distinct redox states of the three copper ions (i.e. $(Cu^{2+})_3$, $(Cu^+)(Cu^{2+})_2$, $(Cu^{2+})(Cu^+)_2$ and $(Cu^+)_3$) coupled with the various accessible protonation states of the copper ligands originating from water or dioxygen (e.g. oxo, hydroxo and peroxo species) (Rulíšek and Havlas, 2003). Therefore, the TNC site (the Cu ions with their first-sphere ligands) possesses a high positive charge (+3 or +4 according to the suggested reaction mechanism), which is partly compensated for by two carboxylate residues in the second coordination sphere

of the TNC, which are conserved throughout the MCO family (Augustine et al., 2008). The second reason is the complicated electronic structure of the TNC. In the putative structure of the so-called native intermediate, NI, the TNC contains three unpaired spins at the vertices of a triangle, all coupled via an O2 molecule in the centre. This leads to so-called spin-frustration, which means that the exchange coupling between the three pairs of Cu2+ ions cannot be satisfied. In this oxidation state, there are two doublet states and one quartet state close in energy (within a few hundred cm-1) (Lee et al., 2002). The third reason is the unique opportunity to couple the theoretical calculations directly to experimental data and provide their theoretical interpretation (Ryde et al., 2007). In the following sections, we review the computational simulations that have contributed to better understand the protein structure–function determinants.

1.4. Theoretical studies on substrate binding

One of the main issues regarding the oxidation activity of laccases is the interaction between the substrate and the enzyme. The contribution of the residues of the substrate binding pocket to the oxidation capability is clearly indicated by the variety of substrate binding sites and the different kinetic behaviors of laccases with similar redox potentials. Understanding the determinants of substrate affinity and specificity of laccases should be of high priority in laccase engineering, since K_m values for e.g. ABTS vary over at least three orders of magnitude ($\sim$1–1000 μM) among different laccases (Dwivedi et al., 2011).

Interactions of some chemical compounds with the laccase was examined by Prasad and coworkers (2012). The docking analysis showed that the active site always cannot accommodate the dye molecules, due to constricted nature of the active site pocket and steric hindrance of the residues whereas some relatively smaller compounds easily be accommodated into the active site pocket, which, thereafter leads to the productive binding (Prasad et al., 2012).

Moreover, Zhang and coworkers (2012) used molecular docking to analyze the interactions between laccase and substrates. They stated that docking results showed that phenol formed hydrogen bonds and hydrophobic interactions with laccase, whereas Triton X-100 formed hydrophobic interactions with

laccase, which may increase the laccase activity and enhance phenol removal. The non-ionic surfactant Triton X-100 was used as additive to study its effects on the removal of phenol (Zhang et al., 2012). Molecular docking was also employed to explore the binding modes and interactional profiles between laccase and phenol or Triton X-100. Chen et al. (2010) analyzed the integration of ligninolytic enzymes with lignin (a lignin derivate was selected as lignin model substrate) using molecular docking (Chen et al., 2010).

The binding properties of these compounds along with identification of critical active site residues can be used for further site directed mutagenesis experiments in order to identify their role in activity and substrate specificity, ultimately leading to improved mutants for degradation of some toxic compounds such as atrazine (Bastos and Magan, 2009), hydroxyl PCBs (Keum and Li, 2004) and phenols (Udayasoorian and Prabu, 2005).

In a similar study on the structural features of natural laccase B (LacB) from *Trametes* sp. AH28-2 was shown a new structural element, a protruding loop near the substrate-binding site, compared with the previously reported laccase structures. This unique structural feature may be involved in modulation of the substrate recognition of LacB (Ge et al., 2010).

Previous docking studies on laccases have emphasized on steric effects as a key determinant for substrate binding. Thus, using available structures, combining rational/directed evolution and molecular docking was able to decrease K_m for ABTS binding to bacterial CotA (Gupta and Farinas, 2010). Specifically, saturation mutagenesis of 19 amino acids lining the CotA binding pocket produced clones with increased specificity for ABTS over syringaldazine. GOLD (Jones et al., 1997) was previously used to rigidly dock six industrial dyes and three mediators (ABTS, acetosyringone, and syringaldehyde) into a homology model of *Pycnoporus cinnabarinus* laccase (Prasad et al., 2012) based on the 82% identical *Trametes hirsuta* laccase (PDB-ID: 3FPX). In another GOLD study (Suresh et al., 2008), 180 pollutants and 71 known laccase substrates from BRENDA (Schomburg et al., 2002) were docked into the crystal

structures of the *Trametes versicolor* alpha laccase 1GYC (Piontek et al., 2002) and *Bacillus subtilis* CotA (1UVW (Enguita et al., 2003)). The study reproduced the crystal structure complex in the latter case, but did not discuss structural features of the poses.

Christensen and coworkers reported the first comparative study of substrate binding into four different laccases from the same organism, to avoid organism-specific effects, i.e. the four isoforms of TvL, by using a density functional-derived description of radical character on ABTS, constructed homology models of all four proteins, and induced fit docking of ABTS at variable pH and oxidation state of the T1 copper (Christensen and Kepp, 2014). Another study has been done by other group. Their docking analyses revealed significantly higher binding efficiency for lignin model compounds, in proportion to their size, for fungal laccase as compared to that of plant laccase. Residues interacting with the model compounds at the respective enzyme active sites were found to be in conformity with their role in lignin biosynthesis and degradation. Molecular dynamics simulation analyses for the stability of docked complexes of plant and fungal laccases with lignin model compounds revealed that tetrameric lignin model compound remains attached to the active site of fungal laccase throughout the simulation period, while it protrudes outwards from the active site of plant laccase (Awasthi et al., 2015).

1.5. Molecular dynamics

Classical MD simulations were carried out for apo-Tth-MCO and holo-Tth-MCO by Bello and coworkers, in order to shed more light onto compare basic features of the structure and dynamics and how copper coordination affects the protein matrix. Their results showed that loop (b21–b24) D2 has enhanced mobility for holo-Tth-MCO and undergoes a conformational change that enables exposure to the proposed electron-transfer site (open conformation), while for apo-Tth-MCO, this loop prevents access to the electron-transfer site (close conformation), revealing the importance of good coordination among the copper ions and the histidine residues in the regulation of substrate binding. On the other hand, extended MD simulation of the open conformation with the electron-donor molecule docked into the protein cavity,

showed that this conformation is required for the optimal electron transfer and that residues near the cavity play an important role in the process (Bello et al., 2012).

The optimization by directed evolution, of the functional properties of *Pleurotus ostreatus* laccases expressed in yeast has been reported. The mutation results were integrated with a structural analysis of the generated mutants that suggest some of the reasons, at a molecular level, for their enhanced activity. In analysis of mutant an increased mobility of loops forming the reducing substrate binding site has been observed leading to higher accessibility of water molecules to the T1 copper site and possibly leading to an increased activity of the enzyme (Festa et al., 2008).

1.6.   Computation of the redox potential calculation

Many methods to calculate the redox potentials of metal sites in proteins have been developed. A first estimate can be obtained by simply calculating the quantum mechanical (QM) energies of the active-site clusters in a continuum solvent. However, to obtain information on the influence of the surrounding protein, more sophisticated methods are needed (Blumberger and Lamoureux, 2008; Noodleman and Han, 2006; Olsson and Warshel, 2004; Sulpizi et al., 2007). Many groups have estimated and rationalized the redox potentials of Cu-T1 proteins (Casella and Contursi, 2007; Datta et al., 2004; Si and Li, 2009). The main problem with the calculation of absolute redox potentials is that it involves a change of the net charge of the studied system. This leads to very large electrostatic energies and long-range solvation effects (Hummer et al., 1998). For example, the Coulombic interaction between two groups with a unit charge is 93 kJ.mol-1 (0.96 V) at 15 Å (although it is probably screened by a dielectric constant of 4–80) and the Born solvation energy in water of a unit charge is 23 kJ.mol-1 (0.24 V) even for a spherical system of a 30-Å radius. This makes the calculation of the absolute redox potentials a formidable task.

For the MCOs, one can exploit the fact that the electron transfer to the TNC proceeds via the Cu-T1 site. It is therefore sufficient to study this internal electron transfer between the Cu-T1 and the TNC, which involves a transport of an electron by ~13 Å but it does not change the net charge of the simulated system.

Therefore, the calculated energies are expected to be more stable. Moreover, the reduction potential of the Cu-T1 site is experimentally known for many enzymes (Hong et al., 2011) and therefore the absolute redox potential of the TNC can be deduced from the calculated difference in the reduction potentials of the two sites.

The general problem with atomic-scale simulations of enzyme catalysis is that thousands of atoms are involved and chemical bonds are modified. The description of bond breaking or forming calls for fairly accurate quantum mechanical (QM) methods, whereas the huge phase space calls for sampling with a cheaper method like molecular mechanics (MM) or semiempirical QM. The most straightforward way to solve the problem is by sampling phase space using a combined quantum mechanics and molecular mechanics (QM/MM) method where a small subset of atoms are treated by QM and the remaining atoms by MM. This can be pursued either by sampling directly on the Born- Oppenheimer surface or by using a Car-Parrinello approach. The problem is that realistic simulation times are currently limited to a few tens of picoseconds for this approach because of the severe computational load even for small QM systems. This is a rather short simulation time for systems as big as enzymes where many events, besides the reaction catalyzed, occur on time-scales much longer than picoseconds (Benkovic and Hammes-Schiffer, 2003).

Various approaches have been proposed and utilized in the literature to solve the problem of computing accurate QM/MM free energies for chemical reactions in solutions (Bandyopadhyay, 2005; Jorgensen, 1989; Muller and Warshel, 1995) including enzymatic reactions (Ishida and Kato, 2004; Kollman et al., 2001; Olsson and Warshel, 2004). A basic idea is to use a fast but less accurate method to sample phase space and use this sampling to estimate high-level QM/MM free energies with a modest number of QM/MM calculations. Below we give a summary of methods based on this idea.

In the quantum mechanical free energy (QM-FE) approach by Jorgensen and co-workers (1989), a reaction pathway for atoms in the QM region is calculated in a vacuum. Free energies for the interaction between the QM and MM atoms are then calculated along the reaction pathway by performing MM free

energy perturbation or thermodynamic integration calculations where electrostatic interactions between the QM and MM atoms are defined via point charge interactions. In the treatment by Jorgensen and co-workers, and later by Kollman and co-workers (1998), point charges to represent the QM atoms were derived from calculations in a vacuum, i.e., without an MM region. Jorgensen and co-workers used the method to study organic reactions in solution, and Kollman and co-workers extended the method to that of enzymatic reactions, namely amide hydrolysis in trypsin (Stanton et al., 1998) and methyl transfer by catechol *O*-methyltransferase (Kuhn and Kollman, 2000).

Yang and co-workers applied their QM/MM free energy method (QM/MM-FE) to the enzymes triosephosphate isomerase (Zhang et al., 1999), enolase (Liu et al., 2000) and 4-oxalocrotonate tautomerase (Cisneros et al., 2003). The QM/MM-FE method is an improvement over the QMFE method in that a QM/MM optimized reaction pathway and QM energies and point charges derived from QM/MM calculations are used. In this way, polarization of the QM region by the MM region is included. Ishida and Kato employed the same approach to study acylation by serine proteases (Ishida and Kato, 2004).

An alternative approach is the ab initio QM/MM approach (QM(ai)/MM) by Warshel and co-workers (Olsson and Warshel, 2004; Villà et al., 2000). They sampled phase space by performing molecular dynamics (MD) simulations with a reference potential given by the empirical valence bond (EVB) method (Warshel and Weiss, 1980). Umbrella sampling ensured that the entire reaction pathway was sampled and made it possible to calculate the potential of mean force (PMF). Free energy changes between the system described by the reference potential and by density functional theory were calculated with free energy perturbation, and in this way a high-level QM/MM PMF can be obtained. The methodology corresponds to using the thermodynamic cycle in Figure 1.3. (With MM replaced by EVB) and is in principle exact with respect to how the free energy changes are calculated. In practice, the free energy did not converge owing to large fluctuations of the difference between the reference potential and the high-level QM/MM potential, although electrostatic interactions converged. Therefore, Warshel and co-workers used more approximate

methods to calculate the free energy difference between the system described by EVB and by a high-level QM/MM method (Olsson and Warshel, 2004; Štrajbl et al., 2002).
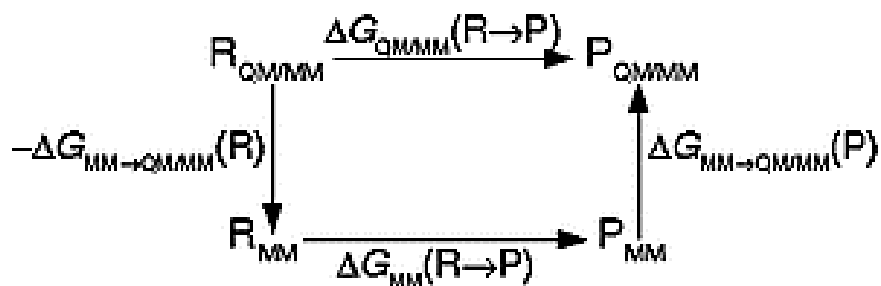
Figure.1.3. Illustration of the QTCP method, where a thermodynamic cycle is employed to calculate QM/MM free energy changes.

Like Warshel and co-workers, Wood and co-workers use free energy perturbation in their ab initio/classical free energy perturbation (ABC-FEP) approach, which was used to compute hydration energies of water and the Na+ and Cl⁻ ions at different physical conditions (Liu et al., 2003; Sakane et al., 2000). In this approach, only solute-solvent interaction energies are perturbed to the QM level. They also studied solute-solvent structural properties as well as water dimer dissociation (Wood et al., 2002). Schofield and co-workers (2000) and Bandyopadhyay (2005) have developed a similar approach termed the molecular mechanics importance based function (MMBIF) method. They also use a MM reference potential to sample the phase space and calculate corresponding high-level QM/MM energies for a set of configurations (Bandyopadhyay, 2005; Iftimie et al., 2000). Based on the two sets of energies, they use a Metropolis-Hastings algorithm to generate a high level QM/MM canonical ensemble from which QM/MM free energies can be calculated.

Unfortunately, the calculated relative redox potentials are sensitive to details in the theoretical treatment (owing to the transfer of a unit charge by ~13 Å). Some researchers have calculated the same difference in the redox potentials with several other methods (Hu et al., 2011). For example, the redox potential difference decreases by 20 kJ.mol⁻¹ if it is calculated by electrostatic embedding rather than mechanical embedding in the QM/MM calculations (i.e. if the electrostatic interactions between the QM and MM systems are calculated by QM rather than by MM). A similar change was observed if the DFT

method was varied, whereas the basis-set effects are ~10 kJ.mol^{-1}. If isolated models of the two Cu sites in a dielectric continuum are used, energy differences of 28–154 kJ.mol^{-1} can be obtained depending on the dielectric constant of the continuum (4–80), showing that such an approach is very unreliable. Standard QM/MM calculations provide an energy difference of ~40 kJ.mol^{-1} with electrostatic embedding but 72–106 kJ.mol^{-1} with mechanical embedding. When these were supplemented with a continuum solvation model of the solvent surrounding the protein using the QM/MM-PBSA approach (Kaukonen et al., 2008) (with mechanical embedding), the energy was somewhat stabilised at 111–120 kJ.mol^{-1}.

Finally, Ryde and co-workers tried also QM/MM free-energy perturbations using the QTCP (QM/MM thermodynamic cycle perturbation) approach . It allows for full flexibility of the protein, except that the two Cu sites are fixed at the QM/MM structures. Interestingly, it yielded an energy difference of ~45 kJ.mol^{-1}. Approximately 10 kJ.mol^{-1} of the difference between the QTCP and MD results comes from differences in the treatment of the long-range electrostatic effects (i.e. solvation outside the ~55 Å radius of the explicitly simulated system; the MD simulations use particle-mesh Ewald summation, whereas the QTCP calculations use the Onsager relation). The rest comes from differences in the geometries in the sampled snapshots. This may indicate that the MM force field of the Cu centres is not accurate enough to extract reliable QM energy differences. On the other hand, the Cu sites have fixed geometries in the QTCP calculations, which is also a somewhat questionable approximation. This shows that it is hard to calculate relative redox potentials to an accuracy better than ~25 kJ.mol^{-1} (0.3 V). On the other hand, it is likely that the differences in the reduction potentials between various states of the TNC site are more accurate (Rulíšek and Ryde, 2013).

In summary, the results show that it is hard to calculate accurate reduction potentials. Several research groups have tried to estimate the reduction potential of various groups in solution and in proteins, involving both metal sites and other redox-active cofactors (Kamerlin et al., 2009; Mehta and Datta, 2007; Olsson and Warshel, 2004; Sulpizi et al., 2007). Again, the active site can either be studied by QM methods (to obtain absolute reduction potentials), or by MM or continuum-solvation methods to study how the protein

modifies the potential of a bound group, or how the potential varies in different proteins or mutants. However, it is still a major effort to estimate acidity constants or reduction potentials in proteins by theoretical methods, especially for metal sites.

1.7.   Directed evolution studies

For most of us, directed evolution represents an elegant shortcut to tailor enzymes with improved features. By mimicking the Darwinist algorithm of natural selection through iterative steps of random mutagenesis and/or DNA recombination, the temporal scale of evolution can be collapsed from millions of years into months rather than weeks of bench work (Romero and Arnold, 2009; Tracewell and Arnold, 2009). In general, it is important to bear in mind three essential aspects when performing laboratory evolution experiments:

i) It is necessary to have a reliable and sensitive screening assay to identify the small improvements obtained in each round of evolution, generally 2 to 10-fold improvements per evolutive cycle. In the last years, colorimetric high-throughput screening assays specifically designed for laccase evolution have emerged. All these assays are based on known natural or surrogate substrates of different chemical nature and complexity (from phenols to recalcitrant compounds: ABTS, 2,6 dimethoxy phenol, syringaldazine, iodide, anthracene, or Poly R478 have been used to screen mutant libraries (Alcalde et al., 2006; Maté et al., 2010; Zumárraga et al., 2007). Depending on the approach, the screening assays can be combined in an attempt to enhance several features at once (e.g. activity and stability (García-Ruiz et al., 2010) or to avoid the laccase becoming dependent of one specific substrate during evolution (Cañas and Camarero, 2010).

ii) Diversity should be generated by random mutagenesis and in vivo or in vitro DNA recombination protocols (Alcalde, 2010). Other approaches such as circular permutation, combinatorial saturation mutagenesis and the combination of rational design with directed evolution are also frequently included in the evolutionary strategy, generally yielding good results (Arnold, 2006; Zumarraga et al., 2008b).

iii) It must be possible to functionally express the genetic products with the desired traits. Although Escherichia coli is the preferred host organism for directed evolution experiments, the broad differences between the eukaryotic expression system of fungal laccases and that of bacteria (codon usage, missing chaperones, post-translational modifications such as glycosylation or the formation of disulphide bridges, and copper uptake) are shortcomings that are not easily overcome. In fact, all attempts to functionally express fungal laccases in bacteria have resulted in misfolding and the formation of inclusion bodies. Alternatively, the secretory machinery of *Saccharomyces cerevisiae* permits post-translational modifications, and it is also an excellent host to carry out laboratory evolution experiments (Bulter et al., 2003).

Directed molecular evolution is a powerful protein engineering tool to improve the known features of enzymes or to generate novel activities that are not required in natural environments (Bloom et al., 2006; Tao and Cornish, 2002). Through this methodology, the scientist recreates the key events of natural evolution in a laboratory environment (mutation, DNA-recombination and selection), thereby making it possible to design interesting and technologically useful enzymes. In the framework of protein engineering, saturation mutagenesis has long been used to carry out semirational studies (Chica et al., 2005) since this approach involves the mutation of any single amino acid codon to all the other codons that will generate the 20 naturally occurring amino acids. This technique is commonly employed to improve the characteristics of enzymes at "hot-spot" residues already identified by conventional random mutagenesis.

In addition, it can be employed to simultaneously mutate several codons (combinatorial saturation mutagenesis, CSM), which will enable all possible combinations of interesting residues to be evaluated in order to identify their optimal interactions and synergies (Zumarraga et al., 2008b). CSM is typically carried out by laborious in vitro protocols that are based on several consecutive PCR reactions and an additional ligation step with the vector in order to clone the whole mutagenized fragment (Fig. 1.4) (Alcalde et al., 2006). The exchange of genetic material by recombination occurs in all living organisms and it is the main process that generates diversity in the evolution of species. The eukaryotic machinery of *S. cerevisiae* offers
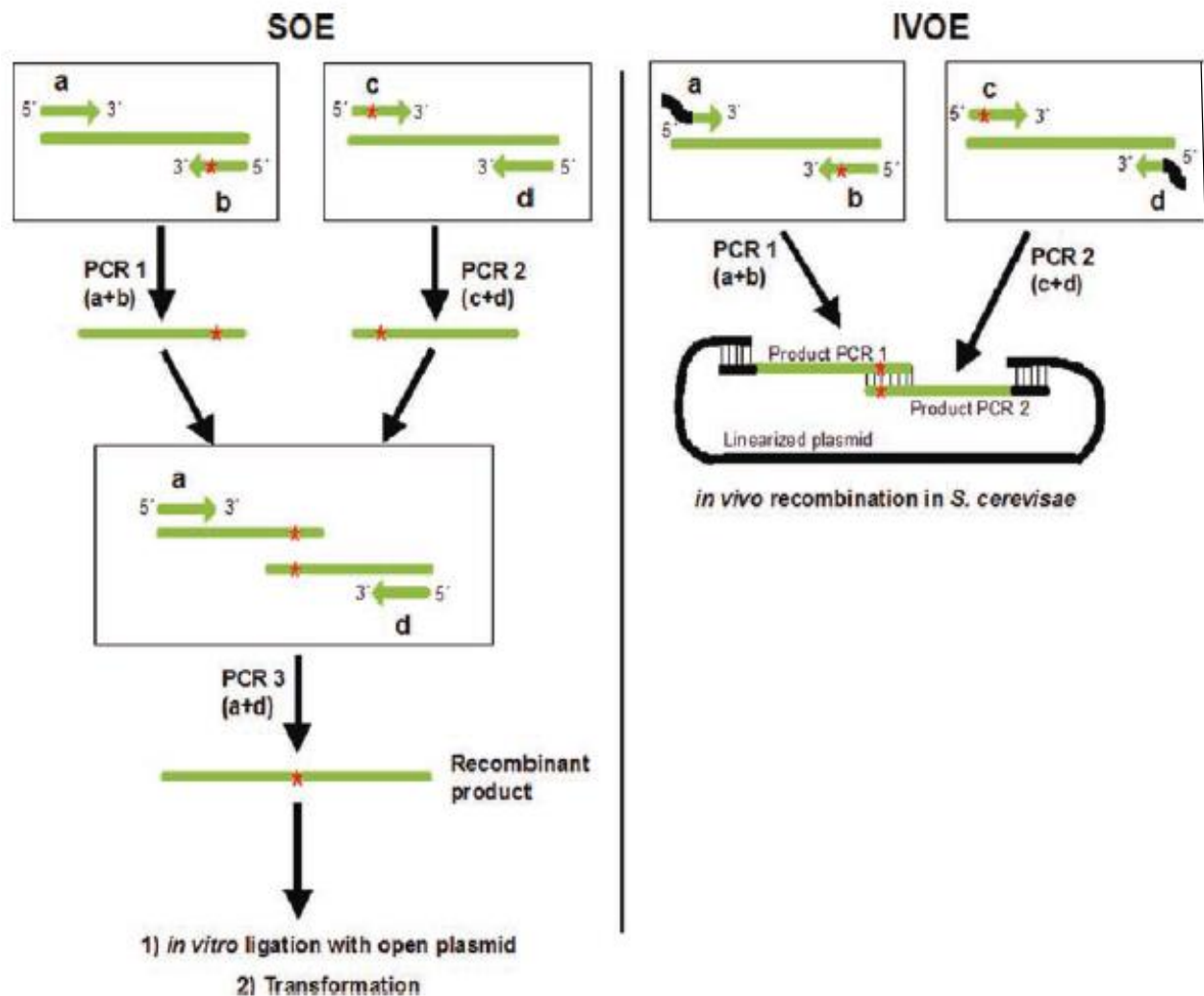
Figure 1.4. Schematic of SOE and IVOE. Sequence splicing by SOE is a mutagenic method that recombines DNA sequences containing mutations through several consecutive PCR reactions. This method requires an additional in vitro ligation step in order to clone the whole fragment within the vector. As an alternative, IVOE eliminates one PCR step and the ligation in vitro with the linearized plasmid. Accordingly, it takes advantage of the eukaryotic apparatus of *S. cerevisiae* and thus, it is necessary to design mutagenized primers with suitable overhangs (Alcalde et al., 2006).

an array of possibilities to construct mutant libraries or to recombine ("shuffle") DNA fragments. Unlike other heterologous hosts used for directed evolution, the high frequency of homologous recombination in *S. cerevisiae* favors its use to clone eukaryotic proteins and in new in vivo protocols aimed at generating diversity (Zumárraga et al., 2008b).

One of the first directed evolution experiments using *in vivo* DNA shuffling was carried out to engineer a low redox potential peroxidase from *Coprinus cinnereus* with oxidative stability (Cherry et al., 1999). This pioneering work opened an array of possibilities that led to many research groups beginning to develop new strategies of DNA recombination (Bulter et al., 2003; Cusano et al., 2009). Taking advantage of yeast physiology, Alcalde and his group have designed several *in vivo* DNA recombination methods (IVOE (*In Vivo Overlap Extension*), IvAM (*In vivo Assembly of Mutant* libraries)) with the aim of generating suitable crossover events or varying the mutational bias in the framework of *in vitro* laccase evolution (Figure 1.5).
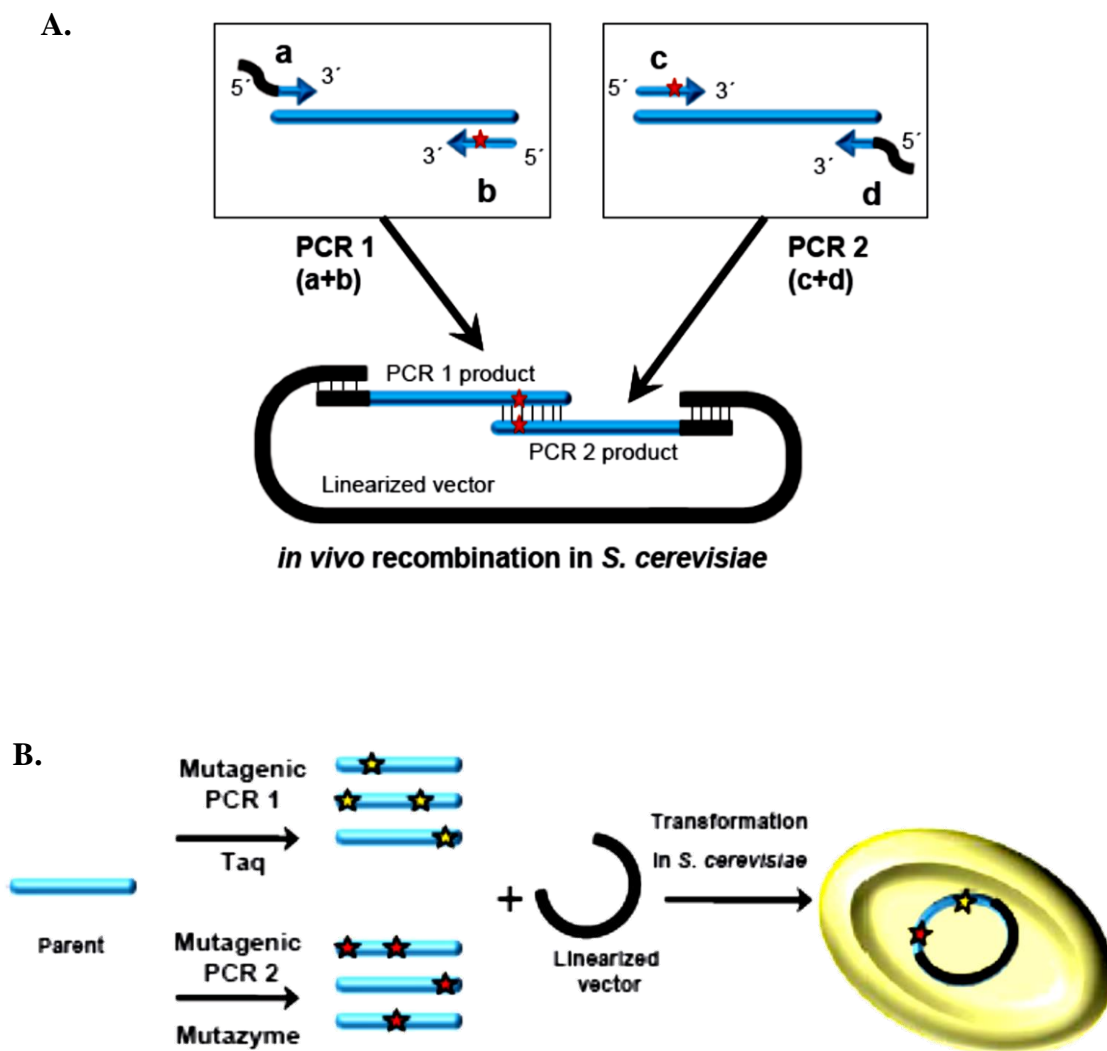
Figure 1.5. Different *in vivo* DNA recombination strategies based on the *S. cerevisiae* apparatus. **A**) IVOE; **B**) IvAM (Maté et al., 2011).

Sequence splicing by IVOE is a robust and reliable method through which combinatorial saturation mutagenesis, deletion and/or insertion mutagenesis, site-directed recombination or site directed mutagenesis can be accomplished straightforwardly (Alcalde, 2010; Alcalde et al., 2006). The method is based on the engineering of mutagenized primers that contain suitable overhangs, with homologous regions that anneal to each other to generate an autonomously replicating vector containing the mutant gene/s. This strategy mimics the classical SOE (*Sequence Overlap Extension*) but it removes several steps, including the *in vitro* cloning. IVOE has been employed to construct mutant libraries for directed evolution of ascomycete and basidiomycete laccases, as well as to carry out semi-rational studies (*i.e.* combinatorial saturation mutagenesis coupled to high-throughput screenings (Zumarraga et al., 2008b).

IvAM is another approach that has been successfully used to engineer fungal laccases for improved organic co-solvent tolerance (Zumárraga et al., 2008b). Generally, error-prone PCR methods are unsatisfactory because they are associated with a limited and predicted mutational spectrum derived from the intrinsic bias of each DNA-polymerase. To overcome this problem, the mutation biases of different polymerases can be combined by alternating between them in successive rounds of evolution. IvAM has allowed us to explore the laccase sequence space through the *in vivo* DNA shuffling of several mutant libraries with different mutational spectra in a single round of evolution.

It is also possible to bring together strategies for *in vitro* and *in vivo* DNA recombination to evolve enzymes in the laboratory. For example, CLERY (*Combinatorial Libraries Enhanced by Recombination in Yeast*) combines *in vitro* and *in vivo* DNA shuffling (Abécassis et al., 2000). In a similar approach, Alcalde and coworkers have combined mutagenic StEP (*Staggered Extension Process*) with *in vivo* DNA shuffling to evolve ligninolytic peroxidases. There is also an interesting report on how to engineer chimeric fungal laccases from *Trametes* C30 by *in vivo* DNA shuffling (Cusano et al., 2009), where a low redox potential laccase gene was used in all the chimeric libraries to guarantee functional expression. This example constitutes a valuable point of departure for the potential application of the *S. cerevisiae* machinery for laccase chimeragenesis.

The first laccase gene subjected to directed evolution was the *Myceliophthora thermophila* laccase (MtL), a low medium redox potential ascomycete laccase that is very thermostable (with T50 values ~75.6ºC) (Bulter et al., 2003). In this work, 10 rounds of laboratory evolution were carried out to achieve the strongest functional expression of a laccase in *S. cerevisiae* yet reported (up to 18 mg/L). The basic tools for the generation of diversity included error prone PCR, StEP and *in vivo* DNA shuffling. The latter was modified in such a manner that error-prone PCR products were recombined *in vivo* to introduce new mutations in conjunction with recombination.

Furthermore, backcrossing recombination was employed to eliminate neutral mutations. In the final rounds of evolution, PCR and *in vivo* gap repair were used to recombine neighbouring mutations in a site-directed fashion, once again taking advantage of the eukaryotic apparatus (referred to as *in vivo* assembly recombination) which proved extremely useful to eliminate some deleterious mutations. The sequence targeted for directed evolution included the native pre-proleader, as well as the C-terminal tail of the gene that encode for parts of the protein that are cleaved during maturation. The ultimate evolutionary product obtained after screening over 20,000 clones, the T2 mutant, harboured 14 mutations. Using combinatorial saturation mutagenesis through IVOE, a direct relationship between the C-terminal plug and a conserved tripeptide in the vicinity of the reducing substrate binding site was determined (Zumarraga et al., 2008a).

The past successes with MtL evolution cannot easily be translated to their high redox potential laccase (HRPL) counterparts, in part because MtL is an ascomycete laccase that facilitates its functional expression in *S. cerevisiae*. Several directed evolution experiments have been attempted by error prone PCR using HRPLs from *Pleurotus ostreatus* (Festa et al., 2008; Miele et al., 2010). The results confirmed a general improvement in the total activity but poor secretion limits their practical engineering for other purposes. Alcalde and his coworkers recently described for the first time how to engineer HRPLs that can be expressed strongly by *S. cerevisiae*, enhancing their activities and thermostabilities. Two different HRPLs were used to achieve this goal, the laccase from basidiomycete PM1 (Maté et al., 2010) and the laccase from *Pycnoporus cinnabarinus* (PcL) (Cañas and Camarero, 2010). The ultimate variant obtained through

this evolutionary process, the OB-1 mutant, was readily secreted by *S. cerevisiae* (up to 8 mg/L) in a soluble, very active and very stable form, particularly with respect to temperature (with a T_{50} value of 73ºC), pH and co-solvents.

Among the strategies engineered to evolve HRPLs, the mutational exchange and the recovery of beneficial mutants should be highlighted. With mutational exchange, several mutations found in both evolutionary programmes (for the α-PM1 and the α-PcL) were switched from one system to another, taking advantage of their close sequence homology (above 75 %). Interestingly, some mutations found in the hydrophobic core of the α-factor preleader were valuable in both systems, which opens the possibility of evolving the α-factor prepro-leader as a universal signal peptide for the heterologous expression of fungal laccases in yeast. With mutational recovery, some beneficial mutations ruled out by the yeast recombination apparatus could be recovered by site-directed mutagenesis of OB-1 having mapped them first in the family tree of the whole evolution experiment (Maté et al., 2010).

1.8.   Structure-activity studies

The role of the axial ligand in tuning the redox potential of the T1 Cu centers has been extensively discussed due to the striking differences found among the different blue copper proteins (Table 1.1). On one end, there is stellacyanin, a single blue copper protein with a redox potential (E^0) as low as +184 mV, which holds a Gln residue as axial ligand. On the other end, fungal laccases, ceruloplasmins and ferroxidases, all holding a Leu or Phe residue, have redox potentials roughly between +500 and +800 mV. However, the small blue copper protein rusticyanin, with a redox potential over +600 mV, shows a Met as axial ligand of the T1 Cu center. When the axial Met was replaced by Leu, the redox potential of rusticyanin raised +100 mV, while it decreased by a similar amount if Met was replaced by Gln (Hall et al., 1999).

The hydrophobicity of the axial ligand seems to correlate with the redox potential of the T1 Cu site in laccases (Durão et al., 2006), so that it might be considered as a rough indicator of their redox potential (Mot and Silaghi-Dumitrescu, 2012). Laccases from plants (e.g., *Rhus vernicifera*) and bacteria (e.g., CotA

laccase from *B. subtilis* or SLAC), with a Met as axial ligand, show the lowest redox potentials (below +500 mV). Middle-potential laccases (up to +700 mV) mainly comprise ascomycete laccases and in general, with the exception of some basidiomycete laccases, have a Leu as non- coordinating axial ligand. Finally, high-redox potential laccases from basidiomycete fungi, with E^0 and +790 mV, commonly have a Phe residue in this position.

Laccase	Sequence alignment												E^0 (V)
StL	^{506}H	C	H	I	A	W	H	V	S	G	G	L^{517}	0.51
MtL	^{502}H	C	H	I	A	W	H	V	S	G	G	L^{513}	0.47
RsL	^{459}H	C	H	I	D	W	H	L	E	A	G	L^{470}	0.71
TvL	^{452}H	C	H	I	D	F	H	L	E	A	G	F^{463}	0.78
PvL	^{451}H	C	H	I	D	F	H	L	E	A	G	F^{462}	0.79
zAO	^{506}H	C	H	I	E	P	H	L	H	M	G	M^{517}	0.34

Table 1.1. Alignment of different laccase sequences. Last raw shows the axial ligand in different structure (Xu et al., 1998).

First site-directed mutagenesis studies on fungal laccases showed the exchangeable contribution to T1 Cu E° of Phe and Leu as non-coordinating axial ligands. The replacement of the non-coordinating axial Leu ligand by Phe in *Rhizoctonia solani* (E° = 710 mV) and *Myceliophthora thermophila* laccases (E° = 470 mV) did not produce a significant increase in their redox potentials nor in the kinetics of the reaction (Xu et al., 1998). Likewise, no significant alteration of *Trametes villosa* laccase properties was observed by changing the non-coordinating Phe axial ligand by Leu. By contrast, Phe replacement to Met resulted in 100 mV redox potential decrease, distorted EPR spectrum, and modified optimum pH and kinetic constants during oxidation of phenolic substrates (Xu et al., 1999). These effects were attributed to a perturbation of the geometry of T1 site. Accordingly, the electric state of the T1 Cu center of the MCO CueO from *E. coli* became similar to those of fungal laccases by changing the Met axial ligand to Leu, obtaining also significant increase of the redox potential (Miura et al., 2009). Substitution of the axial Met with Leu or Phe in *B. subtilis* CotA laccase increased the redox potential by 100 mV, attributed to the weakening in the T1 Cu coordination (Xu et al., 1998), but at the same time, a major drop of the enzyme activity was observed

because the electron transfer between T1 Cu and the TNC became unfavorable (Sakurai and Kataoka, 2007). Interestingly, the Phe mutant laccase underwent an intense drop of thermodynamic stability due to the loss of copper from the T1 site, indicating that copper depletion is a key event in the inactivation of the enzyme (Durão et al., 2006).

Significant perturbation of the electronic structure of *M. thermophila* laccase T1 Cu site was obtained by changing the non-coordinating axial Leu to His. The tetragonal distortion of the T1 site led to a σ overlap between the Cu and Cys(S) orbitals and to the green color of the His variant. The increased charge donation of the axial His coupled with the tetragonal distortion of the T1 site stabilized the oxidized state, hence lowering the redox potential (by 30 mV) and the reactivity of this site (tenfold decrease of k_{cat} respecting the blue wild-type laccase) (Palmer et al., 2003). Directed mutagenesis of the axial Met ligand to His in another MCO, namely bilirubin oxidase, caused the loss of copper and the lack of activity. When the Met ligand was changed to Gln, a coordinating residue not naturally found in MCOs (Sakurai and Kataoka, 2007), T1 Cu parameters resembled those of single-copper stellacyanin, accompanied by a remarkable drop in the enzymatic activity and a ~ 200 mV decrease in the redox potential (Kataoka et al., 2005).

Moreover, along with its redox features, steric hindrance of the substrate largely affects the oxidation proficiency of laccases, as recently demonstrated by Tadesse and coworkers, in *T. villosa* and *Myceliophthora thermophila* laccases, two enzymes markedly differing in redox potential (0.79 and 0.46 V) (Tadesse et al., 2008). The distance between two phenylalanine residues (Phe332 and 265 in TvL1KYA) that mark the entrance to the active site can represent the structural threshold for oxidation of substrates with a compatible redox potential.

In the structure of the laccase from *T. trogii* (2HRG), Matera and coworkers (2008) have suggested that the occurrence of two hydrophobic residues Phe460 and Ile452 in the near surroundings of the Cu1 contributes to the high redox potential observed. Furthermore, residue Phe460 is additionally surrounded by a large number of hydrophobic residues that would also contribute to increasing the redox potential of the Cu1 (Matera et al., 2008).

In addition, the redox potential of laccases is known to be modulated by different factors associated to environment surrounding the T1 Cu. Other residues important for modulating the type 1 copper reduction potential have been identified following site directed mutagenesis and comparison of crystal structures (Kallio et al., 2011; Liu et al., 2011). Thus, the number of residues surrounding the copper ion affects it in such a way that, the lower the coordination of Cu^{2+}, the higher its redox potential is found. Moreover, distortions on the geometry of the copper coordination shell can modify the redox potential, as well as the hydrophobicity of the residues surrounding the copper ion. Finally, the electrostatic field produced by the rest of residues in the protein affects the redox potential and finally, the number of hydrogen bonds of different residues with the sulfur atom of the Cys453 side chain has also found to modulate it (Battistuzzi et al., 1999; Machczynski et al., 2004).

Simulation studies corroborated the crucial role of the axial ligand in defining the chemistry and redox potential of T1 site. QM calculations of six T1 Cu sites (cucumber stellacyanin, *Pseudomonas aeruginosa* azurin, poplar plastocyanin, *Coprinus cinereus* laccase, *Thiobacillus ferrooxidans* rusticyanin, and human ceruloplasmin) confirmed that the low redox potential of stellacyanin was mainly due to the Gln ligand at the axial position, whereas the presence of a non-coordinating hydrophobic residue contributes significantly to the increased redox potentials in *C. cinereus* laccase and human ceruloplasmin (Li et al., 2004). QM/MM and MD simulations data from *T. versicolor* laccase, CueO, CotA and SLAC also correlated at least in part the redox potentials with the hydrophobicity of the T1Cu axial ligand (Hong et al., 2011).

The redox potential of T1 Cu centers is, however, tuned by other factors. One of them, is the T1 Cu-His ligand distance. The longation of the Cu-His (Nd) bond would account for a more electron-deficient copper and, consequently, for the observed higher redox potential in *T. versicolor* laccase as compared to *C. cinereus* laccase (Figure 1.6) (Piontek et al., 2002). Data from the crystal structure of *Rigidosporus lignosus* laccase (Garavaglia et al., 2004) and MD simulations with CotA and SLAC (Hong et al., 2011) were mostly consistent with this hypothesis. However, although the protein fold could, in principle, modulate the T1 Cu redox potential by dictating the positions and orientations of the Cu ligands and

adjusting the coordination bond strengths (Li et al., 2004), overall, the relative changes in the Cu-ligand distances within the rigid His (Nd)-Cys(S)-His(Nd) environment can be assumed small, having a minimal effect on the T1 Cu redox potential for laccases. Conversely, the redox potential in MCOs is also influenced by the solvent accessibility, dipole orientation and H-bonding outside the T1 Cu coordinating sphere. T1 Cu redox potential would increase with N backbone (H)-Cys(S) H-bonding, whereas backbone dipoles would increase the redox potential and dipoles between side-chain and solvent decrease it (Hong et al., 2011).
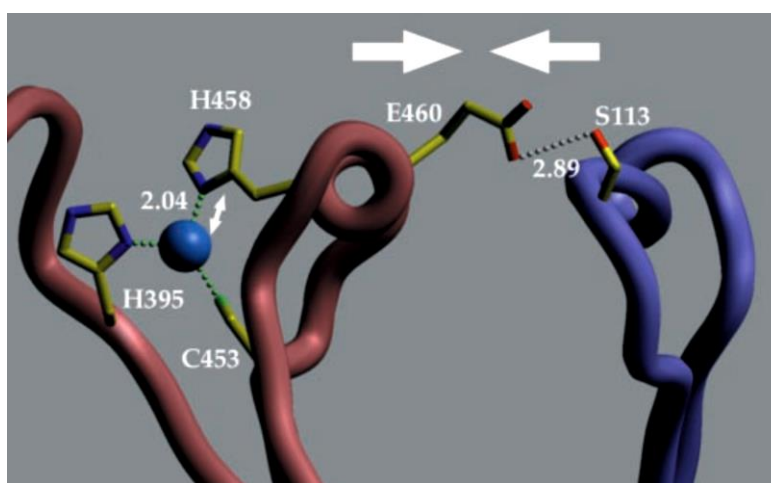
Figure 1.6. Schematic drawing illustrating the movement of a helical segment in TvL. Upon formation of a hydrogen bond between Glu-460 and Ser-113, a movement of the helical segment carrying His-458 could result, which would subsequently cause an elongation of the Cu1-N (His-458) bond at the T1 site (Piontek et al., 2002).

Desolvation effects, protein constraints, metal-ligand, metal-dipole and metal-ion interactions have been proposed to explain the reduction potential modulations. However, the quantitative details of the protein modulations on metal ion reduction potentials have not been fully elucidated (Li et al., 2004). Since the T1 center acts as ''electron gate'' for oxygen reduction, these differences in E° strongly affect the catalytic properties of these enzymes. In particular, a high E° value increases the range of oxidizable substrates and improves the effectiveness and versatility of the enzyme. Indeed, the catalytic efficiency (k_{cat}/K_m) of laccases increases with the E° value of their T1 sites (Shleev et al., 2005). Despite recent

advancements, the understanding of the molecular determinants of the redox potential of the T1 sites in laccases is still not complete and requires further investigation.

Residues that line the substrate binding pocket outside the coordination sphere also influence the reduction potential (Kallio et al., 2009). A Glu-Thr mutation slightly raised the type 1 potential in the heterologously expressed low-potential laccase from *Melanocarpus. albomyces* without a significant change in catalytic activity as measured by ABTS (Rodgers et al., 2010).

Overall, the analysis of possible factors modulating the E° of T1 in different fungal laccases suggests that the value of the E° is actually controlled by several factors. Some of these are dependent on the nature of the coordination ligands of T1, but others can be ascribed to the hydrophobic residues, the nature of the second sphere residues influencing solvent accessibility, hydrogen bind number, dielectric anisotropy around the site, stacking and electrostatic interactions not necessary directly interacting with the copper metal.

2. OBJECTIVES

According to the review described in the previous chapter, there are still some hurdles to overcome and some questions that should be answered: why is the functional expression of laccases in yeast so tremendously difficult? Would it be possible to evolve high-redox potential laccases in bacteria? Is it feasible to enhance the laccase redox potential beyond natural limits by directed evolution or by rational means without disturbing its stability?…and more significantly, would that improvement necessarily mean better activity? We hope that in the near future, new HRPLs engineered by directed evolution and rational approaches can affront the attractive challenges presented by traditional and modern biocatalysis.

One of the goals of this thesis is to characterize the binding pocket of diverse laccases and describe the mechanism of oxidation of substrate in laccase active site. For this purpose we have used three laccase structures with diverse redox potential values, including a high redox potential (HRPL), a low redox potential (LRPL) and one bacterial laccase, to study the differences in active site of this enzyme.

For industrial use of laccase, the current challenge is to obtain improved laccases with desirable physicochemical characteristics such as a higher redox potential. The present study is also aimed at applying a computational method that permits the calculation of the redox potential by taking into account the different residues in binding pocket environment in order to suggest possible mutations. Then, we employed site directed mutagenesis techniques to investigate those mutations effect in biochemical characteristics of laccase and redox potential value.

In order to achieve these main objectives, some activities can be followed up:

1- To study interaction between binding site and different substrates or mediators by computational docking tools

2- To compare different structures of laccase

3- To apply a computational method for calculating redox potential value of laccase

4- To propose mutations that impact on redox potential value

5- To apply site directed mutagenesis techniques to analysis the mutations

6- To characterize biochemical features of those mutants and compare them with parental type

3. MATERIAL AND METHODS

I.   Simulations and computational methodology

3.1. Molecular docking

Molecular docking is a method used to predict the preferred orientation of one molecule to a second when bound to each other to form a stable complex, in other words the protein–ligand complex. By means of docking it is possible to identify the residues that are directly involved in binding and to reveal the nature of the interface itself. Docking studies have been carried out to get insights about the molecular factors affecting the holding of substrate.

Two approaches can be used to carry out molecular docking studies. One approach uses a matching technique that describes the protein and the ligand as complementary surfaces. Whereas, the second approach simulates the actual docking process in which the ligand-protein pairwise interaction energies are calculated using a scoring function.

There are several docking programs available like GOLD, Autodock, MOE or Glide. In the present study we have used GOLD software [Genetic Optimization for Ligand Docking] (Jones et al., 1997, 1995) and the MOE docking program (MOE 2013.08, Chemical computing group lnc., 1010 Sherbooke St. West, Suite #910, QC, Canada.) among others.

In GOLD the score function was used as scoring function to rank different binding modes. This is a molecular mechanics–like function that includes four terms that account for the protein–ligand hydrogen-bonds, protein-ligand van der Waals interactions, intramolecular hydrogen bonds in the ligand and contribution due to intramolecular strain in the ligand. In GOLD a scoring function to rank different binding modes; the GOLD score function is a molecular mechanics–like function with four terms

$$\text{GOLD Fitness} = \text{Shb\_ext} + \text{Svdw\_ext} + \text{Shb\_int} + \text{Svdw\_int}, \qquad \text{Eqn(1)}$$

Where Shb_ext is the protein–ligand hydrogen-bond score and Svdw_ext is the protein-ligand van der Waals score. Shb_int is the contribution to the Fitness due to intramolecular hydrogen bonds in the ligand; this term is switched off in all calculations presented in this work (this is the GOLD default, and generally gives the best results); Svdw_int is the contribution due to intramolecular strain in the ligand.

The docking process using the MOE program was performed in several steps (Figure 3.2). First, each ligand poses can be used to rescore and to refine poses. Additionally, the knowledge of pharmacophore was introduced to constrain the poses. The Alpha Triangle placement which derives poses by random superposition of ligand atom triplets alpha sphere dummies in the receptor site is to determine the poses. The London dG scoring function estimates the free energy of binding of the ligand from a given pose. The functional form is a sum of terms:

$$\Delta G = c + E_{flex} + \underset{h\text{-bonds}}{\Sigma} C_{HB}\ f_{HB} + \underset{m\text{-lig}}{\Sigma} C_M\ f_M + \underset{atom\ i}{\Sigma} \Delta P_i \quad \text{Eqn(2)}$$

Where

c = the average gain/loss of rotational and translational motion.

E_{flex} = the energy due to loss of flexibility of the ligand.

C_{HB} = an hydrogen bond energy

f_{HB} = measures geometric imperfections of hydrogen bonds

C_M = a metal ligation energy

f_M = measures geometric imperfections of metal ligations

D_i = the desolvation energy of each atom i

Docking application in MOE program consists of several steps (Figure 3.1). Each ligand poses can be used to rescore and to refine poses. Additionally, the knowledge of pharmacophore was introduced to

constrain the poses. In MOE the London dG scoring function was used to rank order the different poses generated.

3.2. Molecular dynamics

Besides of molecular docking, the state-of-the-art computational method for obtaining structural and dynamical information about proteins relevant for understanding these issues is molecular dynamics (MD). The aim of computer simulations of molecular systems is to compute macroscopic behavior from microscopic interactions. The main contributions a microscopic consideration can offer are (1) the understanding and (2) interpretation of experimental results, (3) semiquantitative estimates of experimental results, and (4) the capability to interpolate or extrapolate experimental data into regions that are only difficultly accessible in the laboratory.

Some of the typical applications of MD simulations include: characterization of the structural dynamics of proteins, protein function prediction, protein folding and unfolding studies, to study the role of solvents in protein dynamics, validating and improving, molecular mechanics force fields, determination and validation of structures from experimental methods, drug design and development, to gain insights into biological phenomena, occurring at molecular and supra molecular level to cellular level. The equations of motion can only be solved numerically for a multi-body problem. To calculate the dynamics of the system (*i.e.* the position of each atom as a function of time), Newton's classical equations of motion are solved for each atom given an empirical force field:

$$F_i = m_i \, a_i = m_i \, d^2 r_i \, / \, dr^2 \quad \text{Eqn(3)}$$

The force on each atom is the negative of the derivative of the potential energy with respect to the position of the atom:

$$F_i = - \frac{\partial V}{\partial r_i} \qquad \text{Eqn(4)}$$

Once the coordinates of the atoms of a starting structure and their velocities are defined, the force acting on each atom can be calculated for each point in time t + dt and a new set of coordinates can be generated. The repetition of this procedure generates a molecular trajectory corresponding to the time-dependent fluctuations of the atomic positions. The accuracy of the simulations is directly related to the potential energy function that is used to describe the interactions between particles.
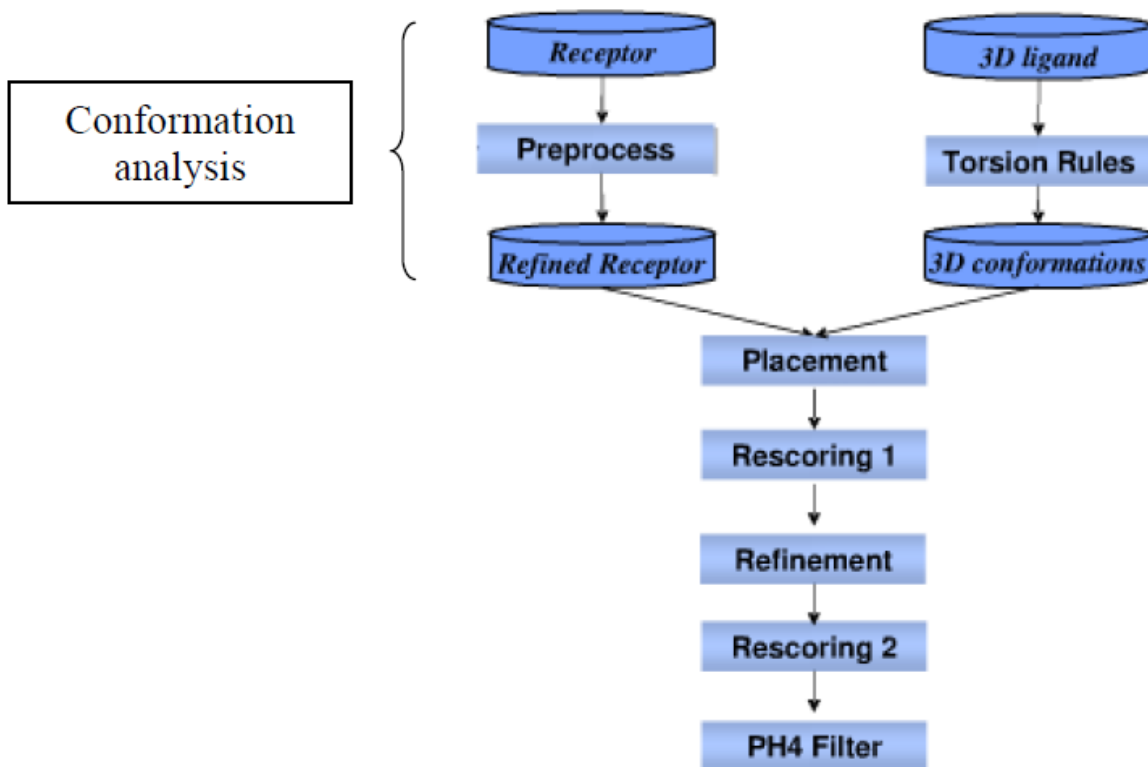
Figure 3.1. Several steps of docking in MOE program.

Normally, a classical potential energy function is used that is defined as a function of the coordinates of each of the atoms. The potential energy function is separated into terms representing covalent interactions and non_covalent interactions. The covalent interactions may be described by the following terms:

$$V_{bond} = \sum_{i=1}^{Nb} \quad \frac{1}{2} K_i^{\ b} (r_i - r_{0,i})^2 \qquad \text{Eqn(6)}$$

$$V_{\text{angle}} = \sum_{i=1}^{N\theta} \quad \frac{1}{2} K_i^{\ \theta} (\theta i - \theta_{0,i})^2 \qquad\qquad \text{Eqn(7)}$$

$$V_{\text{dihedral}} = \sum_{i=1}^{N\phi} \quad \frac{1}{2} K_i^{\ \phi} \cos (n_i (\phi_i - \phi_{0,i})^2 \qquad \text{Eqn(8)}$$

$$V_{\text{improper}} = \sum_{i=1}^{N\xi} \quad \frac{1}{2} K_i^{\ \xi} (\xi i - \xi_{0,i})^2 \qquad\qquad \text{Eqn(9)}$$

The equations correspond to two, three, four and four body interactions, respectively.

These interactions are represented by harmonic potentials for the bond lengths ri, for the bond angles θi, for the improper dihedral (out of the plane) angle ξi and by a more complex potential for the dihedral angles Φi. The non-covalent (non-bonded) interactions, which correspond to interactions between particles separated by more than three covalent bonds, are usually described by Coulomb's law

$$V_{\text{coulomb}} = \sum_{i<j} \quad (1/4\pi \ \varepsilon_0 \ \varepsilon_r) \ (q_i \ q_j/r_{ij}) \qquad\qquad \text{Eqn(10)}$$

for the electrostatic interactions and by a Lennard-Jones potential:

$$V_{LJ} (r) = \sum_{i<j} \quad A_{ij}/r_{ij}^{12} - B_{ij}/r_{ij}^{6} \qquad\qquad \text{Eqn(11)}$$

for the van der Waals (vdW) interactions, where rij is the atomic distance between particles i and j. The force field parameters describe the strength of the interactions. For bonded interactions parameters are defined for bond stretching, bond bending and torsional rotation. Another set of parameters determines the strength of non_bonded electrostatic and van der Waals interactions. Electrostatic interactions are generally represented by point charges located at the center of the atom.

How the system evolves through time is specified by the force field and by an integration time step that determines where the atoms will be positioned at time t + dt. MD requires the use of a very small time-step (1-2 fs) to achieve accurate results, because small time-steps limit the approximations that are

introduced by the numerical integrator. This limits the overall scope of the simulated time and the computable properties. For running the simulation AMBER12 was used (Case et al., 2005).

This is done by simulating the system whilst monitoring important properties such as temperature, the different energy terms, structure etc.. At constant periods of time the velocities are rescaled to the values for the desired temperature. This is done until the simulation becomes stable with respect to time, which means till thermodynamic terms like temperature and energy are retained in a certain, small interval for a sufficiently long time. Only when the average temperature of the system stabilizes one can collect the trajectory information for analysis.

Then for the first time in the course of the MD procedure Newton's equations of motion are integrated to propagate the system in time. This is done for a certain period of time to let the system equilibrate in the new thermodynamic state, giving the energy time to evenly distribute throughout the system. In the next step the velocities are scaled to values corresponding to a slightly higher temperature and another equilibration phase is carried out.

An important parameter to monitor the MD run is the root mean square deviation (RMSD). RMSD indicates how much two structures vary in terms of differences between the coordinates of the structures and is calculated with

$$D_{RMS} = \sqrt{\frac{1}{N} \sum_{i=1}^{N} \quad (x_i{}^{\alpha} - x_i{}^{\beta})^2} \qquad\qquad Eqn(12)$$

where X_i is the coordinate of atom i, α and β correspond to the different structures. RMSD is more appropriate to show that simulations are performed close to experimental structures to convince scientists with a rather critical view on reliability of molecular dynamic simulations. Thus, combined with molecular graphics programs which can display molecular structures in a time dependent way, molecular dynamic simulations provide a powerful tool to visualize and understand conformational changes involved in ligand

binding, catalysis or other functions of biological macromolecules at an atomic level. To give an overview

of the whole procedure described in this process of simulation, it is summarized in Figure 3.2.
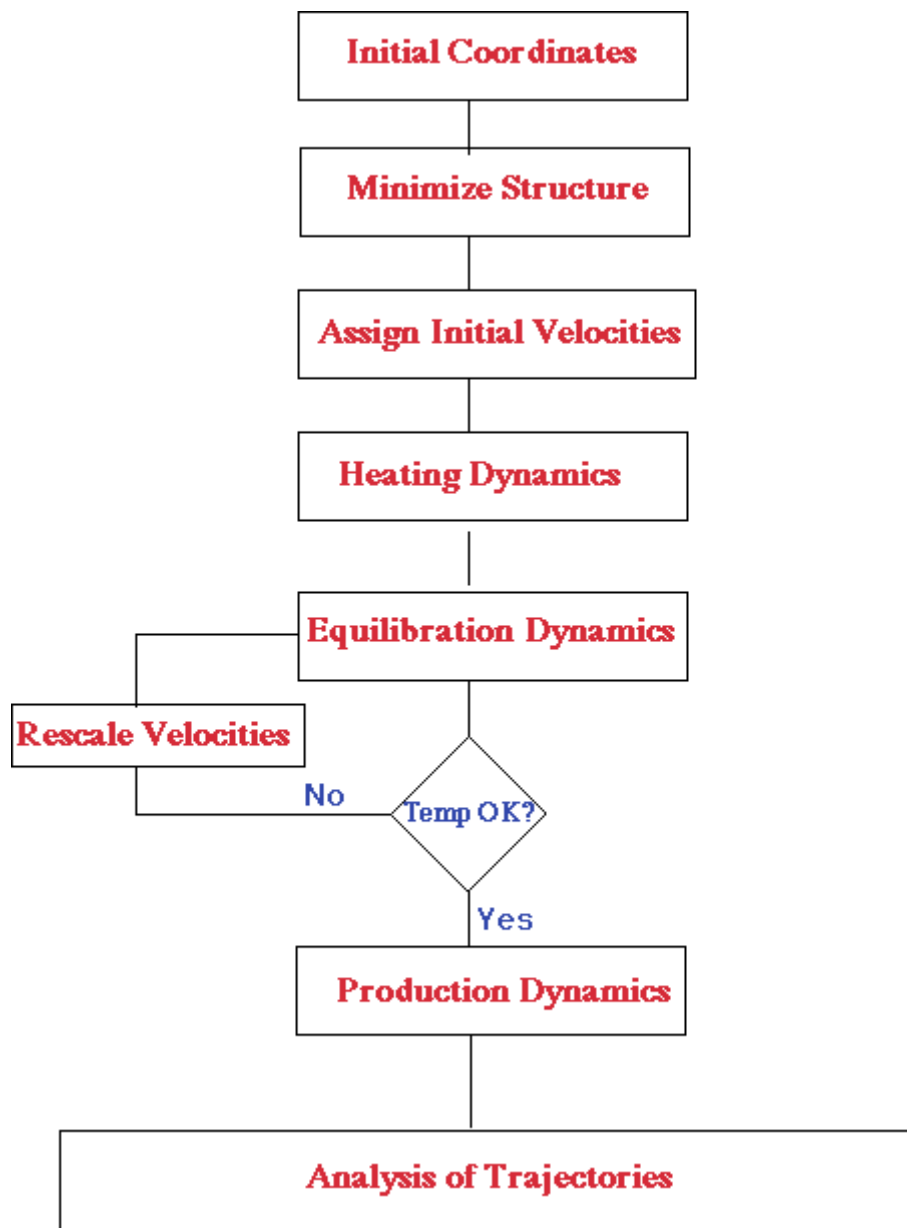
Figure. 3.2. An overview of the whole procedure described in the process of molecular dynamics simulation.

3.3.   QM/MM Calculations

In the QM/MM approach, a small but important part of the total system (called system1 or the QM system) is treated by quantum mechanics (QM), whereas the rest (called system 2 or the MM system) is treated by molecular mechanics (MM). The QM/MM calculations have been performed with the program COMQUM (Ryde and Olsson, 2001), which is a modular combination of the QM software Turbomole 6.5 and the MM software Amber 9. The advantage with this approach is of course that the whole macromolecule is explicitly modelled and that free energies can be calculated.

In this work we used QM/MM-2QM approach. The protein and solvent are divided into three subsystems: the two QM systems (systems 1a and 1b) and the MM system (system 2). In the QM calculations, systems 1a and 1b are represented by a wave function, whereas all the other atoms are represented by an array of partial point charges, one for each atom, taken from MM libraries. Thereby, the polarisation of the QM system by the surroundings is included in a self-consistent manner (electrostatic embedding, EE).

When there is a bond between systems 1 (system 1a or 1b) and 2 (a junction), the hydrogen link-atom approach is employed. The QM region is truncated by hydrogen atoms (called hydrogen link atoms, HL), whose positions are linearly related to the corresponding carbon atoms in the full system (called carbon link atoms, CL) (Ryde, 1996; Ryde and Olsson, 2001). In the point-charge model of the surroundings, all atoms were included, except the CL atoms. Therefore, the CB atom of all His and Met Cu ligands, and the CA atom of the Cys ligand were replaced by HL atoms. In order to avoid overpolarisation of the QM system, point charges on atoms directly bound to junction atoms (i.e. the closest neighbors of the QM system) are zeroed, and the resulting residual charges are equally distributed on the remaining MM atoms in that residue (Ryde, 1996).

In the QM/MM geometry optimizations, the QM/MM energy is calculated as shown in the following Equation:

$$E^{EE}_{QM/MM-2QM} = E^{HL}_{QM1a+ptch1b2} - E^{HL}_{MM1a,\,qa=0} + E^{HL}_{QM1b+ptch1a2} - E^{HL}_{MM1b,\,qb=0} + E^{CL}_{MM1ab2,qa=qb=0}$$

Eqn(13)

Here, $E^{HL}_{QM1a+ptch1b2}$ is the QM energy of system 1a, truncated with HL atoms, and including a point-charge model of the surrounding protein in the one-electron Hamiltonian (also of system 1b). $E^{HL}_{QM1b+ptch1a2}$ is the corresponding QM energy for system 1b. $E^{HL}_{MM1a,\,qa=0}$ is the MM energy of system 1a (still with HL atoms), but with all charges zeroed, and similar for $E^{HL}_{MM1b,\,qb=0}$. Finally, $E^{CL}_{MM1ab2,qa=qb=0}$ is the MM energy of the full system with CL atoms, but with the charges of the two QM systems zeroed (because all electrostatics interactions within the QM systems and between the QM and MM systems are considered in the two QM terms. However, the electrostatic interactions between the two QM systems is still accounted for in both $E^{HL}_{QM1a+ptch1b2}$ and $E^{HL}_{QM1b+ptch1a2}$. This problem was solved by scaling down the point charges of the other QM system by a factor of 2 in both terms. This is not completely satisfactory, because it will underestimate the polarisation of the QM systems by each other, but since the two systems are quite far apart, the effect should be quite small.

The point-charge model of each QM system was obtained by a fit to the electrostatic potential (ESP) calculated for a polarised wavefunction but without the point charges when the ESP was calculated. The ESP points were sampled with the Merz‑Kollman approach, as implemented in Turbomole. The charges were updated in each step of the geometry optimisation. The same charges were used to model the QM systems at the MM level when the surrounding MM system was optimised.

3.3.1. Force-Field Parameterizations

The bonded force-field parameters of the copper sites in the MD simulations were constructed according to the method developed by Norrby and Liljefors, (Norrby and Liljefors, 1998) using the recent implementation for Amber99. This method minimizes a penalty function consisting of the deviation of geometries and Hessian elements between the QM and MM calculations, giving different weights to different kinds of data. The geometries were described as lists of all bonds, angles, and dihedral angles,

rather than by absolute positions. The weight factors of the various data types were 100 Å^{-1} for bonds, 2 deg^{-1} for angles, 1 deg^{-1} for torsions, and 0.01_0.1 mol Å^2/kcal for Hessian elements (0.01 for elements involving interactions of an atom with itself, 0.02 for atoms bound to each other, 0.04 for atoms connected by two bonds, 0.1 for atoms connected by three bonds, and 0.01 for all other elements) (Norrby, 2000). The QM calculations were performed on the vacuum-optimized structures, which were started from the QM/MM-2QM structures in the protein.

The iterative force-field optimizations were started from the corresponding Hess2FF force field, (Nilsson et al., 2003) which is automatically extracted from the Hessian matrix. After convergence, the force field was checked. Typically, some bonds and angles get zero force constants in the first runs of the parameterizations. These were reset to reasonable values, and force constants of other angles around the same central atom were reduced, and then the parameterization was run again. This was repeated until all bonds and angles had nonzero force constants and all other parameters looked reasonable. Specific force fields were calculated for both the reduced and the oxidized forms of the T1 and ligand. We assigned separate atom types for all metals and all atoms that ligated directly to the metals. For the T1 sites, we also used new atom types for all atoms in the ligands, except for hydrogen atoms bound to the same atom.

Charges for all atoms were fitted to the ESP, sampled according to the Merz_Kollman scheme, (Besler et al., 1990) but with a higher-than default density of points, 2000_3000 points/atom. These charges were used directly in the parameterization, whereas in the MD simulations of the whole protein, the charges on the Cl atoms were adapted so that the total charge of the amino acid (including both QM and MM atoms) was the same as the sum of QM charges of the corresponding QM fragment (Ryde and Olsson, 2001). Thereby, we ensure that the total charge of the simulated system is an integer, but we allow for charge transfer within the QM system (the amino acids with QM atoms have noninteger total charges). The van der Waals parameters of the Cu ions were R = 1.17 Å and ε = 4.77 kJ/mol (Bartolotti et al., 1991). Neither the charges nor the van der Waals parameters were changed during the parameterization.

The redox potentials of the two copper sites were estimated. For the minimized QM and QM/MM-2QM structures, we used the relation:

$$E^0 = (E_{OX} - E_{red}) - E_{NHE} \qquad \text{Eqn(14)}$$

where the factor $E_{NHE} = 4.28$ V converts the energy scale to that of the normal hydrogen electrode (NHE) (Kelly et al., 2007). If both copper sites are considered, the correction factor cancels, and we give the energy difference between the OR and RO (a negative sign indicates that the OR state is more stable). For the MD simulations, we instead used the relation:

$$E^0 = (\langle \Delta E_{et} \rangle_{RO} + \langle \Delta E_{et} \rangle_{OR})/2 \qquad \text{Eqn(15)}$$

ΔE_{et} was calculated by the QM/MM-2QM approach. The same charges of each Cu site were used in our calculations. The reason for this is that previous investigations of the accuracy of QM/MM have indicated that the ESP charge fitting often becomes unstable and may give spurious charges and energies in some cases (Hu et al., 2011). The calculations were performed on 1250 snapshots, sampled every 10 ps during the 10 ns production simulation. For the MM components, instead 5000 snapshots were used, sampled every 2 ps. In all calculations of ΔE_{et} with QM/MM-2QM, no periodic boundary conditions were used. Instead, the MM system was centered on the two Cu sites, and an infinite cutoff was employed.

For the MD simulations, we calculated the vertical energy difference between the two electronic states, RO and OR, $\Delta E_{et} = E_{RO} \_ E_{OR}$ for all snapshots obtained in the MD simulations of the two states. Next, the reorganization energy (RE) was estimated from

$$\lambda = (\langle \Delta E_{et} \rangle_{RO} - \langle \Delta E_{et} \rangle_{OR})/2 \qquad \text{Eqn(16)}$$

We run classical MD simulations of a solvated laccase, using tailored accurate MM parameterizations of T1 site and ligand, and then perform QM/MM calculations of the metal site and ligand for over a thousand snapshots from the MD simulations.

II. Experimental methods

3.4. Materials

3.4.1. Chemical Reagents

All chemicals used were of reagent grade purity.

1. dNTPs (Sigma, Spain).

2. Appropriate PCR primers.

3. Low melting point agarose (Bio-rad, Spain).

4. DNA extraction from agarose gels: Zymoclean gel DNA recovery kit (Zymo Research, USA).

5. Yeast transformation: yeast transformation kit (Sigma, Spain).

6. Zymoprep kit (Zymo Research, USA).

3.4.2. Biological Materials

1. *E. coli* XL2-blue competent cells (Stratagene, USA).

2. *S. cerevisiae* (e.g., protease deficient strain BJ 5465, ATCC208289).

3. Expression shuttle vector containing the gene of interest under the appropriate promoter, a signal sequence for secretion (e.g., the native sequence or the alpha factor preproleader), and selection markers for *S. cerevisiae* and *E. coli*. For example: pJRoC30, Gal10 promoter, *Myceliophthora thermophile* T2 mutant laccase with the native signal sequence, and the uracil and ampicillin selection markers (Figure 2.3).

4. Gene variants created by site directed mutagenesis.

5. Restriction endonucleases

6. Proofreading polymerase, e.g., Pfu (Stratagene, USA).
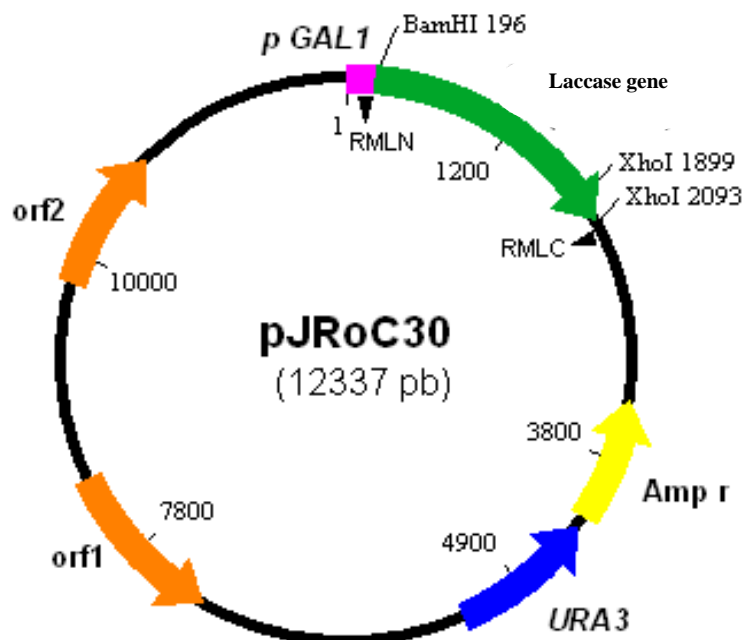
Figure 3.3. pJRoC30 plasmid.

3.4.3. Gene of parental type of laccase (MtL T2)

The parental gene used for the development of this Doctoral Thesis corresponds to the *Myceliophthora thermophila* laccase mutant T2 (MtLT2), which was designed by directed evolution in previous studies conducted at the California Institute of Technology (Caltech), for a functional expression in *S. cerevisiae* (Bulter et al., 2003). MtLT2 contains 14 mutations introduced during 10 cycles of directed evolution, which gives appropriate levels of engineering for laccase expression against various applications.

3.4.4. Culture media

We used LB medium for cultivation of *E. coli*, SOB solution for transformation of *E. coli*, SC medium for cultivation of *S. cerevisiae*, YPD for cultivation of selected clones in rescreening step and laccase selective expression medium (See Appendix A).

3.4.5. Primer design

In order to produce mutated gene and make a library, first we designed different primers for desired positions of laccase gene (See Appendix B).

3.5. Methods

Homologous recombination displayed by eukaryotic machinery to splice mutagenized DNA fragments, and of the yeast gap repair mechanisms to substitute in vitro ligation (Alcalde et al., 2006). In our case, two PCR reactions are carried out using mutagenized primers in order to produce two PCR fragments that share homologous sequences at the 3′ and 5′ ends. These products already contain the mutagenized codons and they are then directly shuffled by *S. cerevisiae* in vivo through their sites of recombination to give rise to a whole gene. Likewise, recombination not only splices the two fragments in a complete gene but it also shuffles the mutagenized codons. The whole mutagenized gene possesses large overhangs that recombine with the ends of the linearized vector, thereby forming an autonomously replicating plasmid. It is not straightforward to determine which event takes place first (the splicing of the PCR fragments between themselves or their linkage to the linearized plasmid) and in fact, it is even likely that both phenomena happen simultaneously.

3.5.1. PCR

Two separate PCR reactions were carried out simultaneously to amplify the two DNA fragments that overlapped at specific positions corresponding to the regions targeted for site-directed mutagenesis of the parental sequence. The primers were designed with Fast-PCR software (University of Helsinki, Finland) and were as follows: RMLN, RMLC, forward and reverse primers for mutagenized region (See Appendix C). The PCR fragments were loaded on low-melting-point preparative agarose gels and purified using the Zymoclean gel DNA recovery kit.

3.5.2. Agarose gel electrophoresis

DNA was separated by gel electrophoresis in 1 % agarose gels. Agarose was boiled in TAE buffer and after cooling to 55 °C the gel was poured into a horizontal gel chamber with a sample comb. After consolidation the gel was covered with TAE buffer and the comb was removed. Gel electrophoresis was run at 110 Volt for 30 min. The gel was stained in GelRed for 15 min and discolored with dH_2O. The fragment was detected under UV light.

3.5.3. DNA isolation from agarose gels

The DNA band of interest was cut out with a clean scalpel and transferred into a 1.5 ml tube. According to the manual of *Agilent Technologies* DNA was isolated from agarose gel with the *StrataPrep DNA Gel Extraction Kit*. The purified DNA was eluted with 20 µl dH_2O.

3.5.4. Determination of DNA concentration

The DNA concentration was determined photo metrically by measuring the absorption at 260 nm (A_{260} = 1 relates 50 µg/mL). The measurement was done by using the *Infinite M200 Pro NanoQuant.*

3.5.5. DNA sequencing

Laccase genes were sequenced by the company *GATC Biotech*. 5 µl (80 – 100 ng/µl) of DNA was mixed with 5 µl of Primer (5 µM). After sequencing the data was analyzed with the software *BioEdit*.

3.5.6. Cultivation of *Escherichia coli*

LB with the appropriate antibiotics were inoculated using a toothpick or spreading 150 µl of a liquid culture and incubated over night at 37 °C. For a preparatory culture, a single colony was transferred into LB and incubated over night at 37 °C and 250 rpm. This culture was applied for plasmid mini preparations.

3.5.7. Cultivation of *S. cerevisiae*

SC dropout medium agar plates were inoculated using a toothpick or spreading of a liquid culture and incubated at 30 °C for 2 days. For a preparatory culture, a single colony was transferred into SC medium and incubated at 30 °C and 220 rpm for 2 days. Those cultures were applied for the inoculation of main cultures for the preparation of chemically competent cells, plasmid isolation and screening of mutants.

3.5.8. Mini plasmid preparation

For the preparation of plasmid DNA a plasmid mini preparation kit was used. A single colony was inoculated in 5 ml of LB medium and incubated at 37°C over night. The cells were harvested by centrifugation and the Miniprep was done according to the manual of *Agilent Technologies*. Then, the pJRoC30 plasmid was linearized with *Xho*I and *BamH*I. After that, purified by agarose gel extraction using a low melting point agarose at 4°C and with an applied voltage of less than 5 V/cm (distance between the electrodes of the unit). To determine its concentration the absorption of the plasmid measured at 260 nm.

3.5.9. *S. cerevisiae* chemically competent cells

The PCR fragments (200 ng -each) were mixed with the linearized vector (100 ng) and transformed into competent yeast cells. According to the *Yeast Transformation Kit* (*Sigma Aldrich*) aliquots of 10 µl of salmon testes DNA (10 mg/ml), 200 ng of insert and 100 ng of plasmid DNA were added to 100 µl competent cells and vortexed. After adding of 600 µl of PLATE buffer and vortexing, the mixture was incubated at 30 °C for 30 min and 700 rpm. To increase the transformation efficiency DMSO were added to 10 %. The heat shock was performed for 15 min in a 42 °C water bath. After briefly spinning, the supernatant was discarded and resuspended in 500 µl of sterile water. 25 – 100 µl were plated on SC dropout plates and incubated at 30 °C for 2 – 3 days. On average, around 1500 individual clones were analyzed per mutation. The selected plasmids were isolated and sequenced to verify the site directed-mutagenesis.

3.5.10. *E. coli* chemically competent cells

For the transformation in *E. coli* (XL1-Blue) aliquots of 10 µl of competent cells were thawn on ice and mixed with 0.2 µl of ß-mercaptoethanol (c_E = 25 mM). The cells were incubated 10 min on ice and 5 µl of Zymoprep were added and mixed by inversion. Afterwards the tubes were incubated on ice for 30 min. The cells were heat shocked at 42 °C for 30 sec and incubated on ice for 2 min. Then 500 µl of SOC medium were added and incubated for 1 h at 300 rpm. The final volume of 100 µl was plated out on LB/amp plates and incubated overnight at 37 °C.

3.5.11. Library construction and screening

For construction of a library 17 96-well plates have been filled with 180 µL of expression medium per well using an 8-channel pipette. Individual clones from the SC-drop out plates have been picked and transfer them into the 96-well plates. Column 6 of each plate, be inoculated with the standard (parental) and one well (H1) not be inoculated (control) (Figure 2.4.). The plates were wrapped in parafilm and incubated for 72 h at 30°C and 220 rpm in a shaker at 80–85% humidity. Then, the parafilm were removed from the culture plates and centrifuged (master plates) for 15 min at 3,000 rpm at 4°C. 20 mL of the supernatants were transferred onto activity plates using a robotic station Freedom EVO (Tecan, Männedorf, Switzerland) onto three replica plates. The first replica plate was filled with 180 µL of 100 mM citric phophate buffer (pH 4.0) containing 3 mM ABTS, the second replica was filled with 180 µL of 100 mM citric phophate buffer (pH 4.0) containing 2 mM Molybdenum hexacarbonyl and the third replica was filled with 180 µL of 100 mM citric phophate buffer (pH 4.0) containing 20 mM Violuric acid. The plates were stirred briefly and the absorption at 418 nm ($\varepsilon_{ABTS}{}^{\bullet+}$ =36,000 M^{-1} cm^{-1}), at 388 nm for Molybdenum hexacarbonyl and at 515 nm (ε_{VA} =13.9 M^{-1} cm^{-1}) was recorded in the plate reader (SPECTRAMax Plus 384, Molecular Devices, Sunnyvale, CA). In case of Molybdenum hexacarbonyl and Violuric acid measurement the plates were incubated at room temperature until the color developed that was after 4 and 24 hours, respectively and the absorption was measured again. Relative activities were calculated from the difference between the

absorption after incubation and that of the initial measurement normalized against the parental type and used as reference in the corresponding plate.
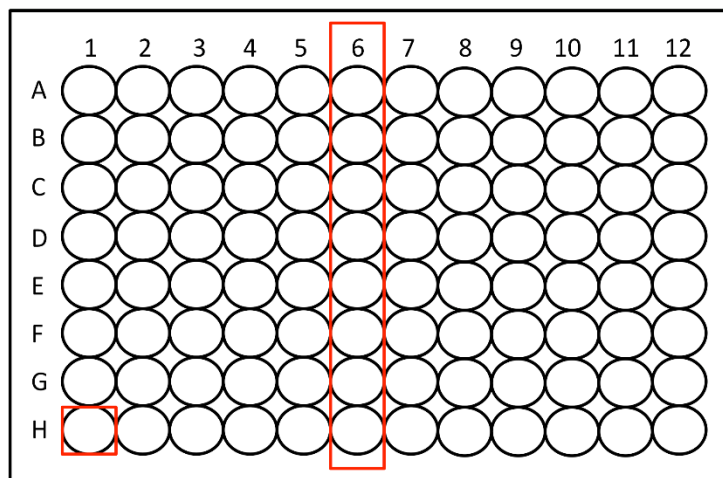
Figure 3.4. Model of a 96 well plate for preparation of HTS. Column 6 contains parental type and well H1 contains negative control.

3.5.12. Re-screening

To rule out false positives, two consecutive rescreenings were carried out.

3.5.12.1.   First re-screening

Aliquots of 5 µL of the best clones were removed from the master plates to inoculate 50 µL of minimal media in new 96-well plates. Columns 1 and 12 (rows A and H) were not used to prevent the appearance of false positives. After a 24 h incubation at 30ºC and 225 rpm, 5 µL was transferred to the adjacent wells and further incubated for 24 h. Finally, 200 µL of expression medium was added and the plates were incubated for 48 h. Accordingly, each mutant was grown in 4 wells. The parental types were subjected to the same procedure (lane D, wells 7-11) and the plates were assessed using the same protocols for the screenings described above.

3.5.12.2.   Second re-screening

An aliquot from the wells with the best clones of the first rescreening was inoculated in 3 mL of YPD and incubated at 30ºC and 225 RPM for 24 h. The plasmids from these cultures were extracted (Zymoprep yeast plasmid miniprep kit, Zymo Research). As the product of the zymoprep was very impure and the concentration of DNA extracted was very low, the shuttle vectors were transformed into super-competent *E. coli* cells (XL2-Blue, Stratagene) and plated onto LBamp plates. Single clones were picked and used to inoculate 5 mL LBamp media and they were grown overnight at 37 ºC and 225 RPM. The plasmids were then extracted and *S. cerevisiae* was transformed with plasmids from the best mutants as well as with the parental type. Five clones for each mutant were picked and rescreened as described above.

3.5.12.3.   Third re-screening

In the third re-screening a single colony of the best mutants and the parental type as the reference from the second re-screening were picked from a SC selective plate and inoculated in SC medium for 2 – 3 days incubation at 30 °C and 220 rpm. The optical density at 600 nm of the precultures were measured and diluted to 0.3. After incubation of approximately 6 hours at 30 °C and 220 rpm the cells reached the OD_{600} of 1. Finally 1 ml of culture was induced with 9 ml of expression medium and incubated at 30 °C and 220 rpm. Every 24 h samples were taken to measure optical density and activity until the mutants achieved their highest activity (~ 36 h). After those three re-screenings a new mutant with a higher activity was determined.

3.5.13. Determination of thermostability

The thermostability of the different laccase samples was estimated by assessing their T50 values using 96/384 well gradient thermocyclers. Appropriate laccase dilutions were prepared. Then, 50 μL was used for each point in the gradient scale and a temperature gradient profile ranging from 55 to 85ºC was established as follows (in ºC): 55.0, 56.8, 59.9, 64.3, 70.3, 75.0, 78.1 and 80.0. After a 10 min incubation,

samples were chilled out on ice for 10 min and further incubated at room temperature for 5 min. Afterwards, 20 µL of samples were subjected to the same ABTS-based colorimetric assay described above for the screening. The thermostability values were deduced from the ratio between the residual activities incubated at different temperature points and the initial activity at room temperature.

3.5.14. Determination of optimal pH activity

pH activity profile of different variants were measured with 100mM Citrate-Phosphate-Borate buffer with different pH (2.0 – 9.0 adjust with acid acetic or NaOH). 20 µL of the supernatant were filled in triplicates for each variants in 96-wells plate. Afterwards, 180 µL of reaction mixure contained 3mM of ABTS was added and activity was measured. Activity was normalized with respect to maximum activity of the sample in each case of variant.

3.5.15. Determination of stability vs. pH

Stability vs. pH for parental type, 3H12, 5B4, 15H11 and 19G8 were determined by incubating enzymes in Citrate-Phosphate-Borate buffer with pH between 2.0 to 9.0 and residual activity after different incubation time was measured. The supernatants of each variants concentrated 50 times with microcon membrane by adding KH_2PO_4 (20mM, pH 4.0). Then, diluted 50 µL of each variants in each pH and after different period of incubation (1, 4, 24, 48, 75, 144 hours) the initial and residual activity were measured. For measuring activity citric phosphate buffer (100mM, pH 4.0) contained 3 mM ABTS was used. Each experiments were performed in triplicate.

3.5.16. Production and purification of laccase

3.5.16.1.   Production of laccase in S. cerevisiae

A single clone from the *S. cerevisiae* containing the parental or mutant laccase gene was picked from a SC drop-out plate, inoculated in 10 ml of minimal medium and incubated for 48 h at 30ºC and 225 rpm

(Micromagmix shaker, Ovan, Spain). An aliquot of cells was removed and inoculated into a final volume of 50 ml of minimal medium in a 500 ml flask (optical density, OD_{600}=0.25). Incubation proceeded until two growth phases were completed (6 to 8 h) and then, 450 ml of expression medium contained $CuSO_4$ (5.6 mM) was inoculated with the 50 ml preculture in a 2 litre baffled flask (OD_{600}=0.1). After incubating for 38-42 h at 30ºC and 225 rpm (maximal laccase activity; OD_{600}=28-30), the cells were separated by centrifugation for 30 min at 6000 rpm (4ºC) (Avantin J-E Centrifuge, Beckman Coulter, Fullerton, CA).

3.5.16.2.   Purification

Laccases were purified by fast protein liquid chromatography (FPLC) equipment, ÄKTA purifier (GE Healthcare, UK) and high performance liquid chromatography (HPLC). The crude extract was first submitted to a fractional precipitation with ammonium sulphate at 60 % (first cut) and the pellet was then removed before the supernatant was subjected to 95 % ammonium sulphate precipitation (second cut). The final pellet was recovered in 20 mM tris buffer pH 7.8 and the sample was filtered and loaded onto the FPLC coupled with a strong anionic exchange column (HiTraP QFF, GE Healthcare) pre-equilibrated with tris buffer. The proteins were eluted with a linear gradient from 0 to 1 M of NaCl in two phases at a flow rate of 1mL/min: from 0 to 40 % over 60 min and from 40 to 100 % over 10 min. Fractions with laccase activity were pooled, concentrated, dialyzed against tris buffer and further purified by HPLC-PDA coupled with a 10μm high resolution anion exchange Biosuite Q (Waters, 10cm; Waters, Milfrod, MA, USA) preequilibrated with tris buffer. The proteins were eluted with a linear gradient from 0 to 1 M of NaCl at a flow rate of 1 mL/min in two phases: from 0 to 25 % in 300 min and from 25 to 100 % in 10 min. The fractions with laccase activity were pooled, dialyzed against 20 mM KH_2PO_4 buffer pH 4.0, concentrated and stored at 4ºC.

3.5.17. SDS-PAGE

Throughout the purification protocol the fractions were analyzed by SDS-polyacrylamide gel electrophoresis (SDS-PAGE) on 10 % gels in which the proteins were stained with Coomassie brilliant blue (Protoblue Safe, National Diagnostics, GA, USA). Sodium dodecyl sulfate (SDS), an anionic detergent, is used to reduce proteins to their primary (linearized) structure and coat them with uniform negative charges so that the mobility of the proteins is solely based on molecular weight. The gel was casted with a composition of 10% separating gel and 6% stacking gel (See Appendix D). The protein sample to be analyzed was diluted with a sample buffer (0.5 M Tris, 2% SDS, 10% glycerol, 0.1% bromophenol blue, β-mercaptoethanol 5%). The prepared samples (5 μl protein and 10 μl buffer), and 8 μl-sample of the protein molecular weight marker, were loaded onto the gel and the electrophoresis was carried out using a gel running buffer (25 mM Tris, 192 mM glycine, 0.1% SDS) at 60 v for 4 h. The run gel was stained for 3 h using a staining solution (0.025% Commassie R-250, 40%methanol, 10% glacial acetic acid diluted in distilled water). The stained gels were destained until visualizing the bands using destaining solution (40% methanol, 10% glacial acetic acid diluted in distilled water). All protein concentrations were determined using the Bio-Rad protein reagent and bovine serum albumin as a standard.

3.5.18. Characterization of purified enzymes

Oxidation of ABTS and DMP was measured at pH 4.0. Steady-state kinetic constants were calculated from oxidation of increasing substrate concentrations. Mean values and standard errors for apparent affinity constant (Michaelis constant, K_m) and maximal enzyme turnover (catalytic constant, k_{cat}) were obtained by nonlinear least-squares fitting of the experimental measurements to the Michaelis-Menten model. Fitting of these constants to the normalized equation $v = (k_{cat}/K_m)[S]/(1 + [S]/K_m)$ yielded the efficiency values (k_{cat}/K_m) with their corresponding standard errors.

3.5.19. Quantification of the enzymes

The routine way and for estimate the factors and performance of the purification, concentration of the enzymes was determined with Bradford method (Bradford, 1976) by using protein assay dye reagent (BioRad). The test is based on maximum absorbance in 595 nm of the acidic solution of Coomasie Blue in combination with a protein. 159μL of water was added to 1 μL of the sample with 40 μL of the Bradford reagent in 96-wells plate. Then, the plate was shaken and after 5 minutes incubation in room temperature absorbance was measured. Data was interpolated in one calibrated curve that performed with BSA.

4. RESULTS AND DISCUSSION

4.1. Geometry optimizaion of the ligands

Table 3.1 shows the chemical structures of the fourteen ligands selected in the present study for docking studies. Initial coordinates of the ligands listed in were generated using GaussView and optimized at the Hartree-Fock level using a 6-31G* basis set by means of the Gaussian09 program (Frisch et al., 2009).

(2Z,2'E)-2,2'-(hydrazine-1,2-diylidene)bis(3-ethyl-2,3-dihydrobenzo[d]thiazole-6-sulfonate)

2,5-dimethylaniline

2,2,6,6-Tetramethylpiperidinyloxy

1H-benzo[d][1,2,3]triazol-1-ol

2-hydroxyisoindoline-1,3-dione

3,4,5-trihydroxybenzoic acid

4-hydroxybenzoic acid

2,6-dimethoxyphenol

1-(4-hydroxy-3-methoxyphenyl)ethanone

5-(hydroxyimino)pyrimidine-2,4,6(1H,3H,5H)-trione

1-(4-hydroxy-3,5-dimethoxy phenyl)ethanone

4-hydroxy-3-methoxybenzaldehyde

(E)-3-(4-hydroxyphenyl)acrylic acid

(E)-3-(4-hydroxy-3,5-dimethoxy phenyl)acrylic acid

2,4,6-trimethylphenol

3,4-dihydroxy-5-methoxy benzaldehyde

4-hydroxy-3-methoxy benzaldehyde

(E)-3-(4-hydroxy-3-methoxy phenyl)acrylic acid

N-(4-hydroxyphenyl)acetamide

4-hydroxy-3,5-dimethoxy benzaldehyde

2-isopropyl-5-methylphenol

4-(hydroxymethyl)-2-methoxyphenol

methyl 4-hydroxy-3,5-dimethoxybenzoate

methyl 4-hydroxy-3-methoxybenzoate

Table 4.1. List of the ligands were used in molecular docking

In case of ABTS; we carried out geometry optimization of the compound in three different protonation states. Results of these optimizations show ABTS with the two benzothiazoline groups in the same planar in the case of ABTS^{2-} and ABTS^{1-}, whereas the two fused rings show a 90° twist when the two nitrogens of azine group are protonated. Comparison the crystallographic structure of ABTS bound to the *B. subtilis* laccase (pdb ID: 1UVW), suggests that the ligand binds doubly protonated. In order to give support to this hypothesis we experimentally determined the pKa of ABTS. Titration curves show that ABTS exhibits two pKa at 1.5 and 9.5 (Figure 4.1), respectively. Consequently at the working pH of around 4 it is expected that the nitrogens are protonated.
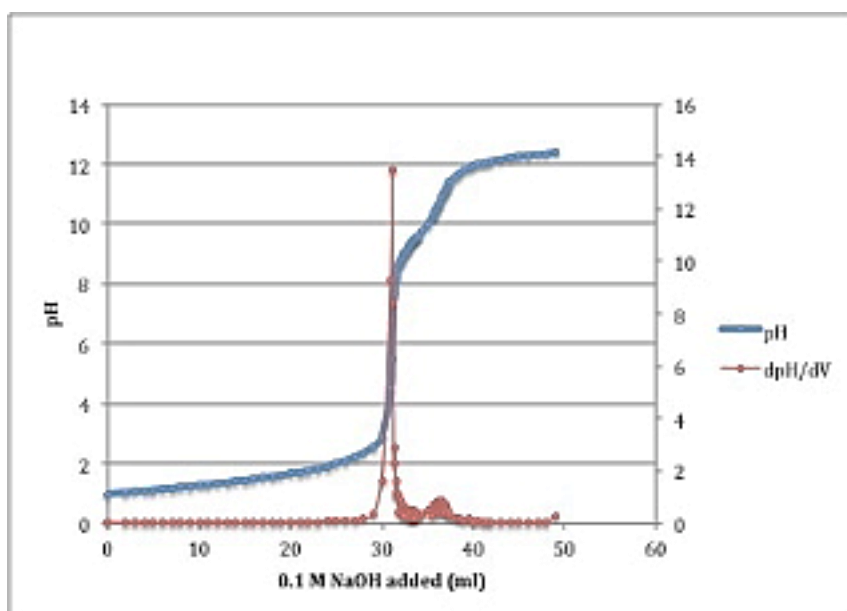
Figure 4.1. Titration of ABTS.
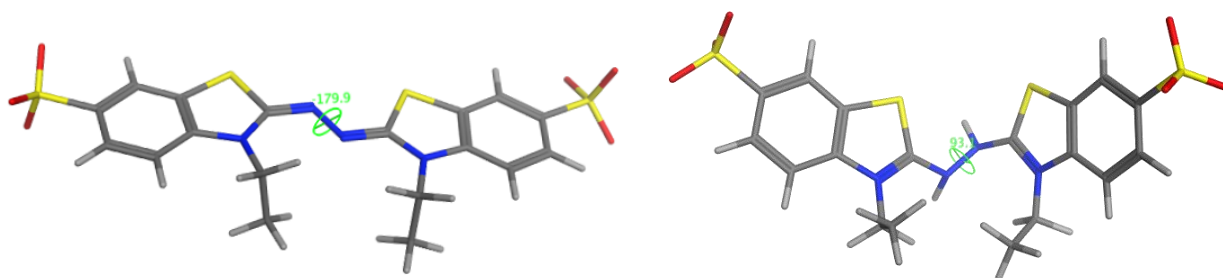
Figure 4.2. Geometry optimization of ABTS. In the left the angle of ABTS^{2-} in the azine group is 179.9 while this angle in ABTS is 93.1.

Christensen and coworkers (2014), have described the possible binding poses of ABTS in different isoforms of laccase. They showed that ABTS contains delocalized radical density on the two azine N and the ring N═C and S in the two adjacent thiazoline moieties and the highest density belonged to two azine N (Christensen and Kepp, 2014). In our investigation, we reported for the first time that the protonation state of ABTS has effect on conformation of this ligand. Our result showed that ABTS in neutral state contained an azine C−N═ N−C dihedral angle of 93.1° which is closed to crystalized structure (68.4°). Although, the azine dihedral angel in other states was bigger (Figure 4.2).

4.2. Docking studies

The set of fourteen ligands were used for docking studies in two fungal laccases: the one corresponding to the species *T. versicolor* (PDB entry 1KYA) and the *M. albomyces* (PDB entry 3FU8) as well as in the bacterial laccase of *B. subtilis* (PDB entry 1UVW).

In order to perform docking studies, substrates and other molecules found in the crystallographic structure were removed and hydrogens added. Residue protonation states were considered taking into account the respective working pH, i.e. pH 5.0 for the fungal laccase and pH 8.0 for the bacterial one. Amber charges were used for protein atoms and RESP charges were calculated for the substrates. Prior to docking, the protein and the ligands were fully minimized with MMFF94 force field.

The surface of the active site of *T. versicolor* is composed of Phe162, Phe265, Phe332, Phe337, Gly334, Gly392, Leu164, Pro391, Asp206, Asn264, His458 and His395 which are mostly hydrophobic and aromatic residues. The active site of *M. albomyces* is set out of Phe371, Phe427, Leu363, Leu429, Ile505, His431, His508, Glu235, Pro192, Ala191 and Trp373 which are hydrophobic but less aromatic than *T. versicolor*, whereas residues Gly417, Thr415, Thr418, Arg416, Pro226, Pro384, Leu386, His497 and His419 define the biding pocket in bacterial laccase, *B. subtilis*. As it has been observed the bacterial active site is not as hydrophobic as the fungal structures. Moreover, the residues are not aromatic. Another difference is that active site is wider than the two fungal laccases active site.

The selected compounds categorized to the structures contained OH or NOH. About ABTS it cannot be in none of these groups. However, it is one of the most popular substrate being used in industry (Bourbonnais and Paice, 1990). Also, 1UVW crystalized structure contained this compound and we considered ABTS in our work to observe the difference binding mechanism of these compounds. Bellow it has been explained the docking results of each selected laccase structures and the substrates.

4.2.1. Fungal laccase: structure of *T. versicolor*

One of the fungal laccase with high redox potential value is a structure with pdb code 1KYA. It is a fungal laccase that has been crystalized with 2,5-xylidine (XYD) (Bertrand et al., 2002). The binding mode of xylidine and 1KYA was shown in figure 4.3. XYD bound in the active site by hydrogen bind to Asp206. The distance between –NH of His458 and –N in xylidine is 2.61 Å. Hydrogen of His is pointed to –N of xylidine which make it possible for electron transfer. Docking results showed that compounds contain –OH and –NOH in their structure bound in the binding pocket of laccase. These compounds bound near His458 in an orientation that oxygen atom of hydroxyl group becomes near to –NH of His. Moreover, the ring of these compounds have π-π interactions with Phe162, 265 and Pro 391.

There are some poses that have hydrogen bind between –H of hydroxyl group of substrates and Asp206, however, those poses there is no possibility for electron transfer to copper because the hydroxyl group of structure is far from His. In some cases –OH group of the compounds indicate interaction with His and Asp and they are in the orientation between these two residues, such as, 3,4-dihidroxy5-methoxy benzaldehyde and 4-(hydroxynethyl)-2-methoxyphenol. In the 1H-benzo-[1,2,3]triazol-1-ol, 2,2,6,6-tetramethyl piperidinyloxy and 2-hydroxyisoindoline-1,3 dione the poses are similar to phenolic compounds. 5-(hydroxyiminolpyrimidine-2,4,6(1H,3H,5H)-trione just showed interaction with His and π-π interactions. In case of ABTS, -SO_3 in some poses indicated interaction with His458 and Asn264. As it is shown in figure 4.4 it contain hydrogen interaction with Asn264 and the hydrogen atom of His458 is perpendicular to the benzothiazoline ring of ABTS. These are the results when Asp206 was non-protonated.
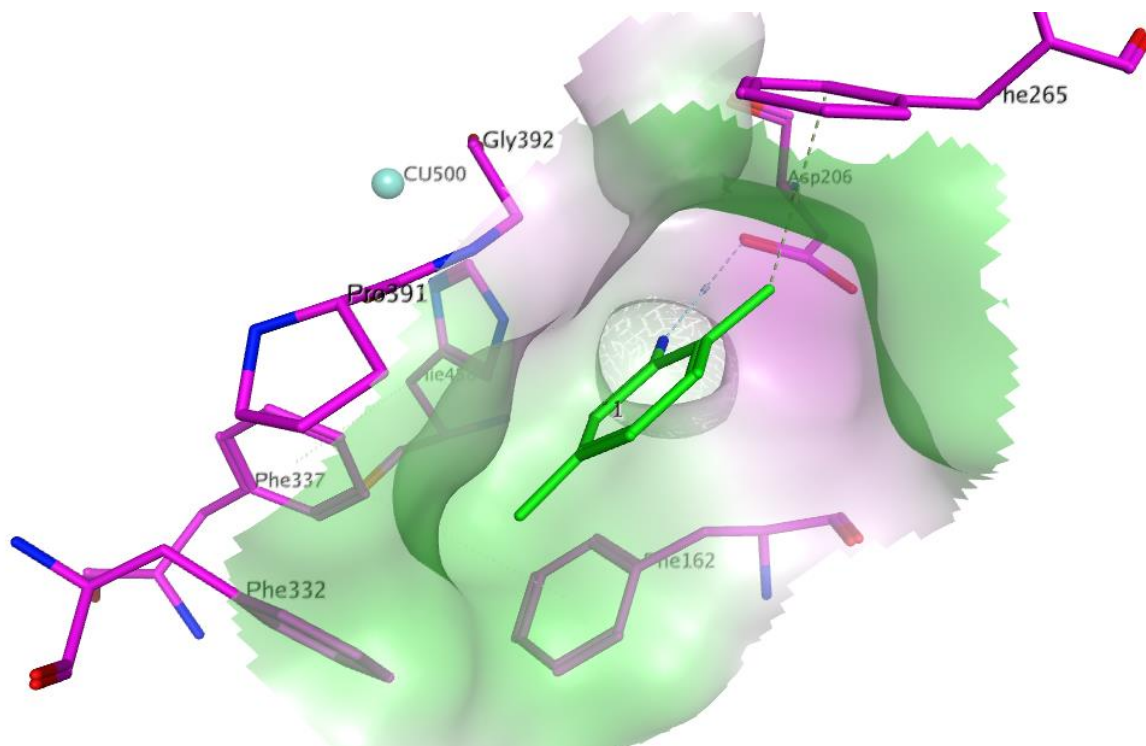
Figure 4.3. Xylidine position in binding pocket of TvL. It bound to the binding pocket of *T. versicolor* laccase (pdb entry 1KYA) showing the side chains surrounding the ligand.
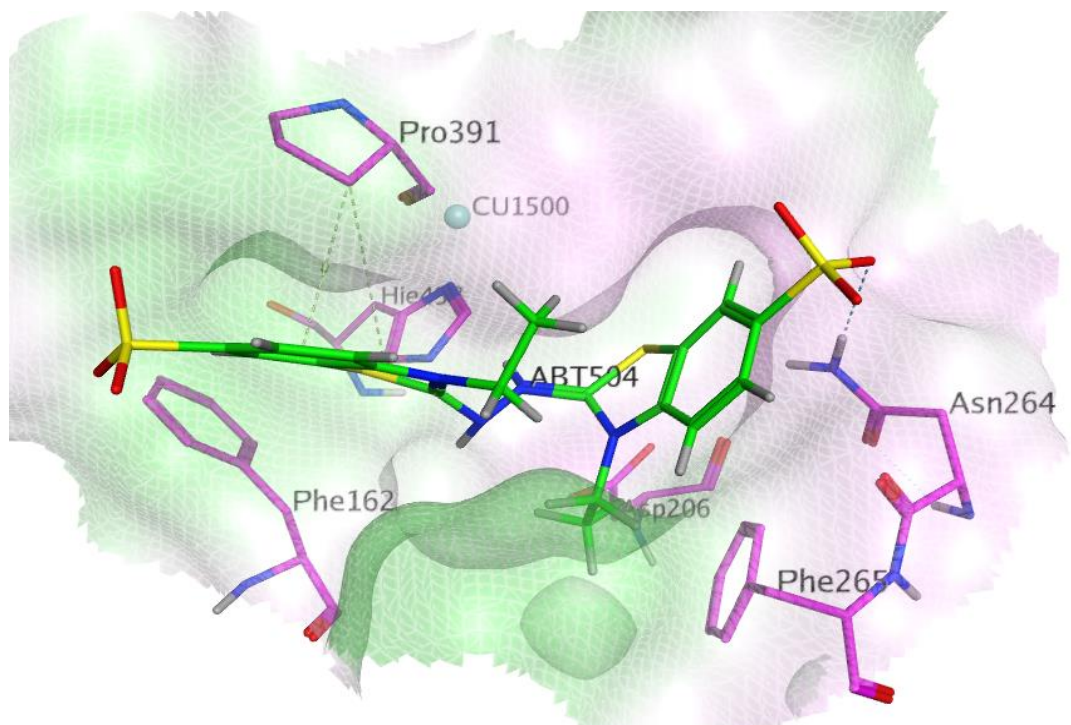
Figure 4.4. Propose conformation of ABTS bound to the TvL.

Molecular docking has been performed in the same way with Asp206 protonated. The results showed again the similar orientation in case of –OH and –NOH containing compounds. The only difference was that –H of protonated Asp206 points to the oxygen atom of hydroxyl group of compounds and there is no hydrogen bind. Also, the scores in all cases were worse except with ABTS. The score showed improvement and it was -8.1307 kcal/mol.

Recently, Christensen and his colleagues (2014) have systematically explored the possible binding modes of ABTS upon binding to four *T. versicolor* laccase isoenzymes. the best poses, represented by the isoform Lccα, which is also experimentally the strongest-binding protein, is that ABTS is bound in a semi-extended conformation with one buried sulfonate group interacting with protonated Asp206 (AspH206) and the other sulfonate interacting with the Arg161 that is unique to the α-isoform. The donor part of ABTS was close to His (Christensen and Kepp, 2014). In our work, MOE produced this pose with worse score, -5.7555 kcal/mol in comparison to the pose that it showed interaction with Asn264.

Previously, it has been discussed that at pH ∼ 2, where the strongest binding isoforms Lcc α and Lcc β have their optimum activity (Koschorreck et al., 2008). At low pH protonated Asp206 helps to keep negatively charged ABTS in the binding pocket. Our result confirm this issue since we observed better score when molecular docking performed with protonated Asp206.

4.2.2. Low redox potential laccase: structure of *M. albomyces*

The structure of this laccase is found in the protein data bank with 2,6-dimetoxyphenol (DMP) bound in binding pocket. As difference with the structure of the *T. versicolor*, this structure contains a glutamate (Glu235) in the biding pocket, instead an aspartate (Asp206). Analysis of the structure suggests that the hydroxyl hydrogen of the hydroxyl group interacts with Glu235 via a hydrogen bond. In addition, one of the hydrogen atoms of His508 interacts via a hydrogen bond with the oxygen of substrate. Furthermore, the substrate is stabilized by a number of π-π interactions between the ring of DMP and residues Phe427, Phe371 and Leu429 of the binding pocket.

The molecular docking study suggests that the substrates containing a hydroxyl group exhibit similar interaction as DMP with the protein. Those structures with an acid function besides of the hydroxyl group, there are some poses in which His interacted with acid group shows a hydrogen bonding interaction with Glu235.

About some compounds such as 2-hydroxyisoindoline-1,3-dione (HPI) in addition to the poses that His points to –OH, there are some poses that His was pointed to the –N and –OH had hydrogen binding with Glu.

In 1H-benzo-[1,2,3]triazol-1-ol, there is a pose that –NH shows hydrogen binding with Glu and His points to the –N in the ring. This is addition to the poses that His had interaction with –OH and π-π interactions. Also, in all structures some poses just had hydrogen binding with Glu, however, in this case it cannot be remarked because then how the electron may pass to copper. About ABTS that does not have –OH in the structure, in some poses –SO_3 has interaction with His508 and Asn236 besides of π-π interactions. There is a pose that two –SO_3 group of ABTS has interaction with Asn236 and Trp373 and –NH is perpendicular to the ring of ABTS but the score was worse.

Docking was performed in the same condition with protonated Glu205. The results showed similar poses with substrates with similar score except in case of ABTS that the score for accepted pose was -11.36 kcal/mol.

4.2.3. Bacterial laccase: structure of *B. subtilis*

Structure of a bacterial endospore coat component was crystalized by Enguita and coworkers in 2003. This protein shows activity the same as multicopper oxidases. ABTS bound in the active site of the crystalized structure. The sulfonate group of ABTS shows hydrogen bond to Gly323 and Arg416; moreover hydrogen of His497 is perpendicular to the benzothiazoline ring. The results presented that Arg416, Gly417, Thr415, Leu386 and Pro384 participate in interaction with the ring of the compounds. Besides, ABTS

bound in the same mode in crystalized structure. However, it indicated other poses. For example it had interaction with Arg416 and Thr262, and –NH of His497 pointed to the sulfur in benzothiazoline ring. Or it had interaction with Arg and Gly and His pointed to the sulfur in benzothiazoline ring. In docking of this structure results in contrary to fungal laccase, the interaction between His497 and –SO$_3$ of ABTS has not been observed. It can be concluded that ABTS interaction is different in fungal and bacterial laccase.

Table 4.2 summarizes the surface of active site of laccase structures. It outlined which of them involved in interaction with different substrates.

	MaL (3FU8)	TvL (1KYA)	BsL (1UVW)
Residues in surface of active site	Ala191, Pro192, Glu235, Leu363, Phe371, Trp373, Phe427,Leu429, His431, Ile505, His508	Phe162, Leu164, Asp206, Phe265, Asn264, Phe332, Gly334, Phe337, Pro391, Gly392, His395, His458	Thr262, Pro384, Leu386, Thr415, Arg416, Gly417, Thr418, His419, His497
Residues participate in the interaction	Glu235, Leu363,Phe371, Phe427, Leu429, His431, His508	Phe162, Asp206, Phe265, Asn264, Pro391, Phe337, His395, His458	Leu386, Pro384, Thr415, Arg416, Gly417, Thr418, His419, His497
Property	Hydrophobic but less aromatic	More hydrophobic than bacteria laccase	Wider

Table 4.2. Comparing of residues in surface of active site and participated residues in interaction among three different laccase structures.

Generally, docking results showed that substrates bound near His. In fact, the hydrogen of N$_e$ of His is oriented to the oxygen atom of the phenolic substrate which is the path for electron transfer from substrate to the enzyme. In previous investigations, the syringaldehyde shown in the active site of the enzyme was positioned on the basis of the binding orientation of 2,5-xylidine observed in the *T. versicolor* structure, assuming a similar orientation of phenolic compounds and aniline derivatives (Lahtinen, 2013). In our study also the orientation of the 21 phenolic compounds were similar to the arylamin compound in crystalized structure *T. versicolor* laccase. Moreover, our docking studies suggest that electron transfers to His458 in

the case *T. versicolor*, His508 in *M. albomyces* and His497 in the case of the bacterial laccase, involved in

the coordination with copper in the T1 site.

Table 4.3 summarized the calculated score by MOE program for 3 different laccase structures and

substrates. The lowest energy belongs to 3FU8 structure that means molecular docking produced more

favorable pose for the same substrates in comparison to other two structures. The worst score resides with

bacterial laccase. This bacterial laccase (1UVW) has less hydrophobic and aromatic residues in the activity

site, consequently, find a pose that interacts with residues needs more energy.

Compound	Score (kcal/mol)		
	1KYA	**3FU8**	**1UVW**
2,4,6-trimethylphenol	-4.02	-4.69	-2.16
2,5-xylidine	-3.84	-4.12	-1.22
2,6-DMP	-4.42	-4.71	-2.18
4-hydroxybenzoic acid	-4.10	-3.92	-2.54
3,4-dihydroxy-5-methoxy benzaldehyde	-4.12	-4.30	-2.37
4-hydroxy-3,5-dimethoxy phenylethanon	-3.50	-5.08	-3.29
4-hydroxy-3-methoxy phenyl ethanone	-3.80	-4.38	-3.36
4-hydroxy-3-methoxyphenyl benzaldehyde	-4.17	-4.81	-3.35
HBT	-3.77	-3.66	-1.69
Methyl-4-hydroxy-3,5-dimethoxybenzoat	-4.60	-5.1	-3.65
Methyl-4-hydroxy-3-methoxybenzoat	-3.83	-4.89	-3.91
2-hydroxyisoindoline-1,3-dione (HPI)	-4.07	-4.49	-3.90
N-4-hydroxyphenylacetamid	-4.36	-4.3	-3.53
3-(4-hydroxyphenyl)acrylic acid	-4.36	4.09	-2.66
3-(4-hydroxy-3,5-dimethoxy phenyl)acrylic acid	-4.66	-5.22	-4.23
3,4-dihydroxy-5-methoxy benzaldehyde	-2.61	-4.02	-2.26
Tempo	-3.59	-4.37	-2.01
violuric acid	-3.99	-3.88	-1.21
ABTS	-4.81	-7.71	-3.51

Table 4.3. Molecular docking scores of 3 different laccase with substrates.

The docking analysis of *Pycnoporus cinnabarinus* laccase with acetosyringone and syringaldehyde revealed the hydrogen binding between these substrates and Asp in active site of the enzyme (Prasad et al., 2012). It was mentioned by Bruyneel and coauthors (2012) that phenolic compounds had one productive docking with the –OH group forming hydrogen bonds with Asp (Bruyneel et al., 2012). In these studies it was suggested that proton may transfer to Asp or Glu conserved residues in fungal laccases.

According to our docking results this residue is far to make it possible except in some cases of substrates. Besides, Asp/Glu does not exist in all fungal laccase, such as *T. hirsuta* (Polyakov et al., 2009). However, there is a water molecule between DMP and Glu in *M. albomyces* crystalized structure. In the case of ABTS it has different mechanism and there is no proton transfer in ABTS_laccase complex (Fabbrini et al., 2002).

Our docking study displayed sulfonate group of ABTS bound to Asn of fungal laccases in the orientation that hydrogen of His became perpendicular to the ring of ABTS which means electron transfers from the ring to the His. This is similar pose to the crystalized structure of *B. subtilis* with ABTS (Enguita et al., 2003). According to the previous study (Bertrand et al., 2002) since there is no difference in K_m of this compound in different pH that it refers to the different protonated state of Asp/Glu in the binding pocket, thus, in case of ABTS no hydrogen can be extracted from the reducing substrate.

According to the Proton-coupled electron transfer (PCET) mechanism proton and electron should transfer to different atoms. As it was mentioned in other articles PCET occurs in metalloenzymes (Fernandez et al., 2012; Hammes-Schiffer, 2001). PCET reactions involving the transfer of an electron and a proton may be sequential, where either the electron or the proton transfers first, or concerted, where the electron and proton transfer simultaneously (Hammes-Schiffer and Soudackov, 2008). In PCET, the proton and the electron (i) start from different orbitals and (ii) are transferred to different orbitals which is occurred in laccase. In case of laccase some QM studies should be performed to make it clear and demonstrate if proton or electron transfers first.

4.3. Molecular dynamics simulations

Structures retrieved from a protein databank that lack hydrogen atoms. So these have to be added to the file. Due to the fact that the methods to retrieve molecular structures are not perfect and especially in x-ray-structures there are crystal contacts, which lead to a compaction of the molecules. Furthermore, hydrogen atoms are added to relatively arbitrary positions near their neighbors. Thus there are atoms lying too close together and the energy is raised high above natural energy levels. These high energy interactions lead to local distortions which result in an unstable simulation. They can be released by minimizing the energy of the structure before starting a simulation.

To raise the temperature from 0K to the desired value, 300K, first initial velocities should be assigned to the atoms corresponding to a Gaussian distribution for a certain temperature to provide the system with energy. After having heated the system so quickly, the structure might be unstable and the temperature may drop too low. That is why the system should be equilibrated properly before running the real dynamic simulation, the production run. As stated before, equilibration is the process where the kinetic energy and the potential energy evenly distribute themselves throughout the system.

Force field parameters and electrostatic charges of atoms for protein and ligand were derived from the AMBER libraries [parm99 version of the all-atom AMBER force field (Cornell et al., 1995)]. The parameter set for the copper center (see Tables 4.3-4.5) involving all Cu–L distances and L–Cu–L_ angles, were taken from the DFT-optimized model structure that has been done Comba and coworkers (2002) (Comba and Remenyi, 2002).

Atom	Mass(u)	Van der Walss Radius [Å]
Cu(I,II)	63.546	1.17 from (Bartolotti et al., 1991)

Table 4.3. Mass and van der Waals Parameters Introduced to the AMBER Force Field.

Bond	kb [kcal/(mol*Å2)]	$r0$(Å)
Cu1-S	5.00	2.87 (De Kerpel and Ryde, 1999)
Cu1-SH	50.61	2.22
Cu1-NB	21.25	2.03
Cu1-OH	10.00	2.35

Table 4.4. Ideal bond distances and stretching force constants introduced to the AMBER force field.

Angle	θ_0 (°)
Cu1-S -CT	113.81
Cu1-SH-CT	101.31
Cu1-NB-CR	122.10
Cu1-NB-CC	122.90
Cu1-NB-CV	122.90
Cu1-OH-H	120.00
S -Cu1-SH	113.39
S -Cu1-NB	96.50
SH-Cu1-NB	122.50
NB-Cu1-NB	99.07
OH-Cu1-NB	90.00

Table 4.5. Ideal valance angles introduced to the AMBER force field.

Three selected structures have been further characterized by means of MD simulations. We evaluated the effect of protonation state of a conserved residue in fungal laccase, Asp/Glu, in binding of substrates. In simulation of 1KYA with XYD as a substrate with protonated Asp206, after 7ns the substrate started going far from His458, then in 11ns it came back near to His. This ligand was unstable in binding pocket, it went far and came back to the binding site in molecular dynamic simulation. This simulation has been repeated with non-protonated Asp206. There is no difference between results. We obtained the same result.

It was stated in other researches, the role of 2,5-xylidine as a weak inhibitor of *Rigidoporus lignosus* laccase. The ABTS and 2,5-xylidine compete one with another, it is suggested that they combine with enzyme at the same *locus* and the inhibition is competitive (Cambria et al., 2010). Therefore, XYD may consider as a weak substrate that was not stable for more than 7ns of MD simulation in the active site of 1KYA structure. In other study, it was pointed that XYD was used as a laccase inducer in the fungus culture. This arylamine is a very weak reducing substrate of the enzyme (Strong, 2011).

Molecular dynamic simulation of 3FU8 with DMP was more stable. DMP stayed in the binding pocket for 20ns when Glu235 was protonated. However, it showed stability for 25ns when Glu235 was non-protonated. As the results showed DMP stayed more stable in the binding pocket in comparison with MD simulation of XYD. In fact, this structure is a phenolic ligand. The phenolic structures are the main group of laccase substrate.

In addition, DMP had interaction with residues in the binding pocket longer when Glu235 was non-protonated. However, if we remark this residue as a protonated one, how the proton may transfer? What about net of water in the environment? The position of water molecules were observed during the simulation. DMP has stayed near His508 and Glu235 until there was a water molecule between Glu and DMP. In the moment that the water molecule moved in the simulation and went far DMP started going far, too. Furthermore, this water molecule was observed in crystal structure. The mode of proton transfer was not the objective of this study. Although, these results illustrate that water molecules have role in the interaction.

In case of 1UVW, as it explained before, there is no Glu/Asp near the active site of enzyme. So, there is just one type of simulation. The results indicated the pose of ABTS in the pocket was similar to crystalized structure for 26ns. Meanwhile in some moments of simulation hydrogen atom of His497 pointed to sulfur in benzothiazoline ring, the similar pose to docking result. These two poses have been observed in docking results. But ABTS stayed in the first pose longer and it is similar pose in crystalized structure. As a conclusion the interaction between ABTS and enzyme occurs in the pose that sulfonate binds to Gly323 and –H of His497 is perpendicular to the ring for electron transfer.

4.4. QMMM

In this study, we calculated redox potential of T1 site for low redox potential laccase structure (3FU8) using QMMM-2QM-MD. Laccase catalyze a substrate, received one electron at T1 site and sequentially reduced the substrate. Therefore, T1 site has two oxidation states, Cu^+ and Cu^{+2}. Likewise, the DMP has two oxidation states, DMP and $DMP^{-\bullet}$. Among three structures that we did other studies about them, we chose 3FU8. Because DMP just has two states in comparison to ABTS that be able to have different states. As well, in MD simulation this ligand was more stable in comparison to XYD in 1KYA structure. Therefore, it is more suitable structure for this calculation.

4.4.1. QM calculation

The QM calculations were performed with the Perdew–Burke–Ernzerhof (PBE) density functional (Perdew et al., 1996), together with the def2-SVP basis set for H, C, N, O, S, and CU basis set (Schäfer et al., 1994, 1992). The calculations were sped up by expansion of the Coulomb interactions in auxiliary basis sets, the resolution-of-identity approximation (Eichkorn et al., 1997, 1995). The calculations were performed with the Turbomole 6.5 package (Case et al. 2005) (a development of University of Karlsruhe and Forschungszentrum Karlsruhe GmbH, 1989-2007). The structures were optimized until the change in energy between two iterations was below 2.6 $Jmol^{-1}$ and the norm of the maximum norm of the gradients was below 10^{-3} a.u. The Cu ion was assumed to be in the high-spin state. The spin-unrestricted formalism was employed. The two QM systems were studied in both the oxidized and the reduced states. This means that the T1 site and ligand had a total charge of either zero or one, with no or one unpaired electron.

4.4.2. MM and MD calculations

All MM calculations were run with the sander module in the Amber software (Case et al., 2005) using the Amber 1999 force field (FF99) (Cornell et al., 1995; Wang et al., 2000). The QM system was represented by charges fitted to the electrostatic potential, sampled according to the Merz–Kollman

scheme,(Besler et al., 1990) as implemented in Turbomole, but with a higher-than default density of points, 2000–3000 points/atom. The charges on the CL atoms were adapted so that the total charge of the amino acid (including both QM and MM atoms) was the same as the sum of QM charges of the corresponding QM fragment (Ryde and Olsson, 2001). Thereby, we ensure that the total charge of the simulated system is an integer, but we still allow charge transfer within the QM system (the amino acids with QM atoms have non-integer total charges).

In the MD simulations, the bond lengths involving hydrogen atoms were constrained using the SHAKE algorithm (Ryckaert et al., 1977). The water solvent was described explicitly with the TIP3P model (Jorgensen, 1989). The electrostatics were treated with the particle-mesh Ewald method (Darden et al., 1993; Essmann et al., 1995) with a grid size of 80, a fourth-order B-spline interpolation, a tolerance of 10^{-5}, and a real-space cut-off of 8 Å. The temperature was kept constant at 300 K and the pressure at 1 atm using the Berendsen weak-coupling algorithm (Berendsen et al., 1984) with a time constant of 1 ps. Five simulations were run. First, the structures were subjected to 1000 steps minimization, keeping all non-hydrogen atoms restrained to the original crystal structure with a force constant of 418 kJ/mol/Å^2. Next, a 20 ps MD simulation with a constant volume was run, still keeping the heavy atoms restrained. Third, a 20 + 50 ps MD simulation with a constant pressure was run to equilibrate the box size. During the first 20 ps, the non-hydrogen atoms were restrained, whereas during the last 50 ps, these restraints were removed. Fourth, a 200 ps equilibration at a constant volume was run without any restraints. Finally, the systems were simulated for 10 ns in a constant volume, and coordinates were sampled every 2 ps. MD simulations were performed for both electronic states, RO and OR. In the QM/MM energy calculations, no periodic boundary conditions were used. Instead, the MM system was centered on the QM system and an infinite cut-off was employed.

The calculations on the laccase are based on the 1.8 Å crystal structure of laccase (PDB code 3FU8). The whole protein was included in the calculations, as well as a varying amount of solvent water molecules. All Glu and Asp residues were assumed to be deprotonated, and all Lys and Arg residues were assumed to

be protonated. The protonation state of the His residues was assigned on the basis of their solvent exposure, the hydrogen-bond network, and the local surroundings: His residues on the protein surface were assumed to be protonated on both N atoms, whereas the remaining His residues, which are ligands of the T1 and T23 Cu ions, were assumed to be protonated on the atom not coordinating to the metal. The Cys ligand of the T1 Cu site was assumed to be deprotonated.

The crystalized structure of this enzyme is a dimer protein. Hence, there are 4 different states to study, each monomer is in oxidized T1site and reduced substrate state (OROR), one monomer has oxidized T1site with reduced substrate whereas the other one has reduced T1 site and oxidized substrate (ORRO or ROOR), and the last state is that each monomer is in reduced T1 site and oxidized substrate state (RORO).

We wanted to calculate the reorganization energy (RE) of the electron transfer between T1 site and the substrate using the methods developed by Warshel, Sprik, and Blumberger, as well as redox potential. The MD simulations were performed at the MM level. Therefore, force-field parameters of the T1 center and the substrate in the two oxidation states are needed.

Several methods exist for the treatment of metal centres by MM94 and there are already several sets of parameters for the T1 site (Comba and Remenyi, 2002; De Kerpel and Ryde, 1999). We have performed a detailed parametrisation of the two metal centres in both oxidation states using the ideal method suggested by Norrby and Liljefors (Hu et al., 2011). This approach uses also QM data in the form of optimised structures and the Hessian matrix. However, in this case it is not assumed that the QM-optimised bonds, angles, and dihedrals are unstrained and double-counting is avoided. Instead, all bonded parameters are optimised by an iterative procedure in which a target function is minimised, involving all bonds, angles, dihedrals, and Hessian elements of the complex, performing a full MM geometry optimisation and frequency calculation for each sets of parameters. Thereby, it is ensured that the final parameters reproduce the QM structure and Hessian as well as possible. This approach has frequently been used to obtain accurate structures and energies for metal sites (Nilsson Lill et al., 2010).

Such a parametrisation was performed as is described in the Methods section both for the T1 and ligand and in both their reduced and oxidised states. The performance of the parametrisations is described in Table 4.6.

	T1ox	T1red	DMP	DMPox
Bonds	0.009	0.01	0.003	0.004
Angles	0.685	0.903	1.113	0.318
Dihedrals	1.029	1.746	0.661	0.17
Coordinates	0.12	0.117	0.034	0.008
Max coord	0.211	0.21	0.074	0.017
R^2 Hessian	0.986	0.993	0.995	0.989

Table 4.6. Performance of the various parametrizations. The quality measures are the correlation coefficient (r^2) between all QM and MM Hessian elements, the root-mean-squared deviations (RMSD) for all bonds, angles, dihedral angles, and coordinates between the MM and QM optimized structures (in A or degrees), the maximum deviation (Max) for the coordinates. Results are shown for the parametrization of the T1 site in the oxidized and reduced state, as well as the substrate.

It can be seen that all four parametrizations perform excellently: They reproduce all bond lengths in the QM structure with a root-mean-squared deviation (RMSD) of less than 0.01 Å, the angles with an RMSD of 0.3-1.1 °, the dihedral angles with an RMSD of 0.1- 1.7°, and the coordinates with an RMSD of 0.008-0.12 Å and with a maximum difference of 0.02-0.21 Å. Moreover, the correlation coefficient between the QM and MM Hessian elements is above 0.98 for all four force fields.

Once the metal sites have been parametrized, 10 ns MD simulations (after equilibration) were run for the four oxidation states, RORO, ROOR, OROR and ORRO (Figure 4.5). The MD trajectories were stable. The reorganization energy is the energy it would take to force the reactants to have the same nuclear configuration as the products without permitting electron transfer. The RE was calculated by the energy difference between the oxidized state in its equilibrium geometry and in the geometry of the reduced state, and vice versa. For the MD simulations, we calculated the vertical energy difference between the two electronic states, ORRO and RORO, $\Delta E_{et} = E_{RORO} - E_{ORRO}$ for all snapshots obtained in the MD simulations of the two states. Then, the RE was estimated from Eqn. 1.

$$OROR \longrightarrow ROOR$$
$$\downarrow \qquad\qquad \downarrow$$
$$ORRO \longrightarrow RORO$$
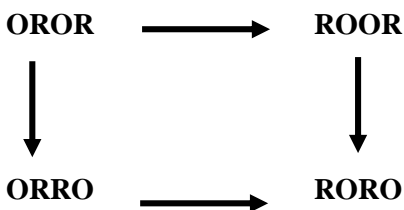
Figure 4.5. Illustration of different states of 3FU8 structure for QMMM-2QM/MD calculation.

Finally, we can also calculate the driving force in the RORO → ORRO reaction, i.e. the difference in the redox potentials of the RORO and ORRO states, using Eqn. 15. Table 4.7 indicates the reorganization energy and redox potential value.

	RE (kJ/mol)	SE	E^0 (kJ/mol)	SE
OROR to ROOR	246	1	92	1
OROR to ORRO	227	1	74	1
ROOR to RORO	240	1	17	1
ORRO to RORO	203	1	7	1

Table 4.7. Reorganization energy and redox potential value of T1 site and DMP in 3FU8 structure calculated by QMMM-2QM/MD.

Since we used dimer structure, the four sites are quite close together. our results indicate that there is a large communication between the various redox states, i.e. that the difference in redox potentials changes from 7-17 to 74-92 kJ/mol if the redox state of T1Cu and DMP in the other subunit changes.

Experimentally, the redox potential of free DMP is +580 mV vs. NHE (Jovanovic et al., 1991) and that of the T1 site of the protein is +470 mV vs. NHE (Kiiskinen et al., 2004). That means the CuT1ox/DMPred state should be around 11 kJ/mol (580-470=110 mV) more stable than the CuT1red/DMPox state. In the experiment DMP was not used for measuring the value, therefore, we do not know how much of the effect comes from DMP and this makes the comparison with experimental value difficult. We can conclude that the sign of our calculated potential is correct, and we correctly predict that CuT1ox/DMPred state is more stable than the CuT1red/DMPox state.

This method has been used before to calculate the RE for the internal electron transfer between the T1 and T23 centers in the MCO enzyme CueO that was 0.94-1.38 eV. They have also estimated the energy difference between the two electron-transfer states and the calculations indicate that the OR state is more stable (Hu et al., 2011). Our result also showed that OR state is more stable than RO state. The reorganization free energies for the intramolecular electron transfer in Ru-modified cytochromes has been calculated 1.2-1.3 eV (Tipmanee et al., 2010). We obtained T1 site RE range of 2.1-2.55 eV for MaL laccase. The value have been measured experimentally for PM1L, 1.93 eV (Pardo et al., 2016). The value that we calculated is overestimated. It has been discussed that using nonpolarizable force field may lead to overestimation of RE value (Blumberger and Lamoureux, 2008; Tipmanee et al., 2010).

4.5. Starting point for directed evolution

Our starting point was high redox potential laccase OB-1 mutant (Maté et al., 2010). In addition to its high redox potential feature, it is highly thermostable and readily secreted by yeast. It has 80% similarity with TvL which our molecular docking and simulations has done with it.

Since we intended to know which residues in binding pocket has effect on redox potential we began with residues that were different in HRPL and LRPL species. Therefore, our starting point for LRPL was MtL T2 mutant (Bulter et al., 2003) which has already 11 mutations. MtL T2 has 76% of identity to MaL which our computational studies was performed on its structure. Table 4.8 and figure 4.6 are shown the comparison of residues in binding pocket of these structures.

4.6. Making the mutagenesis library

The generation of diversity was emulated by taking advantage of the eukaryotic machinery of *S. cerevisiae* (Alcalde, 2010). The high level of homologous recombination of *S. cerevisiae* allowed us to repair the mutagenized products within the linear vector in vivo by engineering specifically overlapping regions.

MtL T2	MaL	TvL	OB-1
G191	A191	F162	A162
A192	P192	L164	T164
L363	L363	F332	F331
L296	A296	F265	S264
W373	W373	F337	F336
L513	L513	F463	F460
E^{o}~ 450 mV	E^{o}~ 470 mV	E^{o}~ 790 mV	E^{o}~ 760 mV
(Zumarraga et al. 2008b)	(Kiiskinen et al. 2004)	(Xu et al. 1996)	(Mate et al., 2013)

Table 4.8. Comparison of binding pocket residues in different laccase structures.

We made saturation mutagenesis library for F331 and 336 positions in OB-1, also, we made site directed mutagenesis in A192L, L296F, L363F, W373F and L513F positions in MtL T2. For our screening we used ABTS to check laccase activity, Molybdenum hexacyanide and violuric acid to assay the improvement of redox potential value. The clones that we saw increasing activity with Molybdenum compound and violuric acid we considered them as a clone that probably it increases the redox potential value.

The results showed that in OB-1 mutagenesis library the best mutant was substitution of F331H. It showed increasing activity with Molybdenum compound. The activity was 2.28 fold higher than the parental type. In case of F336 we did not find any clone that showed improvement in screening assay.

Table 4.9 shows the result of screening on MtL T2 structure. We did not observe any improvement in residues positions 296, 363, 373 and 513. Previously, Cambria and his colleagues (2012) by computational study discussed that putative stacking interactions in HRPL structures such as RlL, TvL and CcL demonstrates the formation of pairs between the histidine imidazole rings involved in the T1-binding site

Figure 4.6. (a) Binding pocket of MtL T2 (red residues) and MaL (green residues), (b) binding pocket of OB-1 (red) and TvL (green).
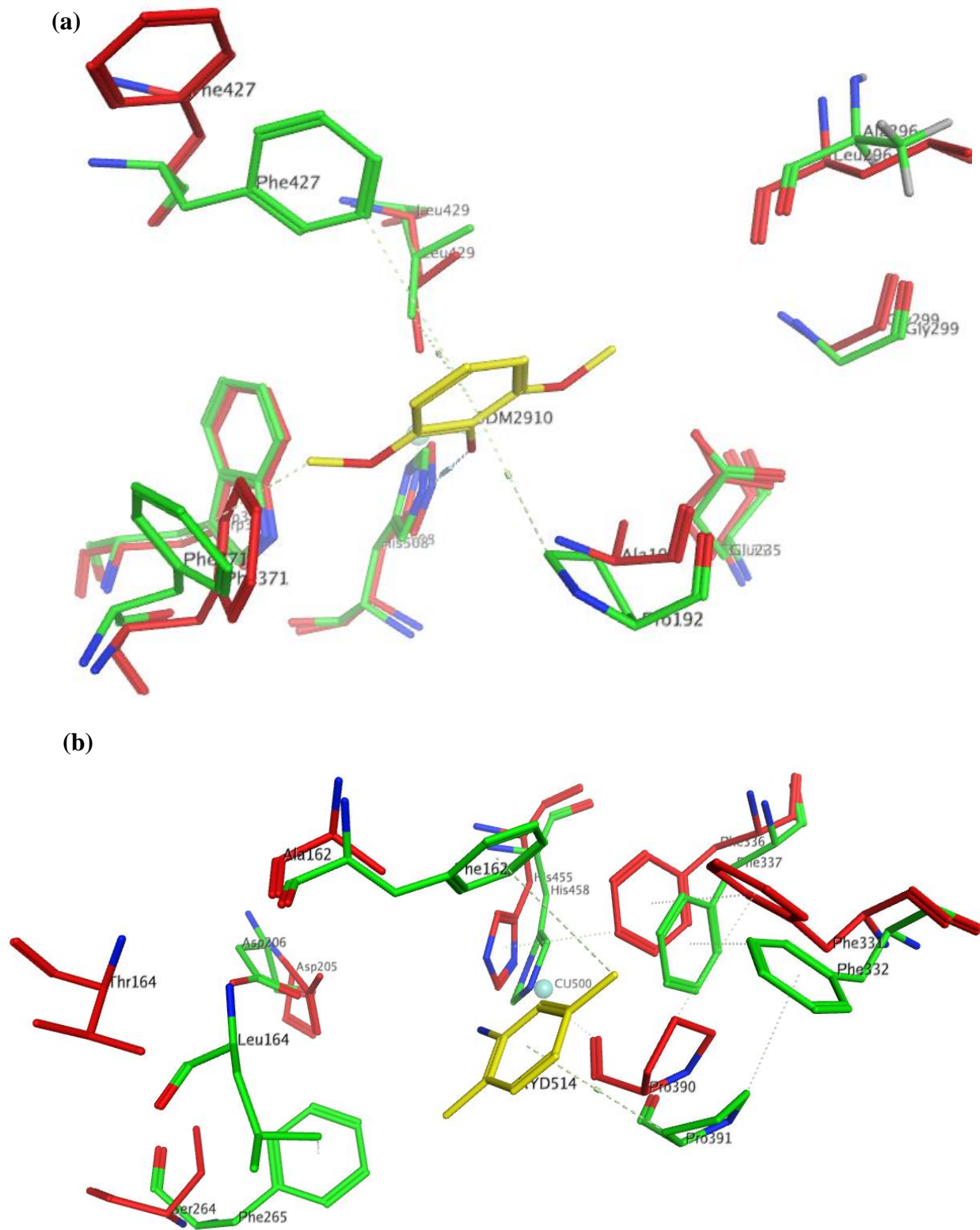
and the conserved phenylalanine aromatic ring in the second coordination shell, whereas in MaL the equivalent residue is replaced by Trp373. Therefore, they concluded that this position could influence the redox properties of the T1 (Cambria et al., 2012). Our result revealed that substitution of Trp373 to phenylalanine did not improve the T1 redox potential value.

In 1998, Xu and coworkers have demonstrated that the replacement of an L513 by phenylalanine at the position corresponding to the T1 Cu axial ligand does not significantly affect the properties (including E^0) of theT1 Cu (Xu et al., 1998). Our results confirmed their result.

In case of A192L the enzyme became inactive. We did not see activity even with ABTS. Therefore, we got the conclusion that this point can be important in redox activity of enzyme and we decided to make a combinatorial library for position 192 and 296 to test the effect on activity and redox potential value.

MtL T2	Activity comparison to parental			
Position	Result	ABTS	Molybdenum hexacyanide	Violuric acid
Ala 192 Leu	inactivated	-	-	-
Leu 296 Phe	The same as parental type	1	1	1
Leu 363 Phe	The same as parental type	1	0.5	0.3
Trp 373 Phe	Very low activity			

Table 4.9. Screening assay results of site directed mutagenesis of MtL T2.

To reduce codon redundancy and screening effort in combinatorial saturation mutagenesis library (Kille et al., 2013) around 1500 clones were explored. Among those clones, 4 of them showed improvement in activity with violuric acid and Molybdenum compound. The clone contained A192P and L296W (3H12) mutation and clone contained A192P and L296L (19G8) showed activity with violuric acid 1.23 and 1.33 fold higher than parental type, respectively (Table 4.10). In figure 4.7, it indicated the different color of interaction with violuric acid between 19G8 and parental type
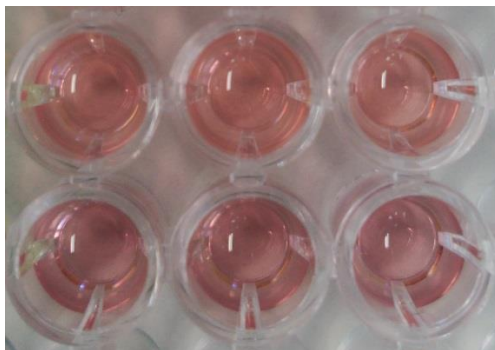
Figure 4.7. Different color in screening assay with violuric acid that related to different activity of 19G8 mutant (up) in comparison of wild type (bottom).

Moreover, the clone contained A192R and L296W (15H11) and clone with mutation A192R and L296L (5B4) showed higher activity with Molybdenum compound in comparison to parental type. However, parental type did not show any activity with Molybdenum compound and we cannot report how many folds of improvement those clones have in comparison to the parental type.

MtL T2			Activity comparison to parental		
Position of mutations	**Method of mutation**	**Mutated**	**ABTS**	**$[Mo(CN)_8]^{4-}$**	**Violuric acid**
Ala192 + Leu296	Combinatorial saturation mutagenesis	A192P L296W	1.34	0.75	1.23
		A192P L296L	1.22	n.d.	1.33
		A192R L296W	1.17	56.03	n.d.
		A192R L296L	1.14	52.57	n.d.

Table 4.10. Activity of best clones. Clones that showed better activity in combinatorial saturation mutagenesis library of MtL T2 has been slected.

We also made another mutagenesis library in T2/T3 site in 433 and 500 position. We performed site directed saturation mutagenesis library for M433 and L500. Nonetheless, we did not detect any improvement in activity with 3 compounds of screening assay.

4.7. Thermostability

Thermostability of the different mutants along directed evolution did not vary significantly, so the final mutant showed thermostability profiles equivalent to the parental type MtLT2 (Figure 4.8). Generally, mutations conferring stability against temperature can also have a beneficial effect against other denaturing factors (such as the presence of organic solvents) and vice versa. In our case, however, mutations introduced during artificial evolution not improved thermostability.

The parental type and 19G8 mutant conserved more than 60% and 70% of their residual activity, respectively, at pH 3.0 after 1 h, but not the rest. In contrast, all mutants were stable in the pH range 5.0-9.0, although parental type kept less than ~80% of its residual activity at pH range 7.0-9.0 and it showed more stability at pH 5.0 and 6.0 (See Figure 4.9). Stability at high pH values can be explained by the fact that inhibition of the TNC by hydroxide ions reduces auto-oxidation of laccase and thereby stabilizes the enzyme (Alcalde, 2007).
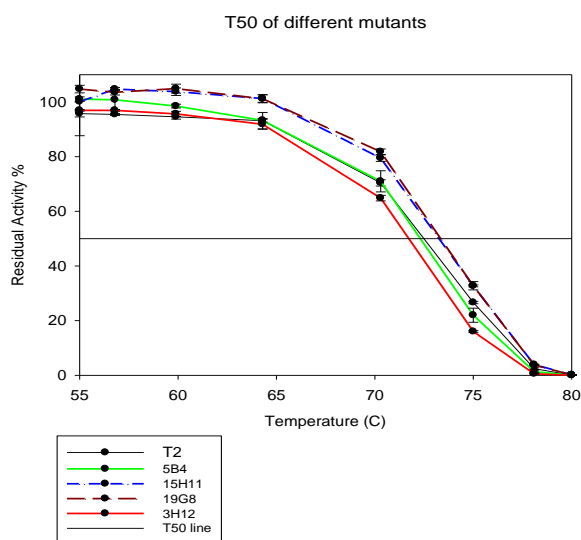
Mutant	T_{50} (°C)
3H12	71.6
T2	72.4
5B4	72.3
15H11	73.2
19G8	73.2

Figure 4.8. Thermostability profile of parental type and mutants. The activities were measured at different times with 3 mM ABTS in citric phosphate buffer pH 4.0. Activities were normalized to the initial activity at room temperature before incubation. Each point represents the mean of three independent experiments.
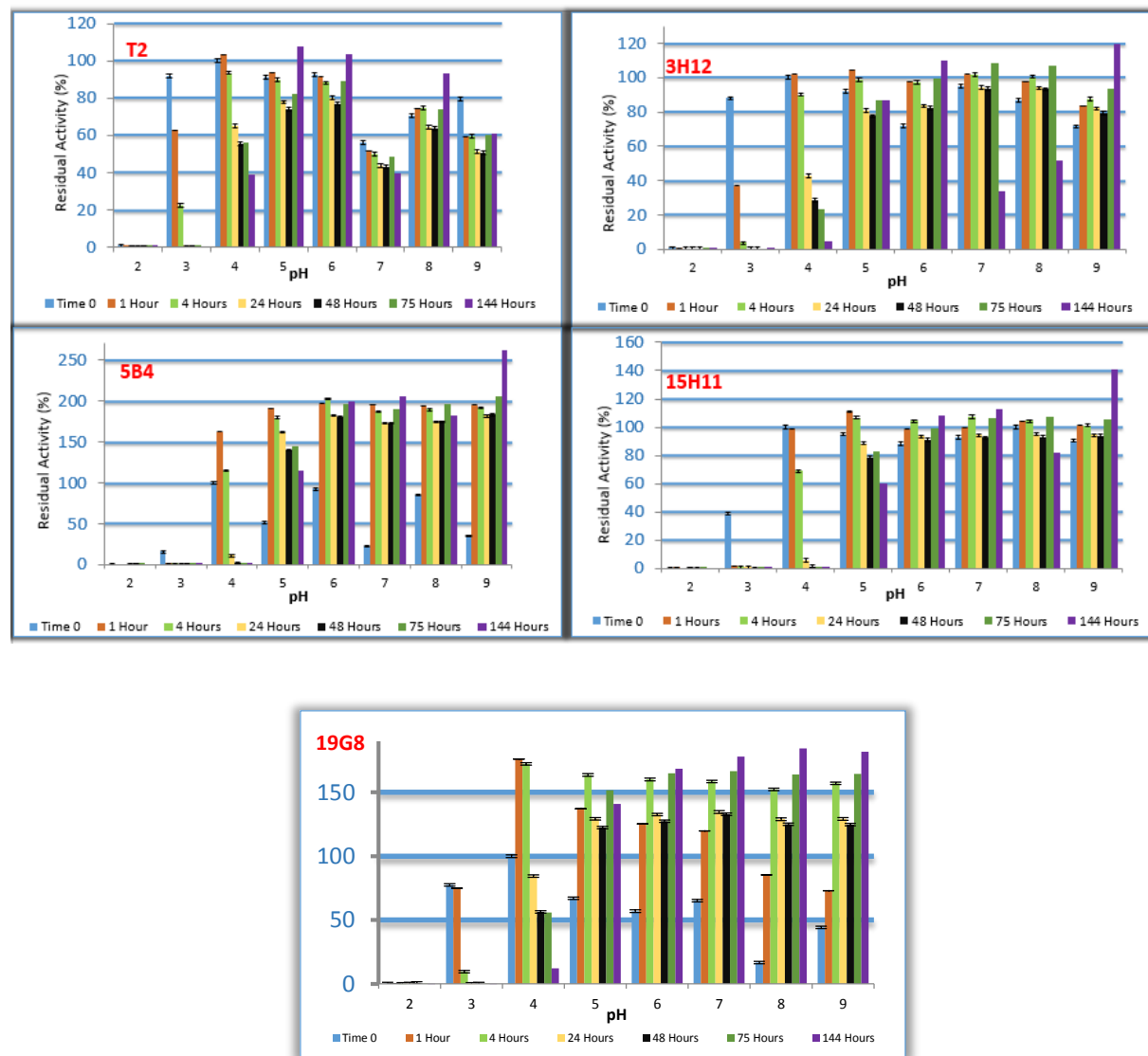
Figure 4.9. pH stability of the parental type and mutants. Enzyme samples were incubated in 100 mM Citrate-Phosphate-Borate buffer at different pH values, and the residual activity was measured with 3 mM ABTS.

4.8. Optimum activity profile and pH stability

The optimum pH for laccases described generally 3.0-5.0 in the range (Shleev et al., 2004). At low pH, the protonated residues such as Asp or Glu in the binding pocket of laccase helps to contain the negatively charged ABTS in the binding pocket, partly explaining why fungal laccases are most active toward ABTS at low pH (for many other substrates, pH_{opt} is substantially higher) (Christensen and Kepp, 2014).

The activity of parental type and all mutants were optimal at pH 4.0 for ABTS and conserved 70% of relative activity at pH 5.0. It retained around 30% of relative activity of MtL T2, 5B4 and 15H11 at pH 6.0 for ABTS. The results showed that the activity of parental type, 3H12 and 19G8 were optimal at pH 3.0 for DMP while it was optimal at pH 4.0 for 5B4 and 15H11. Also, all mutants and parental type hold upto over 60% of relative activity at pH 6.0 for DMP (Figure 4.10).
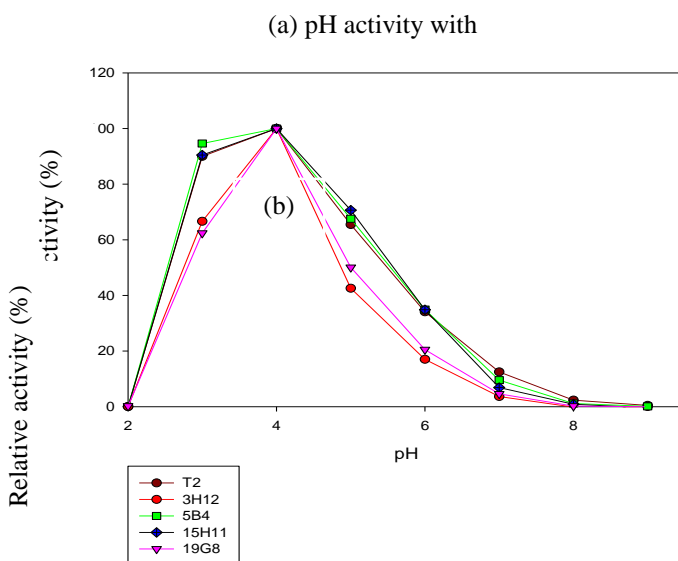
(a) pH activity with

(b) pH activity with DMP
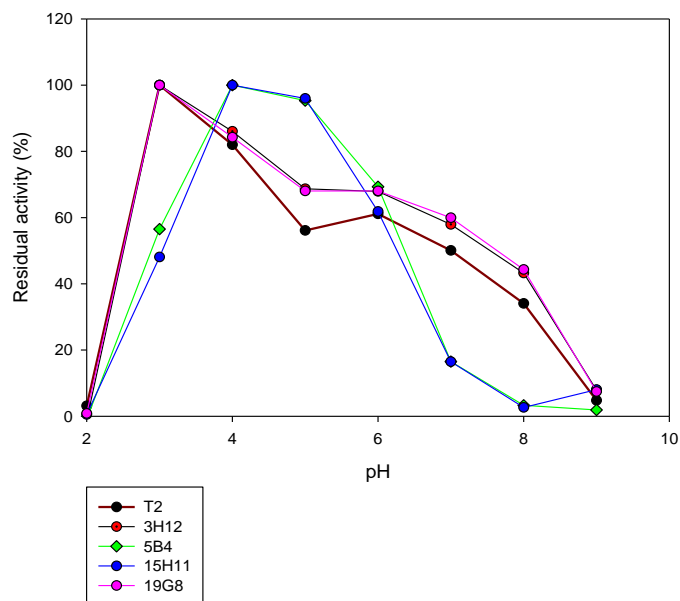
Figure 4.10. Activity profiles at different pHs of MtLT2 parental type and mutants. The activity was measured with (a) ABTS 3 mM and (b) DMP 3 mM. Laccase activity is normalized to activity of its optimum value. Each point represents the average of three independent experiments. Mutants included 3H12, 5B4, 15H11 and 19G8.

Most laccases from fungi such as *Coltricia perennis* (Kalyani et al., 2012), *Paraconiothyrium variabile* (Forootanfar et al., 2011) and *Scytalidium thermophilum* (Ben Younes and Sayadi, 2011) have good stability in near neutral conditions. Laccases from *Trametes pubescens* and *Podospora anserine* were found to have good stability under alkaline conditions (Si et al., 2013), similar to the mutants that have been produced in this project.

4.9. Production and purification of mutants

4.9.1. Expression in *S. cerevisiae*

The different libraries laccases obtained throughout the process of artificial evolution were created using the full laccase gene. *S. cerevisiae* expression of native and mutant laccases cloned into the vector pJRoC30 developed under appropriate conditions of temperature, aeration and agitation (see Section

3.6.19.1 Materials and Methods). Approximately after 36h our cultures reached to maximum OD (OD~36) and activity (0.33 U/mL).

4.9.2. Purification of laccase

The different variants were purified to homogeneity with 4 consecutive steps (see section 3.6.19.2 Materials and Methods). The crude extract (900 mL) was centrifuged. The sample was subjected to two steps of fractional precipitation with $(NH_4)_2SO_4$ 60% to 95% (w/v) (Table 4.11). After treatment, fractions with laccase activity were subjected to two consecutive purification steps on anion exchange columns: first on a DEAE-Sepharose column weak anion exchange and subsequently in a heavy exchange MonoQ column. The average final yield was ~ 80%. All purification steps were carried out at room temperature, given the high stability MtLT2 and its variants. Table 4.12 summarizes the concentration, total and specific activity of MtL T2 and 2 mutants after the purification protocol used in this thesis.

$(NH_4)_2SO_4$ Saturation %	Supernatant Act (U/L)	Pellet Act. (U/L)	Supernatant V (mL)	Pellet V (mL)	Supernatant U	Pellet U	Total U	Supernatant %	Pellet %
650 mL of the fermentation MtL T2 with total activity 223 U/L (145 U)									
60	175	0.019	770.0	9.5	134.8	0.0	134.8	100.0	0.0
95	0.0	10780	850.0	17.3	0.0	186.5	186.5	0.0	100.0
900 mL of the fermentation 5B4 muatant with total activity 531 U/L (478 U)									
60	595	334	1042.0	17.2	620.0	5.7	625.7	99.1	0.9
95	23	12714.0	1147.0	21.0	26.4	267.0	293.4	9.0	91.0
950 mL of the fermentation 19G8 muatant with total activity 152 U/L (144U)									
60	111	1126	1066.0	24.0	118.3	27.0	145.4	81.4	18.6
95	0.0	3393	1185.0	45.0	0.0	152.7	152.7	0.0	100.0

Table 4.11. Fractional precipitation steps.

Enzyme(Laccase)	Total activity U/mL	concentration mg/mL	specific activity U/mg	supernatant U/L	Secretion level mg/L
T2	115	2.02	57.02	223	3.91
5B4	1475	14.46	102.01	531	5.21
19G8	146	2.28	64.15	208	3.25

Table 4.12. Activity of MtL T2 and mutants after purification.

Electrophoresis under denaturing conditions (in the presence of SDS) showed a major band of pure laccase around ~130 kDa (Figure 4.11).
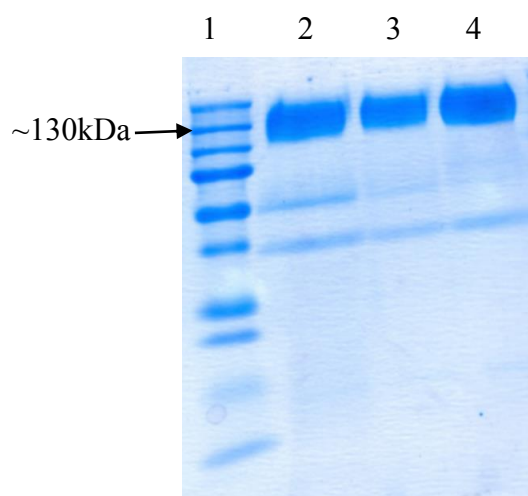
Figure 4.11. SDS-PAGE electrophoresis of laccase after purification. Line 1, molecular weight marker of proteins; line2, MtL T2; line3, 5B4; line4, 19G8.

4.10. Kinetic characterization of purified laccases

Once purified laccase parental MtLT2 and the best mutants directed molecular evolution process, the biochemical characterization of each mutants was carried out. To measure the kinetic properties of a specific enzyme reacting with a particular substrate, several constants are commonly used. From the Michaelis–Menten equation, K_m represents the substrate concentration at which the velocity rate is half maximal; k_{cat} is the number of substrate molecules turned over per enzyme molecule per second. As a result, the

ratio k_{cat}/K_m, so-called specificity constant, is used to compare enzyme efficiency in catalyzing the transformation of their substrate under a given set of conditions.

	Kinetic constants against ABTS			Kinetic constants against DMP		
	k_{cat} (S⁻¹)	K_m(μM)	k_{cat}/K_m	k_{cat} (S⁻¹)	K_m(μM)	k_{cat}/K_m
T2	156 ± 11	14 ± 4	11	105 ± 5	26 ± 6	4
5B4	113 ± 10	20 ± 1	5.6	67 ± 5	147 ± 46	0.5
19G8	171 ± 9	18 ± 5	9.5	86 ± 3	36 ± 7	2.4

Table 4.13. Kinetic constants were measured against ABTS and DMP.

Table 4.13 shows the kinetic constants of the purified laccases with ABTS and DMP as substrate. The lowest K_m values for MtL T2 and mutants were found with ABTS, which indicated higher affinity for this substrate (Table 4.10). This substrate has 2 sulfonate group that negatively charged. Also, it is a substrate with source of electron to donate to T1 site (Christensen and Kepp, 2014). Consequently, it showed better affinity than phenolic substrate such as DMP that does not contain negatively charged group or chain.

Formerly, researchers discussed that optimal proficiency of laccases for ABTS relates to positively charged residues in the binding pocket. Whereas charge interactions appear crucial for tight binding of substrate contained negatively charge group such as ABTS (Christensen and Kepp, 2014). Nevertheless, our result did not confirm that. The mutant that had substitution of A192R, 5B4, did not indicate better affinity to ABTS. We should consider that less bulky Ala sidechains allow increased oxidation of larger substrates. This issue has been investigated in TvL(Galli et al., 2011) and TviL (Tadesse et al., 2008).

The specificity constants, k_{cat}/K_m values, varied from 11 μM⁻¹ S⁻¹ (MtL T2) for ABTS up to 0.5 μM⁻¹ S⁻¹ (5B4) for DMP (Table 4). For MtL T2, the k_{cat}/K_m value was double the 5B4 mutant for ABTS and it was a more efficient catalyst for that substrate. In addition, K_m value of 19G8 that has Pro192 in binding pocket is lower than 5B4 mutant which indicates that it has more affinity to phenolic substrates since the binding pocket is more hydrophobic and allows a better fit for phenolic structures binding site T1.

Zumarraga and colleagues (2008) measured the kinetic constants of MtL T2 against ABTS at pH 4.5. The values for k_{cat} and K_m were 28.3 S^{-1} and 120 μM^{-1}, respectively. Also, the values against DMP were 25.8 S^{-1} and 175 μM^{-1} (Zumarraga et al., 2008a). In our investigation, we measured kinetic values at pH 4.0 and the results showed more efficiency at this pH. There is a Glu in activity site and close to T1 site. The pk$_a$ value for this residue is 4.07. At pH 4.0 it is protonated, therefore, the binding pocket of this structure is less negatively charged. This means that substrate can bind to the activity site easier and consequently less negative charge facilitate that T1 site receive electron easier. However, at pH > 4.0 Glu is non protonated and negatively charged which cause binding and receiving electron with lower efficiency.

4.11. Computational studies of mutants

After characterization of mutants experimentally, we analyzed the mutants by computational study. First, we compared the binding pocket of wild type (3FU8) with the structure that has mutation in position 192 and 296. We compared the wild type structure with P192P and A296L which is similar to 19G8 mutant and P192R and A296L which makes it similar to 5B4 mutant. There was a difference in case of P192R and A296L, the binding pocket is tighter than the wild type (Figure 4.12). In molecular docking simulation it did not show differences and ligands could bind there.

In order to check the redox potential value, we tried the same process for calculation of redox potential (See material and methods 3.4) for the same structure with one mutation in A296L position. In this case we made the structure similar to 19G8 mutant. We calculated the difference in the redox potentials of the RORO and ORRO states. The redox potential value is 167 kJ/mol that illustrates increasing in the value. Our experimental activity assays showed that this mutant has increased the activity with Molybdenum compound that most likely it has higher redox potential value in comparison with parental type. However, it is necessary to measure the redox potential value experimentally. Also, our result indicated that combination of Pro and Leu has effect on redox potential.
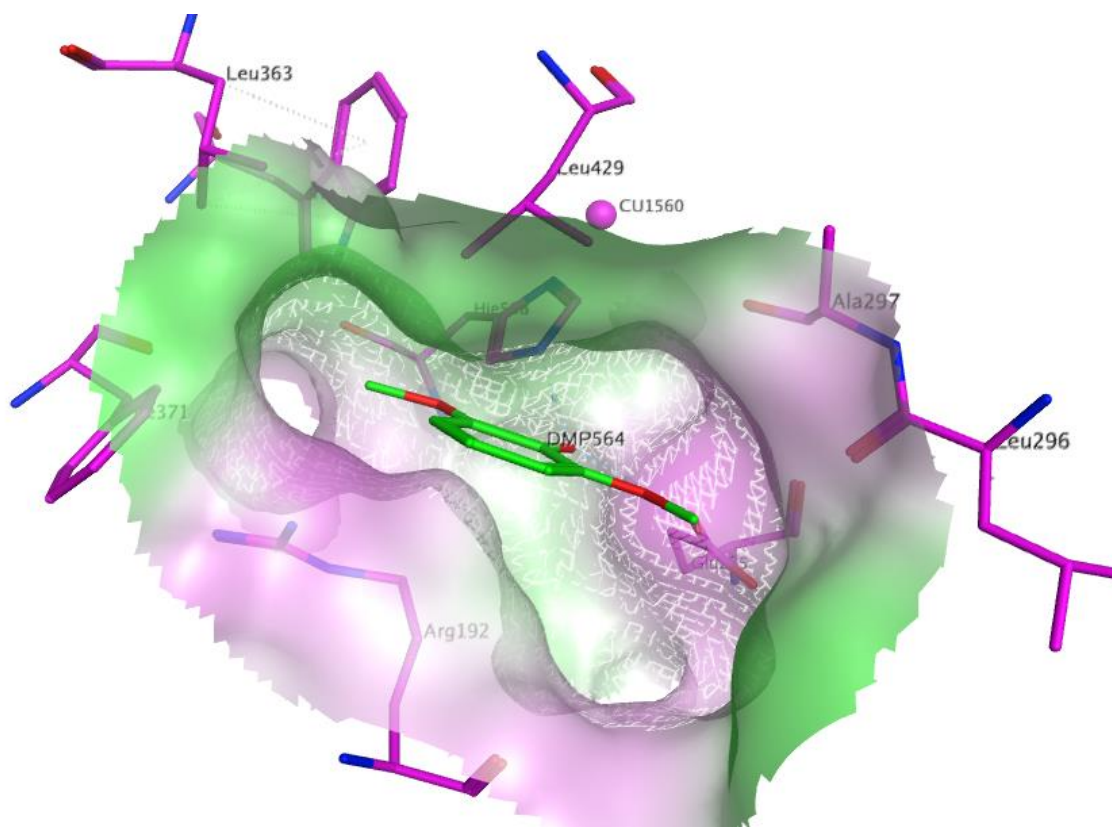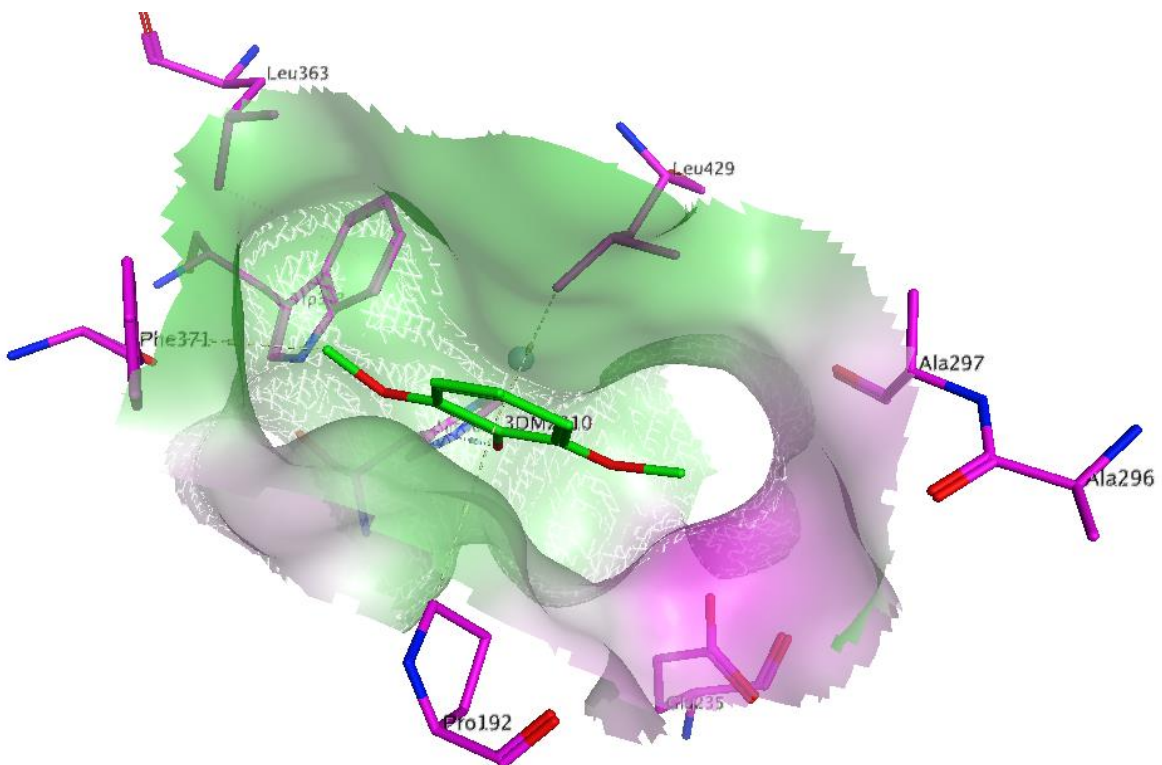
Figure 4.12. 3FU8 structure (upper structure) and 3FU8 contained two mutation, P192R and A296L (down).

Overall, by making different mutagenesis library on MtL T2 laccase, we found that combination of position 192 and 296 has effect on redox potential of this structure. The combination of Pro and Leu, which are hydrophobic residues, or Pro and Trp, which add aromatic residue to the active site lead improvement in activity of enzyme with molybdenum compound ($E°= 780$ mV vs. NHE) and violuric acid ($E°= 912$ mV vs. NHE). Since there was no improvement in kinetic constant of the interaction between these ligands and enzyme, consequently, the improvement in activity refers to redox potential property. Besides, the computational prediction of redox potential of MaL in the same position with the same residue showed increasing in the value.

5. CONCLUSIONS

Laccases can be used in a great variety of process and are the most interesting from a biotechnological point of view due to their higher oxidative capabilities. Yet, some aspects of the reactivity of laccases remain as subjects of debate, such as how the range of redox potentials or the diverse substrate affinities is tuned among laccases, thus hindering their rational design. Besides, one of the remaining challenges in laccase engineering is the increasing of the redox potential at the T1 Cu site beyond the nature limits (above +800 mV) without sacrificing neither the stability nor the catalysis.

Computational studies using protein structure prediction algorithms, molecular dynamics (MD) and hybrid quantum mechanics/molecular mechanics (QM/MM) calculations might aid the design of new laccase variants by reducing the experimental effort required to get the desired properties. Computational simulations and directed evolution will interact to reveal targets for protein engineering to be explored by site-directed mutagenesis (or semi-rational approaches) or for designing smart libraries to reduce the screening efforts in evolutionary strategies. Although, metalloproteins, such as laccase, present many challenges when it comes to computational modeling.

In this work, we tried to characterize structure-activity of laccase by applying computational methods. Then, we proposed the positions for performing mutations to check the effect on redox potential value. Finally, we produced the libraries of mutants experimentally and characterized the best mutant.

The main findings of the present study are:

1. Analysis of the binding site of the diverse laccases studied in this work suggests a differential amino acid composition. Thus, the high redox potential laccase *T. versicolor* exhibits only hydrophobic and aromatic residues. The number of aromatic residues decreases in *M. albomyces* laccase (a low redox potential laccase), whereas this number is even smaller in case of *B. subtilis* laccase, being its binding pocket considerable wider. This results are corroborated by the smaller binding score found in present docking studies.

2. Docking studies performed in this project reveal the importance of residues Asp (D206 in TvL), Glu (E235 in MaL) and His coordinated to copper atom (See Appendix F). Specifically, the acidic moiety of the ligand sits close to Asp/Glu and the oxygen atom of the phenolic substrate is bound at a hydrogen bond distance to the imidazole hydrogen attached to the Nε. Hydrogen abstraction likely occurs by proton donation to the acidic residue and electron transfer to the histidine residue.

3. In the case of ABTS we found a better docking score when Asp/Glu residues were protonated, in contrast with the results found for the rest of the ligands. This finding agrees with experimental results that shows better physicochemical parameters at pH< 4. This suggests that hydrogen abstraction is performed by a different mechanism of the rest of the ligands.

4. The computed value of the redox potential in case of *M. albomyces* laccase, using the dimer structure, ranges between 7-17 when T1 site is oxidized and DMP is reduced in one monomer to 74-92 kJ/mol when T1 site is oxidized and DMP is reduced in both monomers. The subsequent value for reorganization energy ranges between 2.1-2.5 eV. This represent an overestimation in comparison to the experimental value.

5. Saturation mutagenesis studies on position 192 and 296 in MtL T2 structure, shows that A192P, L296L and A192P, L296W produce and increased redox potential mutant in the violuric acid assay. On the other hand, A192R, L296L and A192R, L296W produce an increased redox potential in the Molybdenum hexacyanide assay. This differential behavior can be attributed to the different affinity of the ligands to the enzymes.

6. To further support the improved enzyme performance of redox potential, we measured the physicochemical parameters of the enzymes A192P, L296L and A192R, L296L showing no difference to the parental type.

7. The calculated redox potential of the model of the MaL mutants (P192P, A296L) yields an increase value in regards to the wild type. This suggest that the method can be used as a predictor approach for further studies.

6. BIBLIOGRAPHY

Abécassis, V., Pompon, D., Truan, G., 2000. High efficiency family shuffling based on multi-step PCR and in vivo DNA recombination in yeast: statistical and functional analysis of a combinatorial library between human cytochrome P450 1A1 and 1A2. Nucleic Acids Res. 28, e88.

Alcalde, M., 2010. Mutagenesis Protocols in Saccharomyces cerevisiae by In Vivo Overlap Extension, in: Braman, J. (Ed.), In Vitro Mutagenesis Protocols, Methods in Molecular Biology. Humana Press, pp. 3–14.

Alcalde, M., Zumárraga, M., Polaina, J., Ballesteros, A., Plou, F.J., 2006. Combinatorial saturation mutagenesis by in vivo overlap extension for the engineering of fungal laccases. Comb. Chem. High Throughput Screen. 9, 719–727.

Arnold, F.H., 2006. Fancy footwork in the sequence space shuffle. Nat. Biotechnol. 24, 328–330.

Arnold, F.H., 1993. Protein engineering for unusual environments. Curr. Opin. Biotechnol. 4, 450–455.

Augustine, A.J., Kragh, M.E., Sarangi, R., Fujii, S., Liboiron, B.D., Stoj, C.S., Kosman, D.J., Hodgson, K.O., Hedman, B., Solomon, E.I., 2008. Spectroscopic studies of perturbed T1 Cu sites in the multicopper oxidases Saccharomyces cerevisiae Fet3p and Rhus vernicifera laccase: allosteric coupling between the T1 and trinuclear Cu sites. Biochem. 47, 2036–2045.

Auriol, M., Filali-Meknassi, Y., Adams, C.D., Tyagi, R.D., Noguerol, T.-N., Piña, B., 2008. Removal of estrogenic activity of natural and synthetic hormones from a municipal wastewater: Efficiency of horseradish peroxidase and laccase from Trametes versicolor. Chemosphere 70, 445–452.

Awasthi, M., Jaiswal, N., Singh, S., Pandey, V.P., Dwivedi, U.N., 2015. Molecular docking and dynamics simulation analyses unraveling the differential enzymatic catalysis by plant and fungal laccases with respect to lignin biosynthesis and degradation. J. Biomol. Struct. Dyn. 33, 1835–1849.

Bandyopadhyay, P., 2005. Accelerating quantum mechanical/molecular mechanical sampling using pure molecular mechanical potential as an importance function: the case of effective fragment potential. J. Chem. Phys. 122, 91102.

Bartolotti, L.J., Pedersen, L.G., Charifson, P.S., 1991. Long range nonbonded attractive constants for some charged atoms. J. Comput. Chem. 12, 1125–1128.

Bastos, A.C., Magan, N., 2009. *Trametes versicolor*: Potential for atrazine bioremediation in calcareous clay soil, under low water availability conditions. Int. Biodeter. Biodegr. 63, 389–394.

Battistuzzi, G., Loschi, L., Borsari, M., Sola, M., 1999. Effects of nonspecific ion-protein interactions on the redox chemistry of cytochrome c. J. Biol. Inorg. Chem. 4, 601–607.

Bello, M., Valderrama, B., Serrano-Posada, H., Rudiño-Piñera, E., 2012. Molecular dynamics of a thermostable multicopper oxidase from *Thermus thermophilus* HB27: structural differences between the apo and holo forms. PLoS ONE 7, e40700.

Ben Younes, S., Sayadi, S., 2011. Purification and characterization of a novel trimeric and thermotolerant laccase produced from the ascomycete *Scytalidium thermophilum* strain. J. Mol. Cat. B: Enzym. 73, 35–42.

Benkovic, S.J., Hammes-Schiffer, S., 2003. A perspective on enzyme catalysis. Sci. 301, 1196–1202.

Berendsen, H.J.C., Postma, J.P.M., Gunsteren, W.F. van, DiNola, A., Haak, J.R., 1984. Molecular dynamics with coupling to an external bath. J. Chem. Phys. 81, 3684–3690.

Bertrand, T., Jolivalt, C., Briozzo, P., Caminade, E., Joly, N., Madzak, C., Mougin, C., 2002. Crystal structure of a four-copper laccase complexed with an arylamine: insights into substrate recognition and correlation with kinetics. Biochem. 41, 7325–7333.

Besler, B.H., Merz, K.M., Kollman, P.A., 1990. Atomic charges derived from semiempirical methods. J. Comput. Chem. 11, 431–439.

Bloom, J.D., Labthavikul, S.T., Otey, C.R., Arnold, F.H., 2006. Protein stability promotes evolvability. PNAS 103, 5869–5874.

Blumberger, J., Lamoureux, G., 2008. Reorganization free energies and quantum corrections for a model electron self-exchange reaction: comparison of polarizable and non-polarizable solvent models. Mol. Phys. 106, 1597–1611.

Bourbonnais, R., Paice, M.G., 1990. Oxidation of non-phenolic substrates. An expanded role for laccase in lignin biodegradation. FEBS Lett. 267, 99–102.

Bradford, M.M., 1976. A rapid and sensitive method for the quantitation of microgram quantities of protein utilizing the principle of protein-dye binding. Anal. Biochem. 72, 248–254.

Bruyneel, F., Dive, G., Marchand-Brynaert, J., 2012. Non-symmetrically substituted phenoxazinones from laccase-mediated oxidative cross-coupling of aminophenols: an experimental and theoretical insight. Org. Biomol. Chem. 10, 1834–1846.

Bulter, T., Alcalde, M., Sieber, V., Meinhold, P., Schlachtbauer, C., Arnold, F.H., 2003. Functional expression of a fungal laccase in *Saccharomyces cerevisiae* by directed evolution. Appl. Environ. Microbiol. 69, 987–995.

Cambria, M.T., Di Marino, D., Falconi, M., Garavaglia, S., Cambria, A., 2010. Docking simulation and competitive experiments validate the interaction between the 2,5-xylidine inhibitor and *Rigidoporus lignosus* laccase. J. Biomol. Struct. Dyn. 27, 501–510.

Cambria, M.T., Gullotto, D., Garavaglia, S., Cambria, A., 2012. In silico study of structural determinants modulating the redox potential of *Rigidoporus lignosus* and other fungal laccases. J. Biomol. Struct. Dyn. 30, 89–101.

Cañas, A.I., Camarero, S., 2010. Laccases and their natural mediators: biotechnological tools for sustainable eco-friendly processes. Biotechnol. Adv. 28, 694–705.

Case, D.A., Darden, T.A., Cheatham, T.E., C. L. Simmerling, J. Wang, R. E. Duke, R. Luo, R. C. Walker, W. Zhang, K. M. Merz, B. Roberts, S. Hayik, A. Roitberg, G. Seabra, J. Swails, A. W. Goetz, I. Kolossváry, K. F. Wong, F. Paesani, J. Vanicek, R. M. Wolf, J. Liu, X. Wu, S. R. Brozell, T. Steinbrecher, H. Gohlke, Q. Cai, X. Ye, J. Wang, M. J. Hsieh, G. Cui, D. R. Roe, D. H. Mathews, M. G. Seetin, R. Salomon-Ferrer, C. Sagui, V. Babin, T. Luchko, S. Gusarov, A. Kovalenko, P. A. Kollman, 2005. AMBER 12.

Casella, I.G., Contursi, M., 2007. The electrochemical reduction of nitrophenols on silver globular particles electrodeposited under pulsed potential conditions. J. Electrochem. Soc. 154, 697–702.

Chen, Z., Durão, P., Silva, C.S., Pereira, M.M., Todorovic, S., Hildebrandt, P., Bento, I., Lindley, P.F., Martins, L.O., 2010. The role of Glu498 in the dioxygen reactivity of CotA-laccase from *Bacillus subtilis*. Dalton Trans. 39, 2875–2882.

Cherry, J.R., Lamsa, M.H., Schneider, P., Vind, J., Svendsen, A., Jones, A., Pedersen, A.H., 1999. Directed evolution of a fungal peroxidase. Nat. Biotechnol. 17, 379–384.

Chica, R.A., Doucet, N., Pelletier, J.N., 2005. Semi-rational approaches to engineering enzyme activity: combining the benefits of directed evolution and rational design. Curr. Opin. Biotechnol. 16, 378–384.

Christensen, N.J., Kepp, K.P., 2014. Setting the stage for electron transfer: Molecular basis of ABTS-binding to four laccases from *Trametes versicolor* at variable pH and protein oxidation state. J. Mol. Cat. B, Enzym. 100, 68–77.

Cisneros, G.A., Liu, H., Zhang, Y., Yang, W., 2003. Ab initio QM/MM study shows there is no general acid in the reaction catalyzed by 4-oxalocrotonate tautomerase. J. Am. Chem. Soc. 125, 10384–10393.

Claus, H., Faber, G., König, H., 2002. Redox-mediated decolorization of synthetic dyes by fungal laccases. Appl. Microbiol. Biotechnol. 59, 672–678.

Comba, P., Remenyi, R., 2002. A new molecular mechanics force field for the oxidized form of blue copper proteins. J. Comput. Chem. 23, 697–705.

Cornell, W.D., Cieplak, P., Bayly, C.I., Gould, I.R., Merz, K.M., Ferguson, D.M., Spellmeyer, D.C., Fox, T., Caldwell, J.W., Kollman, P.A., 1995. A second generation force field for the simulation of proteins, nucleic acids, and organic molecules. J. Am. Chem. Soc. 117, 5179–5197.

Cusano, A.M., Mekmouche, Y., Meglecz, E., Tron, T., 2009. Plasticity of laccase generated by homeologous recombination in yeast. FEBS Journal 276, 5471–5480.

Darden, T., York, D., Pedersen, L., 1993. Particle mesh Ewald: An N·log(N) method for Ewald sums in large systems. J. Chem. Phys. 98, 10089–10092.

Datta, S.N., Sudhamsu, J., Pandey, A., 2004. Theoretical determination of the standard reduction potential of plastocyanin in vitro. J. Phys. Chem. B 108, 8007–8016.

De Kerpel, J.O.A., Ryde, U., 1999. Protein strain in blue copper proteins studied by free energy perturbations. Proteins 36, 157–174.

Durão, P., Bento, I., Fernandes, A.T., Melo, E.P., Lindley, P.F., Martins, L.O., 2006. Perturbations of the T1 copper site in the CotA laccase from *Bacillus subtilis*: structural, biochemical, enzymatic and stability studies. J. Biol. Inorg. Chem. 11, 514–526.

Dwivedi, U.N., Singh, P., Pandey, V.P., Kumar, A., 2011. Structure–function relationship among bacterial, fungal and plant laccases. J. Mol. Cat. B: Enzym. 68, 117–128.

Eichkorn, K., Treutler, O., Öhm, H., Häser, M., Ahlrichs, R., 1995. Auxiliary basis sets to approximate Coulomb potentials. Chem. Phys. Lett. 240, 283–290.

Eichkorn, K., Weigend, F., Treutler, O., Ahlrichs, R., 1997. Auxiliary basis sets for main row atoms and transition metals and their use to approximate Coulomb potentials. Theor. Chem. Acta. 97, 119–124.

Enguita, F.J., Martins, L.O., Henriques, A.O., Carrondo, M.A., 2003. Crystal structure of a bacterial endospore coat component. A laccase with enhanced thermostability properties. J. Biol. Chem. 278, 19416–19425.

Essmann, U., Perera, L., Berkowitz, M.L., Darden, T., Lee, H., Pedersen, L.G., 1995. A smooth particle mesh Ewald method. J. Chem. Phys. 103, 8577–8593.

Fabbrini, M., Galli, C., Gentili, P., 2002. Comparing the catalytic efficiency of some mediators of laccase. J. Mol. Cat. B: Enzym. 16, 231–240.

Fernandez, L.E., Horvath, S., Hammes-Schiffer, S., 2013. Theoretical design of molecular electrocatalysts with flexible pendant amines for hydrogen production and oxidation. J. Phys. Chem. Lett. 4, 542–546.

Fernandez, L.E., Horvath, S., Hammes-Schiffer, S., 2012. Theoretical analysis of the sequential proton-coupled electron transfer mechanisms for H2 oxidation and production pathways catalyzed by nickel molecular electrocatalysts. J. Phys. Chem. C 116, 3171–3180.

Festa, G., Autore, F., Fraternali, F., Giardina, P., Sannia, G., 2008. Development of new laccases by directed evolution: functional and computational analyses. Proteins 72, 25–34.

Fiţigău, I.F., Peter, F., Boeriu, C.G., 2013. Oxidative polymerization of lignins by laccase in water-acetone mixture. Acta Biochim. Pol. 60, 817–822.

Forootanfar, H., Faramarzi, M.A., Shahverdi, A.R., Yazdi, M.T., 2011. Purification and biochemical characterization of extracellular laccase from the ascomycete *Paraconiothyrium variabile*. Bioresour. Technol. 102, 1808–1814.

Frisch, M.J., Trucks, G.W., Schlegel, H.B., Scuseria, G. E.; Robb, M. A.; Cheeseman, J. R.; Scalmani, G.; Barone, V.; Mennucci, B.; Petersson, G. A.; Nakatsuji, H.; Caricato, M.; Li, X.; Hratchian, H. P.; Izmaylov, A. F.; Bloino, J.; Zheng, G.; Sonnenberg, J. L.; Hada, M.; Ehara, M.; Toyota, K.; Fukuda, R.; Hasegawa, J.; Ishida, M.; Nakajima, T.; Honda, Y.; Kitao, O.; Nakai, H.; Vreven, T.; Montgomery, J. A., Jr.; Peralta, J. E.; Ogliaro, F.; Bearpark, M.; Heyd, J. J.; Brothers, E.; Kudin, K. N.; Staroverov, V. N.; Kobayashi, R.; Normand, J.; Raghavachari, K.; Rendell, A.; Burant, J. C.; Iyengar, S. S.; Tomasi, J.; Cossi, M.; Rega, N.; Millam, J. M.; Klene, M.; Knox, J. E.; Cross, J. B.; Bakken, V.; Adamo, C.; Jaramillo, J.; Gomperts, R.; Stratmann, R. E.; Yazyev, O.; Austin, A. J.; Cammi, R.; Pomelli, C.; Ochterski, J. W.; Martin, R. L.; Morokuma, K.; Zakrzewski, V. G.; Voth, G. A.; Salvador, P.; Dannenberg, J. J.; Dapprich, S.; Daniels, A. D.; Farkas, Ö.; Foresman, J. B.; Ortiz, J. V.; Cioslowski, J.; Fox, D. J. Gaussian, Inc., Wallingford CT, 2009. Gaussian 09, Revision E.01.

Galli, C., Gentili, P., Jolivalt, C., Madzak, C., Vadalà, R., 2011. How is the reactivity of laccase affected by single-point mutations? Engineering laccase for improved activity towards sterically demanding substrates. Appl. Microbiol. Biotechnol. 91, 123–131.

Garavaglia, S., Cambria, M.T., Miglio, M., Ragusa, S., Iacobazzi, V., Palmieri, F., D'Ambrosio, C., Scaloni, A., Rizzi, M., 2004. The structure of *Rigidoporus lignosus* Laccase containing a full complement of copper ions, reveals an asymmetrical arrangement for the T3 copper pair. J. Mol. Biol. 342, 1519–1531.

García-Ruiz, E., Maté, D., Ballesteros, A., Martinez, A.T., Alcalde, M., 2010. Evolving thermostability in mutant libraries of ligninolytic oxidoreductases expressed in yeast. Microb. Cell Fact. 9, 17.

Gasparetti, C., 2012. BIOCHEMICAL AND STRUCTURAL CHARACTERISATION OF THE COPPER CONTAINING OXIDOREDUCASES CATECHOL OXIDASE, TYROSINASE, AND LACCASE FROM ASCOMYCETES FUNGI.

Ge, H., Gao, Y., Hong, Y., Zhang, M., Xiao, Y., Teng, M., Niu, L., 2010. Structure of native laccase B from *Trametes* sp. AH28-2. Acta Crystallogr. Sect. F Struct. Biol. Cryst. Commun. 66, 254–258.

Gianfreda, L., Xu, F., Bollag, J.-M., 1999. Laccases: a useful group of oxidoreductive enzymes. Bioremediat. J. 3, 1–26.

Giardina, P., Faraco, V., Pezzella, C., Piscitelli, A., Vanhulle, S., Sannia, G., 2010. Laccases: a never-ending story. Cell. Mol. Life Sci. 67, 369–385.

Gunne, M., Höppner, A., Hagedoorn, P.-L., Urlacher, V.B., 2014. Structural and redox properties of the small laccase Ssl1 from Streptomyces sviceus. FEBS J. 281, 4307–4318.

Gupta, N., Farinas, E.T., 2010. Directed evolution of CotA laccase for increased substrate specificity using *Bacillus subtilis* spores. Protein Eng. Des. Sel. 23, 679–682.

Hall, J.F., Kanbi, L.D., Strange, R.W., Hasnain, S.S., 1999. Role of the axial ligand in type 1 Cu centers studied by point mutations of met148 in rusticyanin. Biochemistry 38, 12675–12680.

Hammes-Schiffer, S., 2001. Theoretical perspectives on proton-coupled electron transfer reactions. Acc. Chem. Res. 34, 273–281.

Hammes-Schiffer, S., Soudackov, A.V., 2008. Proton-coupled electron transfer in solution, proteins, and electrochemistry. J. Phys. Chem. B 112, 14108–14123.

Hong, G., Ivnitski, D.M., Johnson, G.R., Atanassov, P., Pachter, R., 2011. Design parameters for tuning the type 1 Cu multicopper oxidase redox potential: insight from a combination of first principles and empirical molecular dynamics simulations. J. Am. Chem. Soc. 133, 4802–4809.

Hong, G., Strajbl, M., Wesolowski, T.A., Warshel, A., 2000. Constraining the electron densities in DFT method as an effective way for ab initio studies of metal-catalyzed reactions. J. Comput. Chem. 21, 1554–1561.

Hu, L., Farrokhnia, M., Heimdal, J., Shleev, S., Rulíšek, L., Ryde, U., 2011. Reorganization energy for internal electron transfer in multicopper oxidases. J. Phys. Chem. B 115, 13111–13126.

Hummer, G., Pratt, L.R., García, A.E., 1998. Molecular theories and simulation of ions and polar molecules in water. J. Phys. Chem. A 102, 7885–7895.

Iftimie, R., Salahub, D., Wei, D., Schofield, J., 2000. Using a classical potential as an efficient importance function for sampling from an ab initio potential. J. Chem. Phys. 113, 4852–4862.

Ishida, T., Kato, S., 2004. Role of Asp102 in the catalytic relay system of serine proteases: a theoretical study. J. Am. Chem. Soc. 126, 7111–7118.

Jones, G., Willett, P., Glen, R.C., 1995. Molecular recognition of receptor sites using a genetic algorithm with a description of desolvation. J. Mol. Biol. 245, 43–53.

Jones, G., Willett, P., Glen, R.C., Leach, A.R., Taylor, R., 1997. Development and validation of a genetic algorithm for flexible docking. J. Mol. Biol. 267, 727–748.

Jones, S.M., Solomon, E.I., 2015. Electron transfer and reaction mechanism of laccases. Cell Mol. Life Sci. 72, 869–883.

Jorgensen, W.L., 1989. Free energy calculations: a breakthrough for modeling organic chemistry in solution. Acc. Chem. Res. 22, 184–189.

Jorgensen, W.L., Chandrasekhar, J., Madura, J.D., Impey, R.W., Klein, M.L., 1983. Comparison of simple potential functions for simulating liquid water. J. Chem. Phys. 79, 926–935.

Jovanovic, S.V., Tosic, M., Simic, M.G., 1991. Use of the Hammett correlation and .delta.+ for calculation of one-electron redox potentials of antioxidants. J. Phys. Chem. 95, 10824–10827.

Kallio, J.P., Auer, S., Jänis, J., Andberg, M., Kruus, K., Rouvinen, J., Koivula, A., Hakulinen, N., 2009. Structure-function studies of a *Melanocarpus albomyces* laccase suggest a pathway for oxidation of phenolic compounds. J. Mol. Biol. 392, 895–909.

Kallio, J.P., Gasparetti, C., Andberg, M., Boer, H., Koivula, A., Kruus, K., Rouvinen, J., Hakulinen, N., 2011. Crystal structure of an ascomycete fungal laccase from *Thielavia arenaria*--common structural features of asco-laccases. FEBS J. 278, 2283–2295.

Kalyani, D., Dhiman, S.S., Kim, H., Jeya, M., Kim, I.-W., Lee, J.-K., 2012. Characterization of a novel laccase from the isolated *Coltricia perennis* and its application to detoxification of biomass. Process Biochem. 47, 671–678.

Kamerlin, S.C.L., Haranczyk, M., Warshel, A., 2009. Progress in ab initio QM/MM free-energy simulations of electrostatic energies in proteins: accelerated QM/MM studies of pKa, redox reactions and solvation free energies. J. Phys. Chem. B 113, 1253–1272.

Kataoka, K., Kitagawa, R., Inoue, M., Naruse, D., Sakurai, T., Huang, H., 2005. Point mutations at the type I Cu ligands, Cys457 and Met467, and at the putative proton donor, Asp105, in *Myrothecium verrucaria* bilirubin oxidase and reactions with dioxygen. Biochem. 44, 7004–7012.

Kataoka, K., Sugiyama, R., Hirota, S., Inoue, M., Urata, K., Minagawa, Y., Seo, D., Sakurai, T., 2009. Four electron reduction of dioxygen by a multicopper oxidase, CueO, and roles of Asp112 and Glu506 located adjacent to the trinuclear copper center. J. Biol/ Chem. 284, 14405-14413.

Kaukonen, M., Söderhjelm, P., Heimdal, J., Ryde, U., 2008. QM/MM−PBSA method to estimate free energies for reactions in proteins. J. Phys. Chem. B 112, 12537–12548.

Kelly, C.P., Cramer, C.J., Truhlar, D.G., 2007. Single-ion solvation free energies and the normal hydrogen electrode potential in methanol, acetonitrile, and dimethyl sulfoxide. J. Phys. Chem. B 111, 408–422.

Keum, Y.S., Li, Q.X., 2004. Fungal laccase-catalyzed degradation of hydroxy polychlorinated biphenyls. Chemosphere 56, 23–30.

Kiiskinen, L.-L., Rättö, M., Kruus, K., 2004. Screening for novel laccase-producing microbes. J. Appl. Microbiol. 97, 640–646.

Kille, S., Acevedo-Rocha, C.G., Parra, L.P., Zhang, Z.-G., Opperman, D.J., Reetz, M.T., Acevedo, J.P., 2013. Reducing codon redundancy and screening effort of combinatorial protein libraries created by saturation mutagenesis. ACS Synth. Biol. 2, 83–92.

Kollman, P.A., Kuhn, B., Donini, O., Perakyla, M., Stanton, R., Bakowies, D., 2001. Elucidating the nature of enzyme catalysis utilizing a new twist on an old methodology: quantum mechanical-free energy calculations on chemical reactions in enzymes and in aqueous solution. Acc. Chem. Res. 34, 72–79.

Koschorreck, K., Richter, S.M., Swierczek, A., Beifuss, U., Schmid, R.D., Urlacher, V.B., 2008. Comparative characterization of four laccases from Trametes versicolor concerning phenolic C-C coupling and oxidation of PAHs. Arch. Biochem. Biophys. 474, 213–219.

Kuhn, B., Kollman, P.A., 2000b. QM−FE and molecular dynamics calculations on catechol O-methyltransferase: free energy of activation in the enzyme and in aqueous solution and regioselectivity of the enzyme-catalyzed reaction. J. Am. Chem. Soc. 122, 2586–2596.

Kumar, S.V.S., Phale, P.S., Durani, S., Wangikar, P.P., 2003. Combined sequence and structure analysis of the fungal laccase family. Biotechnol. Bioeng. 83, 386–394.

Kunamneni, A., Camarero, S., García-Burgos, C., Plou, F.J., Ballesteros, A., Alcalde, M., 2008. Engineering and applications of fungal laccases for organic synthesis. Microb. Cell Fact. 7, 32.

Lahtinen, M., 2013. REACTIVITY AND REACTIONS OF LIGNIN MODEL COMPOUNDS WITH LACCASES.

Li, H., Webb, S.P., Ivanic, J., Jensen, J.H., 2004. Determinants of the relative reduction potentials of type-1 copper sites in proteins. J. Am. Chem. Soc. 126, 8010–8019.

Liu, H., Zhang, Y., Yang, W., 2000. How Is the Active Site of Enolase Organized To Catalyze Two Different Reaction Steps? J. Am. Chem. Soc. 122, 6560–6570.

Liu, W., Sakane, S., Wood, R.H., Doren, D.J., 2002. The hydration free energy of aqueous Na+ and Cl⁻ at high temperatures predicted by ab initio/classical free energy perturbation: 973 K with 0.535 g/cm3 and 573 K with 0.725 g/cm3. J. Phys. Chem. A 106, 1409–1418.

Liu, W., Wood, R.H., Doren, D.J., 2003. Hydration free energy and potential of mean force for a model of the sodium chloride ion pair in supercritical water with ab initio solute–solvent interactions. J. Chem. Phys. 118, 2837–2844.

Liu, Y.H., Ye, M., Lu, Y., Zhang, X., Li, G., 2011. Improving the decolorization for textile dyes of a metagenome-derived alkaline laccase by directed evolution. Appl. Microbiol. Biotechnol. 91, 667–675.

Machczynski, M.C., Vijgenboom, E., Samyn, B., Canters, G.W., 2004. Characterization of SLAC: A small laccase from *Streptomyces coelicolor* with unprecedented activity. Protein Sci. 13, 2388–2397.

Maté, D., García-Burgos, C., García-Ruiz, E., Ballesteros, A.O., Camarero, S., Alcalde, M., 2010. Laboratory evolution of high-redox potential laccases. Chem. Biol. 17, 1030–1041.

Maté, D., García-Ruiz, E., Camarero, S., Alcalde, M., 2011. Directed evolution of fungal laccases. Curr Genomics 12, 113–122.

Mate, D.M., Gonzalez-Perez, D., Falk, M., Kittl, R., Pita, M., De Lacey, A.L., Ludwig, R., Shleev, S., Alcalde, M., 2013. Blood tolerant laccase by directed evolution. Chem. Biol. 20, 223–231.

Matera, I., Gullotto, A., Tilli, S., Ferraroni, M., Scozzafava, A., Briganti, F., 2008. Crystal structure of the blue multicopper oxidase from the white-rot fungus *Trametes trogii* complexed with p-toluate. Inorganica Chimica Acta, Protagonists in Chemistry: Dante Gatteschi (Part II) 361, 4129–4137.

Mayer, A.M., Staples, R.C., 2002. Laccase: new functions for an old enzyme. Phytochem. 60, 551–565.

Mehta, N., Datta, S.N., 2007. Theoretical Determination of the Standard Reduction Potentials of Pheophytin-a in N,N-Dimethyl Formamide and Membrane. J. Phys. Chem. B 111, 7210–7217.

Miele, A., Giardina, P., Sannia, G., Faraco, V., 2010. Random mutants of a *Pleurotus ostreatus* laccase as new biocatalysts for industrial effluents bioremediation. J. Appl. Microbiol. 108, 998–1006.

Miura, Y., Tsujimura, S., Kurose, S., Kamitaka, Y., Kataoka, K., Sakurai, T., Kano, K., 2009. Direct electrochemistry of CueO and its mutants at residues to and near type I Cu for oxygen-reducing Biocathode. Fuel Cells 9, 70–78.

Mot, A.C., Silaghi-Dumitrescu, R., 2012. Laccases: complex architectures for one-electron oxidations. Biochem. Mosc. 77, 1395–1407.

Muller, R.P., Warshel, A., 1995. Ab Initio Calculations of free energy barriers for chemical reactions in solution. J. Phys. Chem. 99, 17516–17524.

Murphy, M.E., Lindley, P.F., Adman, E.T., 1997. Structural comparison of cupredoxin domains: domain recycling to construct proteins with novel functions. Protein Sci. 6, 761–770.

Nakamura, K., Go, N., 2005. Function and molecular evolution of multicopper blue proteins. Cell. Mol. Life Sci. 62, 2050–2066.

Nilsson, K., Lecerof, D., Sigfridsson, E., Ryde, U., 2003. An automatic method to generate force-field parameters for hetero-compounds. Acta Crystallogr. D Biol. Crystallogr. 59, 274–289.

Nilsson Lill, S.O., Forbes, A., Donoghue, P., Verdolino, V., Wiest, O., Rydberg, P., Norrby, P.-O., 2010. Application of Q2MM to stereoselective reactions. Curr. Org. Chem. 14, 1629–1645.

Noodleman, L., Han, W.-G., 2006. Structure, redox, pKa, spin. A golden tetrad for understanding metalloenzyme energetics and reaction pathways. J. Biol. Inorg. Chem. 11, 674–694.

Norrby, P.-O., 2000. Selectivity in asymmetric synthesis from QM-guided molecular mechanics. J. Mol. Struc.: THEOCHEM 506, 9–16.

Norrby, P.-O., Liljefors, T., 1998. Automated molecular mechanics parameterization with simultaneous utilization of experimental and quantum mechanical data. J. Comput. Chem. 19, 1146–1166.

Olsson, M.H.M., Warshel, A., 2004. Solute solvent dynamics and energetics in enzyme ctalysis: the SN2 reaction of dehalogenase as a general benchmark. J. Am. Chem. Soc. 126, 15167–15179.

Palmer, A.E., Randall, D.W., Xu, F., Solomon, E.I., 1999. Spectroscopic studies and electronic structure description of the high potential type 1 copper site in fungal laccase: insight into the effect of the axial ligand. J. Am. Chem. Soc. 121, 7138–7149.

Palmer, A.E., Szilagyi, R.K., Cherry, J.R., Jones, A., Xu, F., Solomon, E.I., 2003. Spectroscopic characterization of the Leu513His variant of fungal laccase: effect of increased axial ligand interaction on the geometric and electronic structure of the type 1 Cu site. Inorg. Chem. 42, 4006–4017.

Pardo, I., Santiago, G., Gentili, P., Lucas, F., Monza, E., Medrano, F.J., Galli, C., Martínez, A.T., Guallar, V., Camarero, S., 2016. Re-designing the substrate binding pocket of laccase for enhanced oxidation of sinapic acid. Catal. Sci. Technol. 6, 3900-3910.

Perdew, J.P., Burke, K., Ernzerhof, M., 1996. Generalized gradient approximation made simple. Phys. Rev. Lett. 77, 3865–3868.

Piontek, K., Antorini, M., Choinowski, T., 2002. Crystal structure of a laccase from the fungus *Trametes versicolor* at 1.90-A resolution containing a full complement of coppers. J. Biol. Chem. 277, 37663–37669.

Polyakov, K.M., Fedorova, T.V., Stepanova, E.V., Cherkashin, E.A., Kurzeev, S.A., Strokopytov, B.V., Lamzin, V.S., Koroleva, O.V., 2009. Structure of native laccase from *Trametes hirsuta* at 1.8 A resolution. Acta Crystallogr. D Biol. Crystallogr. 65, 611–617.

Prasad, N.K., Vindal, V., Narayana, S.L., V, R., Kunal, S.P., M, S., 2012. In silico analysis of *Pycnoporus cinnabarinus* laccase active site with toxic industrial dyes. J. Mol. Model. 18, 2013–2019.

Riva, S., 2006. Laccases: blue enzymes for green chemistry. Trends in Biotechnology 24, 219–226.

Rod, T.H., Ryde, U., 2005. Accurate QM/MM free energy calculations of enzyme reactions: methylation by catechol O-methyltransferase. J. Chem. Theory. Comput. 1, 1240–1251.

Rodgers, C.J., Blanford, C.F., Giddens, S.R., Skamnioti, P., Armstrong, F.A., Gurr, S.J., 2010. Designer laccases: a vogue for high-potential fungal enzymes? Trends Biotechnol. 28, 63–72.

Rodríguez Couto, S., Toca Herrera, J.L., 2006. Industrial and biotechnological applications of laccases: a review. Biotechnol. Adv. 24, 500–513.

Romero, P.A., Arnold, F.H., 2009. Exploring protein fitness landscapes by directed evolution. Nat. Rev. Mol. Cell Biol. 10, 866–876.

Rulíšek, L., Havlas, Z., 2003. Using DFT methods for the prediction of the structure and energetics of metal-binding sites in metalloproteins. Int. J. Quantum Chem. 91, 504–510.

Rulíšek, L., Ryde, U., 2013. Theoretical studies of the active-site structure, spectroscopic and thermodynamic properties, and reaction mechanism of multicopper oxidases. Coord. Chem. Rev. 257, 445–458.

Ryckaert, J.-P., Ciccotti, G., Berendsen, H.J.C., 1977. Numerical integration of the cartesian equations of motion of a system with constraints: molecular dynamics of n-alkanes. J. Comput. Phys. 23, 327–341.

Ryde, U., 1996. The coordination chemistry of the structural zinc ion in alcohol dehydrogenase studied by ab initio quantum chemical calculations. Eur. Biophys. J. 24, 213–221.

Ryde, U., Hsiao, Y.-W., Rulíšek, L., Solomon, E.I., 2007. Identification of the Peroxy Adduct in multicopper oxidases by a combination of computational chemistry and extended X-ray absorption fine-structure measurements. J. Am. Chem. Soc. 129, 726–727.

Ryde, U., Olsson, M.H.M., 2001. Structure, strain, and reorganization energy of blue copper models in the protein. Int. J. Quantum Chem. 81, 335–347.

Sakane, S., Yezdimer, E.M., Liu, W., Barriocanal, J.A., Doren, D.J., Wood, R.H., 2000. Exploring the ab initio/classical free energy perturbation method: The hydration free energy of water. J. Chem. Phys. 113, 2583–2593.

Sakurai, T., Kataoka, K., 2007. Structure and function of type I copper in multicopper oxidases. Cell. Mol. Life Sci. 64, 2642–2656.

Sambrook, J., Fritsch, E.F., Maniatis, T. Molecular cloning: A laboratory manual. 2nd ed. Volumes 1, 2, and 3. Cold Spring Harbor Laboratory Press, New York, 1990.

Santhanam, N., Vivanco, J.M., Decker, S.R., Reardon, K.F., 2011. Expression of industrially relevant laccases: prokaryotic style. Trends Biotechnol. 29, 480–489.

Schäfer, A., Horn, H., Ahlrichs, R., 1992. Fully optimized contracted Gaussian basis sets for atoms Li to Kr. J. Chem. Phys. 97, 2571–2577.

Schäfer, A., Huber, C., Ahlrichs, R., 1994. Fully optimized contracted Gaussian basis sets of triple zeta valence quality for atoms Li to Kr. J. Chem. Phys. 100, 5829–5835.

Schomburg, I., Chang, A., Schomburg, D., 2002. BRENDA, enzyme data and metabolic information. Nucleic Acids Res. 30, 47–49.

Shleev, S., Jarosz-Wilkolazka, A., Khalunina, A., Morozova, O., Yaropolov, A., Ruzgas, T., Gorton, L., 2005. Direct electron transfer reactions of laccases from different origins on carbon electrodes. Bioelectrochem. 67, 115–124.

Shleev, S.V., Morozova, O.V., Nikitina, O.V., Gorshina, E.S., Rusinova, T.V., Serezhenkov, V.A., Burbaev, D.S., Gazaryan, I.G., Yaropolov, A.I., 2004. Comparison of physico-chemical characteristics of four laccases from different basidiomycetes. Biochimie 86, 693–703.

Si, D., Li, H., 2009. Quantum chemical calculation of type-1 Cu reduction potential: ligand interaction and solvation effect. J. Phys. Chem. A 113, 12979–12987.

Si, J., Peng, F., Cui, B., 2013. Purification, biochemical characterization and dye decolorization capacity of an alkali-resistant and metal-tolerant laccase from *Trametes pubescens*. Bioresour. Technol. 128, 49–57.

Solomon, E.I., Lowery, M.D., 1993. Electronic structure contributions to function in bioinorganic chemistry. Sci. 259, 1575–1581.

Stanton, R.V., Peräkylä, M., Bakowies, D., Kollman, P.A., 1998. Combined ab initio and free energy calculations to study reactions in enzymes and solution: Amide hydrolysis in trypsin and aqueous solution. J. Am. Chem. Soc. 120, 3448–3457.

Štrajbl, M., Hong, G., Warshel, A., 2002. Ab Initio QM/MM simulation with proper sampling: "first principle" calculations of the free energy of the auto dissociation of water in aqueous solution. J. Phys. Chem. B 106, 13333–13343.

Strong, P.J., 2011. Improved laccase production by *Trametes pubescens* MB89 in distillery wastewaters. Enzyme Res. 2011, e379176.

Sukan, A., Sargin, S., 2013. Enzymatic removal of phenol from industrial wastewaters. J. Biomater. Nanobiotechnol. 4, 300–307.

Sulpizi, M., Raugei, S., VandeVondele, J., Carloni, P., Sprik, M., 2007. Calculation of redox properties: Understanding short- and long-range effects in rubredoxin. J. Phys. Chem. B 111, 3969–3976.

Sun, X., Bai, R., Zhang, Y., Wang, Q., Fan, X., Yuan, J., Cui, L., Wang, P., 2013. Laccase-catalyzed oxidative polymerization of phenolic compounds. Appl. Biochem. Biotechnol. 171, 1673–1680.

Suresh, P.S., Kumar, A., Kumar, R., Singh, V.P., 2008. An Insilco approach to bioremediation: Laccase as a case study. J. Mol. Graph. Model. 26, 845–849.

Tadesse, M.A., D'Annibale, A., Galli, C., Gentili, P., Sergi, F., 2008. An assessment of the relative contributions of redox and steric issues to laccase specificity towards putative substrates. Org. Biomol. Chem. 6, 868–878.

Tao, H., Cornish, V.W., 2002. Milestones in directed enzyme evolution. Curr Opin Chem Biol 6, 858–864.
Thorum, M.S., Anderson, C.A., Hatch, J.J., Campbell, A.S., Marshall, N.M., Zimmerman, S.C., Lu, Y., Gewirth, A.A., 2010. Direct, electrocatalytic oxygen reduction by laccase on anthracene-2-methanethiol-modified gold. J. Phys. Chem. Lett. 1, 2251–2254.

Thurston, C.F., 1994. The structure and function of fungal laccases. Microbiol. 140, 19–26.

Tipmanee, V., Oberhofer, H., Park, M., Kim, K.S., Blumberger, J., 2010. Prediction of reorganization free energies for biological electron transfer: A comparative study of Ru-modified cytochromes and a 4-helix bundle protein. J. Am. Chem. Soc. 132, 17032–17040.

Tracewell, C.A., Arnold, F.H., 2009. Directed enzyme evolution: climbing fitness peaks one amino acid at a time. Curr. Opin. Chem. Biol. 13, 3–9.

Treutler, O., Ahlrichs, R., 1995. Efficient molecular numerical integration schemes. J. Chem. Phys. 102, 346–354.

Udayasoorian, C., Prabu, P.C., 2005. Biodegradation of phenols by ligninolytic fungus *Trametes versicolor*. J. Biol. Sci. 5, 824–827.

Ulmer, K.M., 1983. Protein engineering. Sci. 219, 666–671.

Valls, C., Vidal, T., Roncero, M.B., 2010. Boosting the effect of a laccase–mediator system by using a xylanase stage in pulp bleaching. J. Hazard. Mater. 177, 586–592.

Villà, J., Bentzien, J., González-Lafont, À., Lluch, J.M., Bertran, J., Warshel, A., 2000. Effective way of modeling chemical catalysis: Empirical valence bond picture of role of solvent and catalyst in alkylation reactions. J. Comput. Chem. 21, 607–625.

Wang, J., Cieplak, P., Kollman, P.A., 2000. How well does a restrained electrostatic potential (RESP) model perform in calculating conformational energies of organic and biological molecules? J. Comput. Chem. 21, 1049–1074.

Warshel, A., Weiss, R.M., 1980. An empirical valence bond approach for comparing reactions in solutions and in enzymes. J. Am. Chem. Soc. 102, 6218–6226.

Wells, A., Teria, M., Eve, T., 2006. Green oxidations with laccase-mediator systems. Biochem. Soc. Trans. 34, 304–308.

Wherland, S., Farver, O., Pecht, I., 2014. Multicopper oxidases: intramolecular electron transfer and O2 reduction. J. Biol. Inorg. Chem. 19, 541–554.

Wood, R.H., Liu, W., Doren, D.J., 2002. Rapid calculation of the structures of solutions with ab Initio interaction potentials. J. Phys. Chem. A 106, 6689–6693.

Xu, F., 1996. Oxidation of phenols, anilines, and benzenethiols by fungal laccases: correlation between activity and redox potentials as well as halide inhibition. Biochem. 35, 7608–7614.

Xu, F., Berka, R.M., Wahleithner, J.A., Nelson, B.A., Shuster, J.R., Brown, S.H., Palmer, A.E., Solomon, E.I., 1998. Site-directed mutations in fungal laccase: effect on redox potential, activity and pH profile. Biochem J 334, 63–70.

Xu, F., Palmer, A.E., Yaver, D.S., Berka, R.M., Gambetta, G.A., Brown, S.H., Solomon, E.I., 1999. Targeted mutations in a *Trametes villosa* laccase. Axial perturbations of the T1 copper. J. Biol. Chem. 274, 12372–12375.

Yang, J., Yang, X., Lin, Y., Ng, T.B., Lin, J., Ye, X., 2015. Laccase-catalyzed decolorization of malachite green: Performance optimization and degradation mechanism. PLOS ONE 10, e0127714.

Zhang, Y., Zeng, Z., Zeng, G., Liu, X., Liu, Z., Chen, M., Liu, L., Li, J., Xie, G., 2012. Effect of Triton X-100 on the removal of aqueous phenol by laccase analyzed with a combined approach of experiments and molecular docking. Colloids Surf. B Biointerfaces 97, 7–12.

Zhang, Z., Komives, E.A., Sugio, S., Blacklow, S.C., Narayana, N., Xuong, N.H., Stock, A.M., Petsko, G.A., Ringe, D., 1999. The role of water in the catalytic efficiency of triosephosphate isomerase. Biochem. 38, 4389–4397.

Zheng, M., Griveau, S., Dupont-Gillain, C., Genet, M.J., Jolivalt, C., 2015. Oxidation of laccase for improved cathode biofuel cell performances. Bioelectrochem. 106, Part A, 77–87.

Zhukhlistova, N.E., Zhukova, Y.N., Lyashenko, A.V., Zaĭtsev, V.N., Mikhaĭlov, A.M., 2008. Three-dimensional organization of three-domain copper oxidases: A review. Crystallogr. Rep. 53, 92–109.

Zumárraga, M., Bulter, T., Shleev, S., Polaina, J., Martínez-Arias, A., Plou, F.J., Ballesteros, A., Alcalde, M., 2007. In vitro evolution of a fungal laccase in high concentrations of organic cosolvents. Chem. Biol. 14, 1052–1064.

Zumárraga, M., Camarero, S., Shleev, S., Martínez-Arias, A., Ballesteros, A., Plou, F.J., Alcalde, M., 2008a. Altering the laccase functionality by in vivo assembly of mutant libraries with different mutational spectra. Proteins 71, 250–260.

Zumarraga, M., Dominguez, C., Camarero, S., Shleev, S., Polaina, J., Martinez-Arias, A., Ferrer, M., De Lacey, A., Fernandez, V., Ballesteros, A., Plou, F., Alcalde, M., 2008b. Combinatorial saturation mutagenesis of the *Myceliophthora thermophila* laccase T2 mutant: the connection between the C-terminal plug and the conserved VSG tripeptide. Comb. Chem. High Throughput Screening 11, 807–816.

7. APPENDICES

APPENDIX A

- **LB medium**

  LB / Amp medium (Sambrook et al., 1990) used for selective growth of *E. coli* transformants containing the vector pJRoC30.

Bacto Tripton	10 g
Yeasr Extract	5 g
NaCl	10 g
Ampicilin esteril (100 mg/mL)[1]	1 mL
Water upto	1 L

[1] Sterilize by filtration.

Adjust to pH 7.0 with NaOH. Autoclave for 15 min at 121 ° C. Add ampicillin when the medium is at ~ 50 ° C.

For solid medium, add 20 g agar / L before sterilization.

- **Solution SOB** (Sambrook et al., 1990)**, Stock solution for transformation into *E. coli*.**

Bacto Tripton	2 g
Yeast Extract	0.5 g
NaCl	0.05 g
KCl (250 mM)	1 mL
Water upto	100 mL

- **SC-medium**

Yeast nitrogen base(YNB)	6.7 g/L
Yeast synthetic drop out medium	1.92 g/L
Glucose	2 g/L
Chloramphenicol[1]	25 g/L

[1] Sterilize by filtration. 25 mg chloramphenicol in 1 mL of ethanol

After mixing the materials, autoclave for 15 min at 121 ° C. Then glucose and chloramphenicol were added.,

- **YPD-medium**

Pepton	20 g/L
Yeast extract	10 g/L
Glucose	200 g/L

- **Laccase selective expression medium**

Compound	1 L	Final concentration
YNB	100 mL	6.7 g/L
Yeast synthetic drop out medium aminoacids supplement	100 mL	1.92 g/L
Galactose (200g/L)	100 mL	20 g/L
Buffer KH_2PO_4 (pH6.0, 1M)	67 mL	67 mM
Ethanol 100%	31.6 mL	25 g/L
$CuSO_4$ (25 g/L)	1 ml	1mM
Chloramphenicol	1 mL	25 mg/L
H_2O	600 mL	

APPENDIX B

- **Synthetic oligonucleotides**

Primer	Sequence
L363F Forward	CGACAACACGCTCGACGTCACCTTTGACACCATGGGCACGCCCCTG
L363F Reverse	CAGGGGCGTGCCCATGGTGTCAAAGGTGACGTCGAGCGTGTTGTCG
W373F forward	GGGCACGCCCCTGTTCGTCTTTAAGGTCAACGGCAGCGCCATCAAC
W373F reverse	GTTGATGGCGCTGCCGTTGACCTTAAAGACGAACAGGGGCGTGCCC
A192L Forward	GGTGGAACTCACCAAGAACTCGGGCTAACCCTTCAGCGACAACGTCC
A192L Reverse	GGACGTTGTCGCTGAAGGGTTAGCCCGAGTTCTTGGTGAGTTCCACC
L296F Forward	CGTCACATTTGGCGGCGGCTTTCTCTGCGGCGGCTCCAGGAGTCC
L296F Reverse	GGACTCCTGGAGCCGCCGCAGAGAAAGCCGCCGCCAAATGTGACG
M433 Forward	CTTTCACCCTACCGCATCCGNNSCACCTGCACGGCCACGACTTTTAC
M433 Reverse	GTAAAAGTCGTGGCCGTGCAGGTGSNNCGGATGCGGTAGGGTGAAAG
L500 Forward	CCGACAACCCGGGCGCCTGGNNSTTCCACTGCCACATCGCCTGGC
L500 Reverse	GCCAGGCGATGTGGCAGTGGAASNNCCAGGCGCCCGGGTTGTCGG
Primers for combinatorial library	
L296 Forward	GCCGAACGCCCGGGAACTACTGGTTTAACGTCACATTTGGCGGCGGCVHGCTCTGCGGCGG
	GCCGAACGCCCGGGAACTACTGGTTTAACGTCACATTTGGCGGCGGCNTDCTCTGCGGCGG
	GCCGAACGCCCGGGAACTACTGGTTTAACGTCACATTTGGCGGCGGCTGGCTCTGCGGCGG
A192 Reverse	CCGGGTGCTTGGCCGTGCCGTTGAACAGGACGTTGTCGCTGAAGGGCHVGCCCGAGTTCTTGG
	CCGGGTGCTTGGCCGTGCCGTTGAACAGGACGTTGTCGCTGAAGGGADNGCCCGAGTTCTTGG

	CCGGGTGCTTGGCCGTGCCGTTGAACAGGACGTTGTCGCTGAA GGGCCAGCCCGAGTTCTTGG
Central Zone Forward	CGACAACGTCCTGTTCAACGGCACGGCCAAGCACCCGG
Central Zone Reverse	CCAAATGTGACGTTAAACCAGTAGTTCCCGGGCGTTCGGC
RMLN	CCTCTATCTTTAACGTCAAGG
RMLC	GGGAGGGCGTGAATGTAAGC

APPENDIX C

	V / μl	**Final concentration**
Buffer Taq 10 x	5	1x
DMSO 50 %	3	3 %
dNTPs mix (40mM)	0.375	0.3 mM
DNA template (100 ng/μl)	1	2 ng/μl
Primer RMLN (10mM)	1.15	0.23 mM
Primer RMLC (10mM)	1.15	0.23 mM
Pfu-Ultra DNA polymerase (2.5 U/μl)	1	0.05 U/μl
dH$_2$O	36.25	
Final volume	50	

Pipetting scheme for error prone PCR

	T / °C	**t**	**Cycles**
Denaturation	95	2 min	1
Denaturation	94	45 sec	
Annealing[*]	50	45 sec	30
Extension	72	1.30 min	
Final Extension	72	10 min	1
Storage	4	∞	

* Annealing temperature with RMLN primer was 50 and with RMLC is 54°C.

Conditions for error prone PCR

APPENDIX D

- **Kits**

Kit	Company
StrataPrep Plasmid Miniprep Kit	Agilent Technologies
StrataPrep DNA Gel Extraction Kit	Agilent Technologies
Zymoprep yeast plasmid miniprep Kit	Orange, California
Yeast Transformation Kit	Sigma Aldrich

APPENDIX E

Reagents	Volume
Acrylamid/Bis 30:1	0.66 mL
Tris-HCl 0.5 M pH 6.8	1.25 mL
SDS 10% (p/v)	0.05 mL
Ammonium persulphate 10%	0.025mL
TEMED	0.01 mL
Water	2.9 mL

Stacking gel condition for SDS_PAGE

Reagents	Volume
Acrylamid/Bis 30:1	4 mL
Tris-HCl 1.5 M pH 8.8	2.5 mL
SDS 10% (p/v)	0.1 mL
Ammonium persulphate 10%	0.05mL
TEMED	0.01 mL
Water	3.3 mL

Separating gel condition for SDS-PAGE

APPENDIX F

Alignment of TvL and MaL sequences

Chain								
	5	10	15	20	25	30	35	40
1							5	10
	GLY———ILE-GLY-PRO-VAL-ALA-ASP-LEU-THR-ILE-T
2	5	10	15	20	25	30	35	40
	GLU-PRO-THR-CYS-ASN-THR-PRO-SER-ASN-ARG-ALA-CYS-TRP-SER-ASP-GLY-PHE-ASP-ILE-ASN-THR-ASP-TYR-GLU-VAL-SER-THR-PRO-ASP-THR-GLY-VAL-THR-GLN-SER-TYR-VAL-PHE-ASN-LEU-T

Chain								
	45	50	55	60	65	70	75	80
1	15	20	25	30	35	40	45	
	-THR-ASN-ALA————————ALA-VAL-SER-PRO-ASP-GLY-PHE-SER-ARG———GLN-ALA-VAL-VAL-VAL-ASN-GLY-GLY-THR-PRO-GLY-PRO-LEU-ILE-THR-GLY-ASN-MET-GLY-ASP-ARG-PHE-GLN-LEU-ASN-
2	45	50	55	60	65	70	75	80
	-THR-GLU-VAL-ASP-ASN-TRP-MET-GLY-PRO-ASP-GLY-VAL-VAL-LYS-GLU-LYS-VAL-MET-LEU-ILE-ASN-GLY-ASN-ILE-MET-GLY-PRO-ASN-ILE-VAL-ALA-ASN-TRP-GLY-ASP-THR-VAL-GLU-VAL-THR-

Chain								
	85	90	95	100	105	110	115	120
1	50	55	60	65	70	75	80	85
	-VAL-ILE-ASP-ASN-LEU-THR-ASN-HIS-THR-MET-LEU-LYS-SER-THR-SER-ILE-HIS-TRP-HIS-GLY-PHE-PHE-GLN-LYS-GLY-THR-ASN-TRP-ALA-ASP-GLY-PRO-ALA-PHE-ILE-ASN-GLN-CYS-PRO-ILE-
2	85	90	95	100	105	110	115	
	-VAL-ILE-ASN-ASN-LEU-VAL———THR————————ASN-GLY-THR-SER-ILE-HIS-TRP-HIS-GLY-ILE-HIE-GLN-LYS-ASP-THR-ASN-LEU-HIS-ASP-GLY-ALA-ASN-GLY-VAL-THR-GLU-CYS-PRO-ILE-

Chain								
	125	130	135	140	145	150	155	160
1	90	95	100	105	110	115	120	125
	-SER-SER-GLY———HIS-SER-PHE-LEU-TYR-ASP-PHE-GLN-VAL-PRO-ASP-GLN-ALA-GLY-THR-PHE-TRP-TYR-HIS-SER-HIS-LEU-SER-THR-GLN-TYR-CYS-ASP-GLY-LEU-ARG-GLY-PRO-PHE-VAL-VAL-T
2	120	125	130	135	140	145	150	155
	-PRO-PRO-LYS-GLY-GLN-ARG-THR-TYR-ARG-TRP-ARG-ALA———ARG-GLN-TYR-GLY-THR-SER-TRP-TYR-HIS-SER-HIS-PHE-SER-ALA-GLN-TYR-GLY-ASN-GLY-VAL-VAL-GLY-THR-ILE-GLN-ILE-A

Chain								
	165	170	175	180	185	190	195	200
1	130	135	140	145	150	155	160	
	-TYR-ASP-PRO-ASN-ASP-PRO-ALA-ALA-ASP-LEU-TYR-ASP-VAL-ASP-ASN-ASP-ASP-THR-VAL-ILE-THR-LEU-VAL-ASP-TRP-TYR-HIS-VAL-ALA-ALA-LYS-LEU-GLY———PRO-ALA———
2	160	165	170	175	180	185	190	
	-ASN-GLY———PRO———ALA-SER-LEU-PRO-TYR-ASP-ILE-ASP———LEU-GLY-VAL-PHE-PRO-ILE-THR-ASP-TYR-TYR-TYR-ARG-ALA-ALA-ASP-ASP-LEU-VAL-HIS-PHE-THR-GLN-ASN-ASN-

Chain								
	205	210	215	220	225	230	235	240
1	165	170	175	180	185	190	195	200
	-PHE-PRO-LEU-GLY-ALA-ASP-ALA-THR-LEU-ILE-ASN-GLY-LYS-GLY-ARG-SER-PRO-SER-THR-THR-THR-ALA-ASP-LEU-SER-VAL-ILE-SER-VAL-THR-PRO-GLY-LYS-ARG-TYR-ARG-PHE-ARG-LEU-VAL-
2	195	200	205	210	215	220	225	230
	-ALA-PRO-PRO-PHE-SER-ASP-ASN-VAL-LEU-ILE-ASN-GLY-THR-ALA-VAL-ASN-PRO-ASN-THR-GLY-GLU-GLY-GLN-TYR-ALA-ASN-VAL-THR-LEU-THR-PRO-GLY-LYS-ARG-HIS-ARG-LEU-ARG-ILE-LEU-

Chain								
	245	250	255	260	265	270	275	280
1	205	210	215	220	225	230	235	240
	-SER-LEU-SER-CYS-ASP-PRO-ASN-TYR-THR-PHE-SER-ILE-ASP-GLY-HIS-ASN-MET-THR-ILE-ILE-GLU-THR-ASP-SER-ILE-ASN-THR-ALA-PRO-LEU-VAL-VAL-ASP-SER-ILE-GLN-ILE-PHE-ALA-ALA-
2	235	240	245	250	255	260	265	270
	-ASN-THR-SER-THR-GLU-ASN-HIS-PHE-GLN-VAL-SER-LEU-VAL-ASN-HIS-THR-MET-THR-VAL-ILE-ALA-ALA-ASP-MET-VAL-PRO-VAL-ASN-ALA-MET-THR-VAL-ASP-SER-LEU-PHE-LEU-ALA-VAL-GLY-

Chain								
	285	290	295	300	305	310	315	320
1	245	250	255	260		265		270
	-GLN-ARG-TYR-SER-PHE-VAL-LEU-GLU-ALA-ASN-GLN-ALA-VAL-ASP-TYR-TRP-ILE-ARG-ALA-ASN-PRO———————ASN-PHE-GLY-ASN———VAL-GLY-PHE-THR-GLY-GLY-ILE-
2	275	280	285	290	295	300	305	
	-GLN-ARG-TYR-ASP-VAL-VAL-ILE-ASP-ALA-SER-ARG-ALA-PRO-ASP-ASN-TYR-TRP-PHE-ASN-VAL-THR-PHE-GLY-GLY-GLN-ALA-ALA-CYS-GLY-GLY-SER-LEU-ASN-PRO-HIS———

Chain								
	285	290	295	300	305	310	315	320
1	245	250	255	260		265		270
	-GLN-ARG-TYR-SER-PHE-VAL-LEU-GLU-ALA-ASN-GLN-ALA-VAL-ASP-TYR-TRP-ILE-ARG-ALA-ASN-PRO———————ASN-PHE-GLY-ASN———VAL-GLY-PHE-THR-GLY-GLY-ILE-
2	275	280	285	290	295	300	305	
	-GLN-ARG-TYR-ASP-VAL-VAL-ILE-ASP-ALA-SER-ARG-ALA-PRO-ASP-ASN-TYR-TRP-PHE-ASN-VAL-THR-PHE-GLY-GLY-GLN-ALA-ALA-CYS-GLY-GLY-SER-LEU-ASN-PRO-HIS———

Chain								
	365	370	375	380	385	390	395	400
1	315	320	325	330		335	340	
	-ALA-VAL-PRO-GLY-SER-PRO———VAL———ALA-GLY-GLY-VAL-ASP-LEU-ALA-ILE-ASN-MET-ALA-PHE-ASN-PHE-ASN-GLY———————THR-ASN-PHE-PHE-ILE-ASN-GLY-ALA-SER-PHE-
2	345	350	355	360	365	370	375	380
	-SER-VAL———————PRO-VAL-ASN-SER-PHE-VAL-LYS———ARG-PRO-ASP-ASN-THR-LEU-PRO-VAL-ALA-LEU-ASP-LEU-THR-GLY-THR-PRO-LEU-PHE-VAL-TRP-LYS-VAL-ASN-GLY-SER-ASP-ILE-

Chain								
	405	410	415	420	425	430	435	440
1	345	350	355	360	365	370	375	380
	-THR-PRO-PRO-THR———VAL-PRO-VAL-LEU-LEU-GLN-ILE-ILE-SER-GLY———ALA-GLN-ASN-ALA-GLN-ASP-LEU-LEU-PRO-SER-GLY———SER-VAL-TYR-SER-LEU-PRO———SER-ASN-ALA-ASP-ILE-
2	385	390	395		400	405	410	415
	-ASN-VAL-ASP-TRP-GLY-LYS-PRO-ILE-ILE-ASP-TYR-ILE-LEU-THR-GLY-ASN-THR———————SER-TYR-PRO———VAL-SER-ASP-ASN-ILE-VAL-GLN-VAL-ASP-ALA-VAL-ASP-GLN-TRP-THR-

Chain								
	445	450	455	460	465	470	475	480
1	385	390		395	400	405	410	
	-GLU-ILE-SER-PHE-PRO-ALA-THR-ALA———ALA———ALA-PRO-GLY-ALA-PRO-HIS-PRO-PHE-HIS-LEU-HIS-GLY-HIS-ALA-PHE-ALA-VAL-VAL-ARG-SER-ALA———GLY-SER———
2	420	425	430	435	440	445	450	
	-TYR-TRP-LEU-ILE-GLU-ASN-ASP-PRO-GLU-GLY-PRO-PHE-SER———LEU-PRO-HIS-PRO-MET-HIS-LEU-HIS-GLY-HIS-ASP-PHE-LEU-VAL-LEU-GLY-ARG-SER-PRO-ASP-VAL-PRO-ALA-ALA-SER-GLN-

Chain									
	485	490	495	500	505	510	515	520	
1		415	420	425	430	435	440		
	THR—VAL—TYR—ASN—TYR—ASP—ASN—PRO—ILE—PHE—ARG—ASP—VAL—VAL—SER—THR—GLY—THR—PRO—ALA—ALA—GLY—ASP—ASN—VAL—THR—ILE—ARG—PHE								
2		455	460	465	470	475	480	485	490
	GLN—ARG—PHE—VAL—PHE—ASP—PRO—ALA—VAL—ASP—LEU—ALA—ARG—LEU—ASN—GLY—ASP—ASN—PRO—PRO—ARG—ARG—ASP—THR—THR—MET—LEU—PRO—ALA—GLY—GLY—TRP—LEU—LEU—LEU—ALA—PHE								

Chain									
	525	530	535	540	545	550	555	560	
1		445	450	455	460	465	470	475	
	ARG—THR—ASP—ASN—PRO—GLY—PRO—TRP—PHE—LEU—HIS—CYS—HIS—ILE—ASP—PHE—HIS—LEU—GLU—ALA—GLY—PHE—ALA—VAL—VAL—PHE—ALA—GLU—ASP—ILE—PRO—ASP—VAL—ALA—SER—ALA—ASN—PRO								
2		495	500	505	510	515	520	525	530
	ARG—THR—ASP—ASN—PRO—GLY—ALA—TRP—LEU—PHE—HIS—CYS—HIS—ILE—ALA—TRP—HIS—VAL—SER—GLY—GLY—LEU—SER—VAL—ASP—PHE—LEU—GLU—ARG—PRO—ALA—ASP—LEU—ARG—GLN—ARG—ILE—SER—GLN—GLU								

Chain									
	545	550	555	560	565	570	575	580	585
1	5	470	475	480	485	490	495		
	L—VAL—PHE—ALA—GLU—ASP—ILE—PRO—ASP—VAL—ALA—SER—ALA—ASN—PRO—VAL—PRO—GLN—ALA—TRP—SER—ASP—LEU—CYS—PRO—THR—TYR—ASP—ALA—ARG—ASP—PRO—SER—ASP—GLN								
2	5	520	525	530	535	540	545	550	555
	L—ASP—PHE—LEU—GLU—ARG—PRO—ALA—ASP—LEU—ARG—GLN—ARG—ILE—SER—GLN—GLU—ASP—GLU—ASP—ASP—PHE—ASN—ARG—VAL—CYS—ASP—GLU—TRP—ARG—ALA—TYR—TRP—PRO—THR—ASN—PRO—TYR—PRO—LYS—ILE—ASP—SER—GLY—LEU								